Mutation of adjacent cysteine residues in the NSs protein of Rift Valley fever virus results in loss of virulence in a murine model infection

By

Gaby Ermelindo Roberto Monteiro

Submitted in partial fulfillment of the requirement for the degree of **Philosophiae Doctor** in the Department of Veterinary Tropical Diseases, Faculty of Veterinary Science, University of Pretoria

Supervisor

Prof. dr hab. Janusz T. Paweska

Co-supervisors

Prof. dr. Jeroen Kortekaas

Dr. Petrus Jansen van Vuren

January, 2019

DECLARATION

I, Gaby Monteiro (12120431), hereby declare that this thesis is a result of my own unaided work, except where I have indicated otherwise. It is submitted in partial fulfilment of the degree, Philosophiae Doctor, at the Faculty of Veterinary Science, University of Pretoria, South Africa. It has not been submitted before for any degree or examination at any other university, nor has it been prepared under the aegis or with the assistance of any other organization or person outside the University of Pretoria, other than as indicated in the acknowledgements.

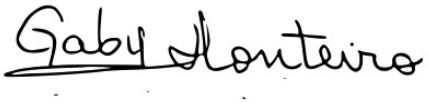

Gaby E.R. Monteiro

January, 2019

ACKNOWLEDGEMENTS

I would like to address my sincere acknowledgements to The Lord for the gift of life, wisdom, strength and success, and the following individuals, institutions and organizations:

Prof. dr hab. Janusz Paweska, Head Centre for Emerging Zoonotic and Parasitic Diseases (CEZPD), National Institute for Communicable Diseases, a division of the National Health Laboratory Service (NICD-NHLS), my supervisor, for his mentorship, expert advice, supervision and funding throughout the long journey of my studies.

Dr. Petrus Jansen van Vuren, medical scientist at CEZPD, NICD-NHLS, my co-supervisor, for his expert advice and support throughout my studies.

Prof. dr. Jeroen Kortekaas, my co-supervisor, Molecular virologist/Group leader at Wageningen Bioveterinary Research, Lelystad, the Netherlands and at the Laboratory of Virology, Droevendaalsesteeg 1, Wageningen, the Netherland, for the opportunity to receive training in reverse genetics at his laboratory in Lelystad, for his expert advice and continuous support throughout my studies.

Dr. Paul Wichgers Schreur (Department of Virology, Wageningen Bioveterinary Research, Lelystad, the Netherlands) for his expert advice and technical support in reverse genetics.

Prof. Dr. Luis Carlos Bernardo Gil das Neves, (University of Pretoria (UP), Department of Veterinary Tropical Diseases (DVTD), my mentor, for his expert advice, encouragement, support and for the opportunity to undertake my studies at the DVTD.

Dr. Ursula Buchholz, National Institutes of Health (NIH, USA) for providing the BSR T7/5 cells.

Dr. Benjamin Brennan from the University of Glasgow for providing the NSs antiserum.

Dr. Christiaan Potgieter (Deltamune, South Africa) for technical support and assistance with transfections.

The NICD-NHLS and CEZPD staff for making their facility available for this project and for their technical support.

Prof. Caroline Tiemessen and the staff at the Department of HIV Cell Biology, Centre for HIV and STIs, the National Institute for Communicable Diseases (NICD-NHLS), and special thanks to Dr. Shayne Loubser. I am grateful to them for making their facility available for the gene expression studies and for making my PhD journey pleasant through their technical, academic and social support.

My sponsors, Wellcome Trust (Grant WT087546MA) through the Southern African Centre for Infectious Disease Surveillance (SACIDS).

Cannon Collins Trust (Graça Machel Trust) for the scholarship awarded.

Eduardo Mondlane University, especially to the Veterinary Faculty and Centre of Biotechnology for their support.

Special acknowledgement goes to my beloved husband Samuel Mudaca and my adorable children Ákila, Hossana and Malvin, for their love, understanding, encouragement and patience throughout the period of my studies.

All my family and friends for their encouragement and immeasurable support.

THESIS SUMMARY

Mutation of adjacent cysteine residues in the NSs protein of Rift Valley fever virus results in loss of virulence in a murine model infection

by

Gaby Ermelindo Roberto Monteiro

Supervisor:

Prof. dr. hab. JT Paweska

Head Centre for Emerging Zoonotic and Parasitic Diseases,

National Institute for Communicable Diseases,

a division of the National Health Laboratory Service

Extraordinary Professor

Department of Medical Virology

School of Medicine

Faculty of health sciences

University of Pretoria

Co-supervisors:

Prof. dr. Jeroen Kortekaas

Molecular virologist/Group leader

Wageningen Bioveterinary Research,

Lelystad, the Netherlands

Laboratory of Virology, Droevendaalsesteeg 1,

Wageningen, the Netherland.

Dr. Petrus Jansen Van vuren

Medical Scientist

Centre for Emerging Zoonotic and Parasitic Diseases,

National Institute for Communicable Diseases,

a division of the National Health Laboratory Service.

Extraordinary Professor

Department of Medical Virology

School of Medicine

Faculty of health sciences

University of Pretoria

For the Degree: PhD in Veterinary Science (Veterinary Tropical Diseases)

Rift Valley fever virus (RVFV) is a mosquito-borne virus of the *Phlebovirus* genus, family *Phenuiviridae,* Order *Bunyavirales*. It has a negative-sense, single-stranded RNA genome, arranged in three segments; large (L), medium (M), and small (S). The S segment employs an ambisense coding strategy, coding for the nucleocapsid (N) protein in the negative sense orientation and the non-structural protein (NSs) in the positive sense orientation. The NSs protein is the major virulence factor of RVFV that inhibits host innate antiviral defense mechanisms. NSs suppresses the induction of type-I interferon (IFN) responses by forming a repressor complex on the IFN-β promoter; promotes the degradation of specific proteins such as Protein Kinase R (PKR) and also induces a general transcription shut-off in infected cells. NSs contains five highly conserved cysteine residues at positions 39, 40, 149, 178 and 194, which are thought to stabilize the tertiary and quaternary structure of the protein. Deletion of the NSs gene results in attenuation of RVFV, but less is known about the exact role of specific amino acid residues of the NSs protein.

This thesis reports on clinical, virological, histopathological and host gene responses in BALB/c mice infected with wild type RVFV (wtRVFV) and genetic mutants having cysteine-to-serine substitution at residues 39 and 40, 149, 178 and 194 of the NSs protein. The wtRVFV and four mutant viruses were rescued from transcription plasmids using a three plasmid-based reverse genetics system. BSR-T7/5 cells were infected with a recombinant fowlpox virus expressing T7 polymerase and subsequently transfected with pUC57 plasmids encoding RVFV S, M and L segments. The rescued viruses were used for animal experiments. BALB/c mice were inoculated subcutaneously (s.c.) with wtRVFV isolate 35/74 or one of the four mutants, and monitored for clinical signs, weighed and temperatures recorded. Samples were collected from mice at regular intervals post inoculation and from any moribund animals, including whole blood, liver, spleen, brain, lungs, heart and kidney tissues, for virus titration, histopathology and gene expression studies. Mice infected with the wtRVFV developed a fatal acute disease characterized by high levels of viral replication, severe hepatocellular necrosis, and up-regulation of transcription of genes encoding type-I and -II interferon (IFN), as well as pro-apoptotic and pro-inflammatory cytokines. The RVFV-C39S/C40S mutant did not cause clinical disease and its attenuated virulence was consistent with virological, histopathological and host gene expression findings in BALB/c mice. Clinical signs in mice infected with viruses containing cysteine-to-serine substitutions at positions 178 or 194 were similar to those occurring in mice infected with the wtRVFV, while a mutant containing a substitution at position 149 caused mild, non-fatal disease in mice.

As mutant RVFV-C39S/C40S showed an attenuated phenotype in mice, the molecular mechanisms underlying this attenuation were further investigated, including the ability of the mutant virus to suppress the type-I IFN response, trafficking to the nucleus, degradation of PKR and the functional transcription factor II Human (TFIIH) subunit p62. Expression levels of IFN-β mRNA transcripts were quantified in MRC-5 cells infected with the wtRVFV and the mutant RVFV-C39S/C40S. The results showed significant ($p<0.05$) upregulation of IFN-β mRNA gene expression in the lysates of cells infected with the mutant C39S/C40S, while IFN-β mRNA levels were reduced in wtRVFV infected cells. This result suggests that the C39S/C40S mutations compromise the antagonism of the IFN response by NSs. *In vitro* experiments in Vero

cells demonstrated that both wtRVFV and the mutant C39S/C40S NSs proteins traffic to the nucleus and form filaments, although the mutant appeared less efficient in forming these structures. Infection of Vero cells with wtRVFV resulted in the degradation of PKR between 8 and 12 hours post infection hours post infection (hpi), whereas PKR levels were maintained in cells infected with mutant C39S/C40S. The attenuated phenotype of the mutant C39S/C40S virus is correlated with the compromised ability of mutant NSs to degrade PKR and to downregulate IFN-β mRNA transcription.

TABLE OF CONTENTS

Declaration i

Acknowledgements ii

Thesis summary iv

Table of contents viii

List of tables xii

List of figures xiv

List of abbreviations xviii

1 General introduction 1

1.1 RVFV pathology and epidemiology 1

1.2 Virus structure and genome organization 3

1.3 Viral entry, packaging and release 5

1.4 Reverse-genetics of bunyaviruses 7

1.5 Natural variation in the RVFV genome 9

1.6 Virus host interactions 10

1.6.1 Interferon pathways 11

1.6.2 Interferon-stimulated genes and restriction factors 13

1.7 RVFV virulence factors 14

1.7.1 RVFV NSs protein 14

1.8 Animal models for Rift Valley fever virus 16

1.8.1 Mice 17

1.8.2 Rats 17

1.8.3 Ruminants 18
1.8.4 Non-human primates 18
1.9 Thesis objectives 19
1.9.1 General objective: 19
1.9.2 Specific objectives: 19
1.10 Hypothesis 20
2 Materials and methods 21
2.1 Ethics statement 21
2.2 Experimental animals 21
2.3 Viruses 22
2.4 Cell lines 22
2.5 Mutagenesis of the five cysteine residues of the NSs protein 25
2.5.1 Extraction of the DNA Plasmid pUC57 26
2.6 Synthesis of the mutant strand 28
2.6.1 Digestion of the parental supercoiled plasmid DNA 30
2.6.2 Transformation of the mutated plasmid in ultracompetent cells 30
2.6.3 Extraction of mutated plasmids 32
2.6.4 Viruses rescue 32
2.6.5 Sequencing analysis of the rescued viruses 36
2.7 Characterization of the rescued virus 37
2.7.1 Viral growth kinetics analysis 37

2.7.2 Characterization of viral foci morphology by plaque assay 38
2.7.3 Western blot analysis 39
2.7.4 Immunofluorescence analysis 40
2.7.5 Two-step quantitative TaqMan RT-PCR assays 40
2.8 Study of the virulence of the mutated viruses in BALB/c mice 41
2.8.1 Virus inoculation in BALB/c mice and collection of samples 41
2.8.2 Extraction of RNA 43
2.8.3 Viral loads 44
2.9 Sequencing analysis of the virus extracted from infected organs 46
2.10 Histopathology examination 46
2.11 Immunohistochemistry examination 49
2.11.1 Inflammatory cytokines and receptors and Type-I inflammatory response 51
2.12 Relative quantification data analysis 52
2.13 Statistical analysis 53
3 Rescue and characterization of wtRVFV and NSs mutants 54
3.1 Introduction 54
3.2 Results 57
3.2.1 Rescue of recombinant RVFV from transcription plasmids 57
3.2.2 Characterization of the rescued virus 57
3.3 Discussion 65
4 Virulence study in BALB/c mice 67

4.1 Introduction 67
4.2 Results 70
4.2.1 Evaluation of RVFV virulence in BALB/c mice 70
4.2.2 Survival of mice 71
4.2.3 Detection of viral RNA by Q-RT-PCR in infected mice 72
4.2.4 Histopathology 75
4.3 Immunohistochemistry 77
4.4 Discussion 81
5 Cytokine gene expression studies 83
5.1 Introduction 83
5.2 Results 85
5.2.1 Cytokine gene expression in RVFV infected mice 85
5.3 Discussion 89
6 Conclusions and future directions 91
7 References 93
8 APPENDICES 119

LIST OF TABLES

Table 2.1.Primers used for the generation of the mutant NSs viruses. 26

Table 2.2. Sample reaction used for the mutant strand synthesis. For the control reaction, the pWhitescript 4.5-kb DNA template (provided by the kit) was used. 29

Table 2.3. Control reaction. The plasmid pWhitescript 4.5-kb DNA template (provided with the kit) was used as control along with 2 primers to amplify the gene of interest. 29

Table 2.4. Thermal cycling parameters used for the four NSs mutant strand synthesis reactions. 30

Table 2.5. Sequence of primers used for amplification of the three genome segments of RVFV used for full genome sequencing. 37

Table 2.6. Outline of the main experiment. BALB/c mouse experimental group I was inoculated with the parental wtRVFV isolate 35/74. Groups II to V were inoculated with the mutant viruses generated. Group VI was mock inoculated with 100µl of EMEM and served as the control group. 43

Table 2.7. Sample reaction for the amplification of the M segment of RVFV using One step RT-PCR kit from Qiagen. The Ar 20368 mosquito isolate 1981 SA was used as control and for the generation of a standard curve. Primers were designed by Drosten et al., 2002. 45

Table 2.8. Thermal cycling parameters used for RT-PCR. Lightcycler 480 (Roche). 45

Table 2.9. Description of liver histopathology scoring in BALB/c mice experimentally infected with wtRVFV and the NSs mutants. 47

Table 2.10. Description of spleen histopathology scoring in BALB/c mice experimentally infected with wtRVFV and the NSs mutants. 48

Table 2.11. Description of liver and spleen immunolabelling scoring in tissues of BALB/c mice experimentally infected with wtRVFV and the NSs mutants. 50

Table 4.1. Histopathology (HP) and immunohistochemistry (IHC) scoring of mouse tissues infected with wtRVFV and the NSs mutants. Experimental groups are arranged according to the severity of the lesions. 78

Table 5.1. Number of transcripts up- and downregulated in the livers and spleens of mutant NSsC39S/C40S and wtRVFV. Samples were collected on day 3 and 5 p.i. 85

LIST OF FIGURES

Figure 2.1. Diagram representing the primers and the position of the cysteine-to-serine mutation in the NSs gene of RVFV isolate SA35/74. 26

Figure 2.2 Transfection plates layout. Two six-well plates were seeded with 2mL per well of the BSR-T7/5 cell suspension (500 000 cells/well in 2mL) the day before transfection. The wtRVFV 35/74 was used as backbone for the generation of the NSs plasmids and each well in duplicate was then transfected with 200µl of DNA plasmid-Jetpei mix accordingly. The reaction was incubated at 37^{o}C, 5% CO_2 for 4-7 days. 34

Figure 2.3 Representation of the rescue of RVFV from transcription plasmids using a three plasmid reverse genetics system. BHK-21 cells (clone BSR-T7/5) were infected with recombinant fowlpox T7 (step 1) and subsequently transfected with plasmid pUC57 encoding RVFV S, M and L segments. After four days, the culture media was collected (step 3). Transcription from the plasmids is controlled by the T7 promoter (T7p). Untranslated regions are depicted as black boxes (adapted from Kortekaas et al., 2011). 35

Figure 2.4. RT^2 PCR Array format for 96 wells. Each well comes with primers for amplification of a specific gene. One plate was used for one sample and three replicates of each sample. 52

Figure 3.1. RVFV replication kinetics in IFN-competent and IFN-deficient cells. Replication kinetics of wtRVFV and the mutants RVFV-C39S/C40S, -C149S, -C178S and -C194S in Vero cells (A) and MRC-5 cells (B). The points in the growth curves are shown as means +/- standard deviation from nine replicates. Asterisk (*) indicates statistically significant differences (Kruskal-Wallis test; $p < 0.05$). 59

Figure 3.2 Plaque morphology. Morphology of plaques produced by (A) wtRVFV and (B) the mutant C39S/C40S. No differences were observed in the morphology and size of plaques produced in Vero cells infected with the wtRVFV and the attenuated mutant C39S/C40S. The cells were fixed in 10% neutral-buffered formalin and stained with 2% crystal violet. Plaques were inspected and measured under inverted microscope, Olympus CellSens Dimension 1x53Camera SC30, 40x magnification. 61

Figure 3.3 Induction of IFN-β gene transcription in RVFV infected cells. At indicated time points post infection, total RNA was extracted from MRC-5 cells infected with either wtRVFV, the mutant C39S/C40S or mock infected. cDNA was amplified using specific primers for human IFN-β and GAPDH. (TaqMan gene expression, ThermoScientific, Waltham, USA). Data represents mean and SD of three replicates. (*) indicates statistical significance (student's t-test $p < 0.05$). 62

Figure 3.4 Western blot detection of NSs and host proteins PKR, p62 in infected vero cells. Vero cells were seeded in 75cm^2 cell culture flasks and infected with wtRVFV or the mutant C39S/C40S at an MOI of 4. After 4, 8 and 12 h.p.i., cell lysates were prepared and subjected to western blot analysis for dettection of NSs, PKR and p62, as described in the material and methods. ß-actin was used as cell lysate control. Infection with wtRVFV resulted in degradation of PKR between 8 and 12 h.p.i while p62 was equally degraded by the wtRVFV and the mutact C39S/C40S. The NSs protein was detected in both wtRVFV and the mutant C39S/C40S from 8 h.p.i. 63

Figure 3.5 Subcellular localization and filament formation of wtRVFV and mutant C39S/C40S NSs proteins. Monolayers of Vero cells on coverslips were infected either with wtRVFV or the mutant C39S/C40S at a MOI of 2. Cells were fixed at 12 h.p.i. and stained with NSs-specific antibodies for the detection of infected cells by immunofluorescence analysis. The left panels show distribution of the nonstructural NSs protein detected with anti-NSs rabbit polyclonal antibody stained with FITC (green), the middle panels show counterstain of the nucleus with DAPI (blue) and the merged image of NSs and DAPI are shown in the right panels. Bars = 20µm. 64

Figure 4.1 Clinical responses in BALB/c mice inoculated with different doses of wtRVFV. Three groups of BALB/c mice each containing five animals were inoculated subcutaneously (s.c.) with 100µl of tissue culture supernatant containing wtRVFV isolate 35/74 ($10^{6.85}$, $10^{3.85}$, or $10^{1.85}$ PFU/mL, respectively). The fourth group was mock inoculated s.c. with 100µl culture media serum free EMEM. 70

Figure 4.2 BALB/c mice survival following subcutaneous inoculation with 100µl of inoculum containing 102.85 PFU/mL wtRVFV isolate SA35/74 and the NSs mutants: RVFV-C194S, RVFV-C178S, RVFV-C149S and RVFV-C39S/C40S. The drop in the percentage of survival on the RVFV-C149S, day 14, is due to the death of a mouse with neurological disease, euthanized on day 14 p.i. Each experimental group consisted of 15 animals. 72

Figure 4.3 RVFV viral loads in tissues and sera of BALB/c mice infected with wtRVFV isolate 35/74 and the RVFV mutants (C194S, C178S, C149S and C39S/C40S). Samples collected on day 3 and 5 p.i. from mice infected with wtRVFV or mutants RVFV-C194S and RVFV-C178S and on day 3, 5, 7 and 14 p.i. for the RVFV-C178S and RVFV-C178S. Each bar represents the mean of RNA copies/g tissue or per mL of serum of mice in each of the experimental groups. The error bars represent the standard deviation. (*) indicates statistically significant differences (Kruskal-Wallis test $p < 0.05$). 75

Figure 4.4 (A-I) Liver and spleen histopathological and immunohistochemical findings in BALB/c mice experimentally infected with wtRVFV and NSs mutants. Samples in panels A, B, C, G, H and I were stained with hematoxylin and eosin. Antigens in samples depicted in panels D, E and F were detected by immunoperoxidase methods with NovaRED chromogen and hematoxylin counterstain. Polyclonal hyperimmune mouse serum was used as the primary antibody and a rabbit anti-mouse antibody as the secondary antibody. Scale bars represent 100µm and 50µm resolution. A: Moderate hepatocellular hydropic change (histopathology score 0) in mouse 21 infected with RVFV-C39S/C40S. B: Multifocal hepatocyte apoptosis (arrowheads) involving single cells to small groups of 2-5 cells (histopathology score 1) in mouse 66 infected with RVFV-C194S. C: Severe diffuse hepatocyte necrosis (histopathology score 3) in mouse 9 infected with wtRVFV. D: Fine diffuse granular cytoplasmic immunolabelling of a few normal hepatocytes (arrowhead) in mouse 21 from the RVFV-C39S/C40S group. E: RVFV-specific positive labelling in multifocal hepatocytes in mouse 66 from the RVFV-C194S group. F: Diffuse intracytoplasmic RVFV-specific positive signal within necrotic foci in mouse 9 from the wtRVFV group. G: Normal spleen showing the ratio of white pulp to red pulp approaching 1:1.5 in control mouse 78. H: Prominent expansion and coalescence of the white pulp (histopathology score 1) in mouse 24 infected with RVFV-C39S/C40S. I: Prominent lymphocyte apoptosis associated with tingible body macrophages (arrowheads) and severe diffuse red pulp atrophy (histopathology score 2) in mouse 56 infected with RVFV-C178S. 80

Figure 5.1 Heat map showing relative levels of RVFV-responsive gene trancripts related to the type-I IFN response. Expression profiles show significant up- or downregulation of gene transcripts in the livers and spleens of mice inoculated with wtRVFV and RVFV-C39S/C40S, on days 3 and 5 p.i. Green and red squares represent reduced and induced levels, respectively. Yellow squares indicate no changes in expression levels. The color scale at the bottom indicates the magnitude of change. Data from three biological replicates are shown for each experimental condition. Please refer to appendix 3 for the description of gene names corresponding to the symbols in the picture. 88

LIST OF ABBREVIATIONS

β-ME	Beta-mercaptoethanol
BSL-3	Biosafety laboratory level 3
BSR-T7/5	Baby hamster kidney cells expressing T7 polymerase
CDC	Centres for Disease Control and Prevention
cDNA	Complementary DNA
CEZPD	Centre for Emerging Zoonotic and Parasitic Diseases
CPE	Cytopathic effect
DC-SIGN	Dendritic cell-specific intercellular adhesion molecule-3-grabbing non-integrin
DMEM	Dulbecco's minimum essential medium
DNA	Deoxyribonucleic acid
DNAse	Deoxyribonuclease
dNTP	Deoxyribonucleotide triphosphate
d.p.i	Days post infection
dsRNA	Double-stranded RNA
EDTA	Ethylenediaminetetracetic acid
ELISA	Enzyme-linked immunosorbent assay
EMEM	Eagle's minimum essential medium
FBS	Fetal bovine serum
G1	Glycoprotein 1

G2	Glycoprotein 2
Gc	C-terminal protein
Gn	N-terminal protein
HIER	Heat-induced epitope retrieval
IFITM	Interferon inducible transmembrane protein
IFN	Interferon
IgG	Immunoglobulin G
IgM	Immunoglobulin M
IGR	Intergenic region
I.m.	Intramuscular
IRF	Interferon regulatory factors
ISG	Interferon stimulated genes
L RNA	Large RNA segment
LB-ampicilin	Lysogeny broth containing ampicilin
M RNA	Medium RNA segment
MEGA	Molecular Evolutionary Genetics Analysis (software)
MOI	Multiplicity of infection
mRNA	Messenger RNA
N protein	Nucleocapsid protein
NCR	Non-coding region

NEAA	Non-essential amino acids
NHLS	National Health Laboratory Service
NICD	National Institute for Communicable Diseases
NSm	Non-structural protein/gene of the M RNA segment
NSs	Non-structural protein/gene of the S RNA segment
OAS	Oligoadenylate synthase
OD	Optical density
ORF	Open reading frame
PAMP	Pathogen associated molecular pattern
PBS	Phosphate buffered saline
PFU	Plaque forming units
PKR	dsRNA-dependent protein kinase R
Pol-I	Polymerase I
PPE	Personal protective equipment
PRR	Pathogen recognition receptors
RNA pol II	RNA polymerase II
RNP	Ribonucleoprotein
RNPs	Ribonucleoproteins
RT-PCR	Reverse transcription polymerase chain reaction
RVF	Rift Valley fever

RVFV	Rift Valley fever virus
S RNA	Small RNA segment
SAP 30	Sin3A associated protein 30
Sc	Subcutaneous
SMLV	Smithburn modified live virus
SNS	Smithburn neurotropic strain
Taq	Thermus aquaticus
TBE	Tris-borate-ethylenediaminetetraacetic acid
$TCID_{50}$	50% Tissue culture infective dose
TFIIH	Transcription factor II human
TIR	Toll/Interleukin-1 receptor
TLR	Toll-like receptors
Tm	Melting temperature
TNF	Tumor necrosis factor
TRAF	TNF-receptor associated factors
TRIF	TIR-domain-containing adapter-inducing interferon-β

CHAPTER 1

1 General introduction

1.1 RVFV pathology and epidemiology

Rift Valley fever (RVF) is a mosquito-borne zoonotic disease caused by RVF virus (RVFV), a member of the *Phlebovirus* genus, family *Phenuiviridae* of the recently established order *Bunyavirales* (Maes et al., 2018, Briese et al., 2016). RVFV was first isolated in 1930, during an outbreak with sudden deaths and abortions among sheep along the lake Naivaska in the Rift Valley of Kenya (Daubney et al., 1931). The first human disease caused by RVFV was reported in 1951 from South Africa (Woods et al., 2002; Mundel and Gear, 1951). Outbreaks then occurred in Egypt 1977/1978 (between 18,000 and 200,000 human infections and 598 deaths), Mauritania 1987 (approximately 200 human deaths), East Africa and Madagascar 1991 (89,000 human infections and more than 500 deaths) and East Africa 1998 (98,000 human infections and 250 deaths) (Swanepoel and Paweska, 2011; Swanepoel and Coetzer, 2004). The disease emerged for the first time outside Africa on the Arabian Peninsula in 2000-2001 and caused an outbreak among livestock and humans (Balkhy and Memish, 2003). RVF outbreaks in Saudi Arabia and Yemen in 2000 affected 882 humans and resulted in 124 deaths (Balkhy and Memish, 2003; Jupp et al, 2002). More recently, RVF outbreaks in humans were recorded in East Africa between 2006 and 2011 (Archer et al., 2011; Mohamed et al., 2010; Nguku et al., 2010; Shieh et al., 2010), Madagascar in 2008 (Andriamandimby et al., 2010; Swanepoel and Coetzer., 2004) South Africa in 2008 and between 2009 and 2011 (Metras et al., 2012; Archer et al., 2011; Swanepoel and Paweska., 2011) and for the first time on the Archipelago of Comoros on the French Island of Mayotte in 2012 (Lernout et al., 2013, Cetre-Sossah et al., 2012; Sissoko et al., 2009). Outbreaks of RVF are usually associated with prolonged and heavy rainfall occurring at irregular intervals, leading to an upsurge in mosquito populations (Swanepoel and Paweska, 2011; Swanepoel and Coetzer, 2004). Mosquitoes of the *Aedes* and *Culex* genera are usually involved in transmission of RVFV, but other mosquito genera (*Anopheles, Eretmapoites* and *Mansonia*) have also been shown to be potential vectors of the virus (Turell et al., 2008). Biting flies such as midges, phlebotomids, stomoxids and simulids might act as mechanical

vectors of infection. Transovarial transmission of the virus in *Aedine* mosquitoes, combined with low-level cycling between mosquitoes and wildlife, is responsible for virus survival during inter-epidemic periods (Evans et al., 2008; Linthicum et al., 1985).

RVF is most severe in sheep, goats and cattle, in which it causes abortion of pregnant animals and high mortality rates among newborns. Adult and non-pregnant animals, although susceptible to infection, are more resistant to clinical disease. Young domesticated ruminants are highly susceptible to disease, while some species of wild animals e.g. camels, and various species of rodents are also susceptible (Swanepoel and Coetzer., 2004). Studies with different species of laboratory rodents have shown that the susceptibility to infection and the severity of clinical symptoms varies among the different species (Ritter et al., 2000; Anderson et al., 1987; Peters and Slone, 1982). There are a number of animals which can become infected with RVFV without clinical symptoms of the disease, including a wide range of wildlife species such as gerenuk, waterbuck, and eland which might play a role in inter-epidemic maintenance of RVFV (Evans et al., 2008).

Fatality rates reach up to 100% in newborn lambs (<2 weeks of age), whereas 20-30% of infected adult sheep may succumb to the infection. Up to 90% of pregnant ewes abort after being infected. This is generally attributed to very high levels of virus replication in multiple organs, which also increases the chances of transmission to humans that handle infected tissues (Woods et al., 2002). Antibodies against RVFV have been found in African buffalo, black rhino, lesser kudu, impala, African elephant, Thompson's gazelle, gerenuk and waterbuck (Rostal et al., 2017; Evans et al., 2008).

Transmission of RVFV to humans can occur through contact with infected tissues, through aerosols created during ruminant abortion or slaughtering, or less frequently through bites by infected mosquitoes (Archer et al., 2011; Daubney et al., 1931). The virus can cause serious disease in laboratory workers and must therefore be handled under high biosafety conditions (BSL 3 or higher). Laboratory workers can be infected by the inhalation of aerosols produced during necropsy, via contact with blood, body fluids or tissues of infected animals, through inoculation, for example via a wound from an infected needle or knife, or through contact with broken skin. Human infections may result in one of four clinical forms: i) uncomplicated, febrile, influenza-like illness; ii)

hemorrhagic fever with liver involvement, thrombocytopenia, icterus and bleeding; iii) encephalitis following a febrile episode with confusion and coma or even death; iv) ocular disease with blurred vision and loss of visual acuity due to retinal hemorrhage and macular edema (Mohamed et al., 2010; Al-Hazmi et al., 2003).

The presence of potential mosquito vectors in RVF-free regions (Turell et al., 2008; Moutailler et al., 2008), the intensification of international trade of live animals, and the impact of climate change has raised international concerns about the potential establishment of RVFV endemicity in RVFV-free countries (Danzetta et al., 2016). In addition, RVFV has also been identified as a potential bioterrorism agent (Sidwell and Smee, 2003).

1.2 Virus structure and genome organization

RVFV has a negative-sense, single-stranded RNA genome, divided into three segments. The large segment (L) encodes the RNA-dependent RNA polymerase (L-protein) in the negative sense orientation. The medium (M) segment encodes the precursor of the envelope glycoproteins Gn and Gc, a 78-kilodalton (kDa) minor structural glycoprotein and a non-structural 14-kDa protein, named NSm, in the negative sense orientation. The small segment (S) employs an ambisense coding strategy, with the open reading frame (ORF) of the nucleocapsid (N) protein in the negative sense orientation and a non-structural protein (NSs) in the positive sense orientation (Giorgi et al., 1991). The nucleocapsid protein and viral polymerase protein associate with the viral genome segments to form ribonucleoproteins (RNPs), which make up the replication machinery of the virus. The three genome segments contain untranslated regions (UTRs) that contain promoters for transcription and replication by the viral polymerase. The UTRs have complementary 5'-3' ends with conserved phlebovirus-specific sequences that base-pair to form panhandle structures that play a role in replication, transcription and packaging (Kolakofsky and Hacker, 1991, Simons and Petterson, 1991).

The RVFV virion has a diameter of 80-120 nanometers (nm), with short spikes (5-8 nm in length) consisting of Gn and Gc glycoproteins projecting through the lipid envelope (Freiberg et al., 2008). These glycoprotein spikes or capsomers are regularly arranged on the virion surface, similar to those reported for the related Uukuniemi

phlebovirus (von Bonsdorff and Petterson, 1975). The capsomeres resemble hollow cylinders situated at five or six-coordinated positions. Inside the envelope, a layer of RNPs is present which bends the inner leaflet membrane toward the glycoproteins, of which the transmembrane segments are discernible (Huiskonen et al., 2009). This suggests a strong interaction between the cytoplasmic tail of the glycoproteins (most likely Gn) and the RNPs which is believed to be essential for packaging of the genome into the particles (Overby et al., 2008).

The N protein is the most abundant protein in infected cells, and also the most immunogenic viral antigen (Magurano and Nicoletti, 1999; Swanepoel et al., 1986). The RVFV N protein is the first viral protein to be produced upon infection (Ikegami et al., 2005) and was shown to be released from infected cells independently of the glycoproteins (Liu et al., 2008). NSs is the most variable protein among phleboviruses (Kortekaas et al., 2011; Sall et al., 1997). The NSs protein forms filamentous structures in the host nucleus and interacts with cellular nuclear proteins (Le May et al., 2008; Yadani et al., 1999; Swanepoel and Blackburn, 1977). The structural glycoproteins, Gn and Gc, are responsible for attachment and entry of the virus into cells and carries neutralizing epitopes (Besselaar and Blackburn, 1992).

RVFV RNA synthesis occurs in the cytoplasm and each segment is a template for replication and transcription (Elliot, 1990). The viral sense strand generates an exact copy in the viral anti-sense orientation, whereas transcribed mRNAs are slightly shorter, terminating in the non-coding region at the 5’ and 3’ ends. Non-coding regions of most phleboviruses contain conserved complementary termini (3’-UGUGUUUC/GAAACACA-5’) resulting in the segment forming “panhandle” structures that serve as promoters for RNA synthesis (Prehaud et al., 1997). The mRNA of the M segment terminates at 3’-CGUCGUCG-5’ (Ikegami et al., 2005) while the mRNA of the L segment is disputed and may produce an mRNA that is identical to the viral anti-sense strand (Albarino et al., 2007) or use a stem-loop terminator or a 5’-CGAUG-3’ motif (Ikegami et al., 2005). The S segment’s transcription termination signals are between the NSs and N open reading frames (ORFs) which falls within an 82 nucleotide (nt) intergenic region (IGR) (Giorgi et al.,1991). The signals for termination within the IGR are 3’-CGUCG-5’ motifs in combination with poly-G/C tracts (Albarino et al., 2007). Both L and N proteins are required for replication and transcription

(Prehaud et al., 1997). Bunyaviruses employ host mRNA “cap snatching” within the cytoplasm. Bunyaviral N protein binds host mRNA caps to protect them from degradation (Mir et al., 2008). N protein then stabilizes the cap at the 3’ end of viral RNA (Mir et al., 2010) while the cap-dependent endonuclease activity of the L protein (Reguera et al., 2010) possibly cleaves the cap into smaller primer fragments. Bunyaviruses use a "prime-and-realign” mechanism to ensure that complete viral RNA is synthesized (Garcin et al., 1995). RVFV mRNA transcripts do not possess a polyadenylated tail (Ikegami et al., 2005). Poly-homodimer formation of the N protein is essential for RNA synthesis (Raymond et al., 2010). Different levels of proteins are expressed from each segment, suggesting varying promoter strengths of the non-coding regions (Gauliard et al., 2006).

1.3 Viral entry, packaging and release

Although the complete life cycle of RVFV has not been fully elucidated, reverse genetics, non-spreading virus particles, and minigenome systems have helped define critical processes of attachment, RNA synthesis, packaging and release (Wichgers Schreur and Kortekaas 2016; Kortekaas, 2011; Lopez et al., 1995). Virions have an icosahedral symmetry with a spherical shell in a T=12 lattice (Sherman et al., 2009; Freiberg et al., 2008). There are 122 capsomeres consisting of hexamers and pentamers of Gn-Gc heterodimers (Huiskonen et al., 2009), which comprise a Gn head and Gc base (Rusu et al., 2012). Gn is most likely the binding partner of the surface receptor while Gc facilitates membrane fusion through acid-triggered type-II fusion (Halldorsson et al., 2018). Due to their location at the site of initial infection, dermal macrophages and dendritic cells (DCs) are believed to be responsible for phlebovirus spread through the host, including RVFV (Léger et al., 2015). The Dendritic cell-specific intercellular adhesion molecule-3-grabbing non-integrin (DC-SIGN) is a C-type lectin highly expressed on dermal dendritic cells and macrophages, and was found to act as an authentic entry receptor for phleboviruses including RVFV (Léger et al., 2016). However, RVFV infect other cells such as hepatocytes and cells of the central nervous system (cells that do not express DC-SIGN) suggesting that additional receptors remain to be identified. Interestingly, it was demonstrated that heparan sulphate, a molecule that is abundantly present on the surface of most

mammalian cell types, is required for efficient infection, suggesting an important role of this attachment factor in the virulence of RVFV (de Boer et al., 2012).

Entry of bunyaviruses is mediated by clathrin-dependent endocytosis (Schudel et al., 2013) and RNPs are released by endosomal acidification (Lozach et al., 2010). The L protein is packaged into mature virions and is required for transcription upon viral entry (Piper et al., 2011). A unique characteristic of bunyaviral replication is the formation of viral tubules associated with the Golgi apparatus, which concentrates L protein for RNA synthesis at viral "factories" (Fontana et al., 2008). In contrast, it was demonstrated for RVFV that replication of RVFV genome segments occurs in the cytoplasm, and the segments are subsequently recruited to the Golgi apparatus (Wichgers Schreur and Kortekaas, 2016). When RVFV Gc is expressed alone, it associates with the endoplasmic reticulum (ER) because of an ER retention signal, and upon forming a heterodimer complex with Gn, which has a Golgi localization signal, the complex is transported to the Golgi apparatus (Gerrard and Nichol, 2007). The N protein forms oligomeric rings when associated with RNA (Ferron et al., 2011) through N-terminal arms which facilitates multimerization (Le May et al., 2005). These multimers can bind RNA in a conserved binding slot which interacts with an RNA backbone to encapsidate the genome (Raymond et al., 2010). The newly formed ribonucleoprotein (RNP) complex is trafficked to the Gn-Gc heterodimers. The N protein probably binds Gn's cytoplasmic tail as this would be essential for the virion's stability in the absence of a matrix protein (Piper et al., 2011). The complementary termini bind to the Gn cytoplasmic tail acting as a signal for viral release (Piper et al., 2011). It was demonstrated in recent studies that RVFV utilizes a non-selective genome packaging strategy (Wichgers Schreur and Kortekaas, 2016), rather than a co-ordinated packaging system previously described in the literature (Terasaki et al., 2013).

The Gn, Gc and N are required for the formation of virus and, when co-expressed, form virus-like particles (VLPs) that are similar in architecture to a mature RVFV virion (Habjan et al., 2009). When Gc and N are co-expressed, the VLPs are more diverse in structure, which reinforces the notion that both glycoproteins are required (Liu et al., 2008). Immature virus will bud into the lumen of the Golgi apparatus for further glycoprotein modification and viral maturation. The later step of RVFV trafficking

through the lumen within vacuoles to the host cell membrane is not a well understood process and may be cell-type specific (Anderson and Smith, 1987).

1.4 Reverse-genetics of bunyaviruses

The study of molecular biology of negative strand RNA viruses has been revolutionized by the development of reverse genetics techniques. These techniques comprise two approaches. The first approach involves a “rescue system” where changes are introduced in the viral genome and the effects of these changes on viral phenotype and biology are directly studied. In this approach, a cDNA copy of the altered viral RNA genome is generated and delivered into permissive cells, where it serves as a template for the production of new viral proteins and new virus particles. The second approach involves “minigenome systems”, in which genome analogues containing a reduced number of viral genes and an easily measurable reporter gene are transcribed and replicated by coexpressed viral proteins (Reviewed in Bouloy and Weber, 2010).

Minigenome systems are available for all the families of negative sense RNA viruses, and rescue systems are also available for nonsegmented and segmented viruses. In bunyavirus research, the T7-based system was used for the rescue of Bunyamwera virus (Lowen et al., 2004; Bridgen and Elliot 1996), LaCrosse virus (Blakqori and Weber 2005) and RVFV (Ikegami et al., 2006), while the Pol I system was used for the rescue of Acabane virus (Ogawa et al., 2007) and RVFV (Billecocq et al., 2008, Habjan et al., 2008). The last two studies compared the two systems and concluded that that both were equally efficient for the rescue of RVFV. When the Pol I system is used, the nucleocapsid protein and the viral polymerase protein must be provided in trans to start virus replication. In contrast, the rescue using the T7 system depends on only the three plasmids encoding the viral cDNA in antigenomic-sense orientation. This demonstrated that the antigenomic sense transcripts act not only as replication intermediates but also as mRNAs (Lowen et al., 2004). Several groups have developed minigenome systems (Gauliard et al., 2006; Ikegami et al., 2005; Kohl et al., 2004; Blackqoni et al., 2003; Flick et al 2003; Lopez et al., 1995). In this approach, a gene encoding a reporter protein such as fluorescent proteins, luciferase or acetyltransferase are most often used. Expression of the reporter protein is only

possible if nucleoprotein N and polymerase L are provided in trans, allowing the assembly of RNPs. Both T7 and Pol-I systems have been employed for transcription and replication of minigenomes. Further studies on minigenome systems by Habjan et al demonstrated the successful packaging of minigenomes in particles (Habjan et al., 2009).

One of the most important requirements for successful rescue of negative-strand RNA viruses is the generation of RNA transcripts that contain termini closely resembling those of the authentic viral genome. Only then, the generated RNA transcripts can function as template for the genome replication by the viral polymerase. To accomplish this requirement, both eukaryotic polymerase I (Pol-I) and phage T7 polymerase have been employed (Ikegami et al., 2006, Kortekaas et al., 2011). Pol-I is an endogenous nuclear protein that produces transcripts lacking 5' caps and 3' polyadenilated tails. Viral genome sequences inserted between the promoter and the terminator sequences of Pol-I contain the exact viral genomic termini. T7 polymerase allows cytoplasmic transcription of viral RNA and is therefore often used for reverse genetics of virus that replicate in the cytoplasm such as bynyaviruses. The T7 polymerase can be expressed from plasmids, recombinant viruses such as vaccinia or fowlpox viruses or constitutively in cell lines (Bridgen, 2012). To create RNAs with 3' termini that exactly correspond to those of the viral genome, the self-cleaving hepatitis delta virus ribozyme sequence can be introduced (Perrotta and Been, 1991).

1.5 Natural variation in the RVFV genome

Viral genome characterization is essential to improve understanding of the role sequence variation has on virulence. The RVFV genome is overall highly conserved and stable (Grobbelaar et al., 2011; Aitken., 2008; Bird et al., 2007b; Sall et al., 1997; Battles and Dalrymple, 1988). Despite their geographical dispersion, all strains of RVFV remain closely related at the nucleotide and amino acid level. Sequencing of geographically diverse RVFV isolates revealed only a 4% and 1% variation in the S-segment, a 5% and 2% variation in the M-segment and a 4% and 1% variation in the L-segment at nucleotide and deduced amino acid sequences, respectively (Bird et al., 2007b). Similar results were obtained from partial M-segment sequences (Grobbelaar et al., 2011). This is likely because the time to most recent common ancestor (TMRCA) for RVFV is recent, with an estimated time of 120-130 years (Grobbelaar et al., 2011; Bird et al., 2007b). Another explanation for this low divergence is the so called "double-filter" hypothesis, which suggests that arbovirus genomes are subject to selective pressures in both the mammalian and insect host, thus leading to tighter genomic constraint (Bird et al., 2007b). This hypothesis has been supported for RVFV *in vitro* in which the genomic stability of NSs was dependent upon alternative passage between insect and mammalian cells (Moutailler et al., 2011). Initial phylogenetic studies indicated that RVFV groups into two major lineages (Egyptian and sub-Saharan), based on sequences of the NSs gene (Sall et al., 1997). Full-genome sequencing, however, revealed that seven distinct lineages can be distinguished (Bird et al., 2007b). Viruses from the Egyptian and the sub-Saharan lineages differ in amino acids that are generally highly conserved. These sequence differences might be involved in the putative differences in virulence observed in the Wistar-Furth rat model (Bird et al., 2007a). Changes in amino acid composition of the surface glycoproteins might have an effect on tropism and antigenicity and not necessarily on virulence. However, changes in the NSs protein might alter its ability to counteract the host innate immune response, thereby leading to increased virulence or attenuation. Changes in the replication machinery of the virus, the N protein and the polymerase, might yield viruses that are less or more fit for rapid replication as a result of altered RNP formation or polymerase activity (Bird et al., 2007a).

Alignment of the NSs protein demonstrated that 5 cysteine residues at positions 39, 49, 150, 170 and 195, are highly conserved among the isolates analyzed (Aitken., 2008; Sall et al., 1997). These residues are important for conservation of the three-dimensional structure of the protein. Cysteine, encoded by two possible codons, UGU and UGC, is a highly reactive, hydrophobic amino acid, capable of forming covalent disulphide bridges which stabilizes the tertiary and quaternary structures of the proteins (Carmenes et al., 1989).

The NSs protein is implicated as the major virulence factor and its pathogenicity is associated with the blocking of interferon production (Le May et al., 2004). Any amino acid changes that result in changes in the filamentous structures of the NSs protein might impact on binding kinetics between NSs protein and SAP 30. Therefore, in hypothesis, loss of cysteine residues in the NSs protein due to point mutations in the NSs gene might influence its ability to fold correctly and thereby compromise interactions with host proteins and DNA.

1.6 Virus host interactions

The host cell has developed mechanisms that survey for markers of viral genetic material. Upon identification, surveillance proteins will activate signal cascades, resulting in production of antiviral proteins that will suppress viral replication (Liu et al., 2008) and signal the adaptive immune response (Meyer, 2009). Viruses have developed means with which to subvert host defenses to establish infection. This includes genomes that are not recognized as foreign, as they do not produce markers that will be detected by the surveillance proteins (Habjan et al., 2008a). Viruses also produce virulence factors that are proteins that have elaborate mechanisms with which to counteract innate immunity and prevent activation of antiviral responses. There is a complex interplay between the two competing mechanisms, which can result in disease prevention or a spectrum of pathogenesis, ranging from mild symptoms to host death. Understanding the molecular basis of host defense pathways and how viruses circumvent these pathways, can lead to a better understanding of pathogenesis as well as assist in the identification of important viral genes involved in antagonism of the immune response.

1.6.1 Interferon pathways

1.6.1.1 Viral recognition and interferon activation

The interferons (IFNs) are a large family of multifunctional secreted proteins involved in antiviral defense, cell growth regulation and immune activation. They have been well described in the literature (reviewed in Wuerth and Weber, 2016 and Liu et al., 2008). The IFN family comprises the type-I IFN-α/β (Levy et al., 2011), type-II IFN-γ (Pestka et al., 2004) and type-III IFN-λ (Prokunina-Olsson et al., 2013; Kotenko., 2011). For the purposes of this section, the type-I IFN response will be focused on due to the fact that it is induced directly by viral infection and that RVFV NSs protein antagonizes the effect of type-I IFNs.

Invading genetic elements are recognized by pathogen recognition receptors (PRR) that survey the host cell for virus markers in the form of pathogen-associated molecular patterns (PAMP). As PRRs of the cytoplasm, the RNA helicase retinoic acid-inducible gene 1 (RIG-1) and melanoma differentiation-associated protein 5 (MDA5) react to infection by distinct sets of RNA viruses (Kato et al., 2006). RIG-1 and MDA5 primarily recognize short 5'-triphosphate dsRNA, or long dsRNA and its analogue polyinosinic:polycytidylic acid (poly (I:C), respectively (Yoneyama et al., 2015; Schlee., 2013; Pichlmair et al., 2009). The prototypical RIG-I possesses two N-terminal caspase recruitment domains (CARDs), a central helicase domain and C-terminal domain, and is kept in an auto-inhibited conformation by intramolecular interactions involving the CARDS and the helicase domain. Ligand binding by the helicase and C-terminal domains induces both ATP-dependent RIG-I oligomerization and a conformational switch, resulting in the exposure of the CARDs (Yoneyama et al., 2015; Sparrer and Gack., 2015). The latter then engage in K63-polyubiquitin-mediated homotypic CARD-CARD interactions with the adaptor mitochondrial antiviral signaling (MAVS), which in turn assembles prion-like fibrillary aggregates that are necessary for the recruitment of tumor necrosis factor (TNF) receptor associated factor (TRAF) 2, 5, and 6 for downstream signaling (Davis and Gack., 2015). The kinase TRAF family member-associated nuclear factor Kappa-light-chain-enhancer of activated B cell (NF-κB) activator (TANK)-binding kinase 1 (TBK1) and inhibitor of kappa B kinase epsilon (Ikκe) subsequently activate the transcription factor IFN regulatory factor 3 (IRF3) by

phosphorylation, followed by its dimerization and nuclear accumulation, where it induces the production of type-I IFN together with the transcription factors NF-κB and activator protein (AP-1) (Yoneyama et al., 2015).

Within the endosomal compartment, toll-like receptor 3 (TLR3) recognizes circular dsRNA and poly (I:C), and signals via the adaptor Toll-interleukin 1 receptor (TIR) domain-containing adapter-inducing IFN-β (TRIF) to activate IRF3, NF-κB, and AP-1, and consequently induces the production of type-I IFNs as well as inflammatory cytokines (Mogensen., 2009). Furthermore, recognition of ssRNA by TLR7/8 and subsequent signaling via the adaptor myeloid differentiation primary response gene 88 (MyD88) results in the secretion of IFN-α, particularly by specialized plasmacytoid dendritic cells (Goubau et al., 2013).

IFN-α/β bind to a common heterodimeric receptor, consisting of the subunit interferon-α/β receptor IFNAR1 and IFNAR2, on both infected and uninfected bystander cells. Signaling via the receptor-associated tyrosine kinase, Janus kinase 1 (JAK1) and tyrosine kinase 2 (TYK2) leads to phosphorylation of signal transducer and activator of transcription 1 (STAT1) and STAT2, which then undergo heterodimerization and translocation to the nucleus. There, in a complex with IRF9, they bind to IFN-stimulated response elements (ISRE) within ISG promoters, finally resulting in the transcription of ISGs (Schneider et al., 2014).

1.6.1.2 Activation of the interferon system by phleboviruses

Phleboviruses do not produce substantial amounts of dsRNA during infection (Zielecki et al., 2013; Weber et al., 2006). As shown for RVFV, their naked virion RNA is nonetheless a strong activator of RIG-I due to the presence of 5'-triphosphorylated dsRNA panhandle formed by the genome ends (Habjan et al., 2008a). Additionally, *in vivo*, the cytoplasmic RNA helicase/MAVS axis was demonstrated to be the primary IFN induction pathway for RVFV (Ermler et al., 2013). The *in vivo* role of the TLRs, by contrast, is less clear. While Ermler et al. found that neither the TLR7/8-MyD88 nor the TLR3-TRIF pathway play a significant role in RVFV IFN induction (Ermler et al., 2013), Gowen et al. showed for Punta Toro virus (PTV) that TLR3 was activated and contributed to increased liver damage and mortality (Gowen et al., 2006). It remains

to be investigated whether these discrepancies are due to different experimental conditions or a differential ability of distinct phleboviruses to activate or inhibit TLR3.

Studies in a range of animal models suggest a protective effect of type-I IFN in phleboviral infection. Treatment with synthetic type-I IFN inducers, such as poly (I:C) or polyinosinic-polycytidylic acid, poly-L-lysine and carboxymethylcellulose [poly(ICLC]) in a prophylactic or therapeutic regimen was reported to protect mice and hamsters from lethal RVFV infection (Peters et al., 1986). Similarly, administration of poly(I:C), poly(ICLC) or IFN itself protect against PTV-induced liver damage and mortality in a mouse model (Gowen et al., 2007; Sidwell et al., 1994; Sidwell et al., 1992) whereas treatment with IFN-neutralizing antibodies rendered otherwise resistant mice susceptible to PTV-associated death (Pifat and Smith, 1987). Several *in vivo* studies correlated the onset of type-I IFN synthesis with increased survival after lethal RVFV and PTV infection (Mendenhall et al., 2009; Bouloy et al., 2001). Thus, induction of type-I IFNs at an early point during infection is crucial for protective effects.

1.6.2 Interferon-stimulated genes and restriction factors

The Interferon-stimulated genes (ISGs) encode many proteins, but several have been identified as antiviral proteins known as restriction factors. Different viruses are targeted by distinct sets of ISGs (Schoggins et al., 2014; Schoggins et al., 2011). Mx proteins inhibit the replication of several phleboviruses, including RVFV (Schoggins et al., 2014). Human MxA proteins are large guanosine triphosphates (GTPases) functioning like membrane-associated dynamin-like proteins and have potent antiviral activity at the early stages of the viral life cycle (Haller and Kochs, 2002). It was shown that MxA sequesters RVFV N into large perinuclear complexes, thereby inhibiting primary and secondary transcription (Habjan et al., 2009b; Kochs et al., 2002). Replication of RVFV is also affected by IFITM2 and IFITM3, but not IFITM1, in accordance with their localization in the endocytic pathway and at the plasma membrane, respectively (Mudhasani et al., 2013). The PKR phosphorylates elongation initiation factor 2α (eIF2α), which leads to general down-regulation of translation (Williams, 1999). PKR is activated during phleboviral infection and can act as potent restriction factor targeted by different phleboviruses (Habjan et al., 2009a;

Ikegami et al., 2009). Furthermore, the 2'-5'-oligoadenylate synthase like 2 (OASL2) phosphorylates the 5' end at the 2' and 5' linked oligoadenylates known as 2-5A, which activates RNAse L causing degradation of both viral and host mRNA (Silverman., 1994). OASL2 and the ISG15 also influence the replication of RVFV (Atasheva et al., 2012; Pichlmair et al., 2011; do Valle et al., 2010).

1.7 RVFV virulence factors

1.7.1 RVFV NSs protein

Rift Valley fever virus have developed mechanisms to inhibit the IFN pathway. At the heart of these mechanisms are virulence factors that potently suppress IFN-β activation. The importance of virulence factors has been demonstrated in several *in vivo* studies. The NSs protein is an important virulence factor of RVFV (Vialat et al., 2000). The loss of NSs results in a highly attenuated virus, as observed by the naturally-attenuated isolate strain Clone 13 (C13), which has a large internal deletion of 549 nucleotides (from nucleotide 80 to 628) that removes 69% of the open reading frame but conserves in-frame the N and C termini (15N and 67-C terminal amino acids) of the predicted translation product. This deletion results in a NSs related peptide with 82 amino acids that conserves the 15N and 67-C terminal amino acids (Muller et al. 1995). The Clone 13 is used as a veterinary vaccine (von Teichman et al., 2011) and demonstrates the importance of the NSs protein in RVFV pathogenesis. NSs was identified as an IFN antagonist (Bouloy et al., 2001) and demonstrates several mechanisms such as suppression of host mRNA transcription, suppression of the IFN-β promoter (and other host genes) and the regulation of RVFV life cycle.

1.7.1.1 Suppression of host mRNA transcription

NSs can interfere with the antiviral defense through its ability to downregulate global host transcription (Billecocq et al., 2004). XPD, XPB, p62 and p44 are important factors of TFIIH (Reviewed by Zurita and Merino., 2003). NSs enters into the nucleus by sequestering p44 and then binds XPB through p44 (Le May et al., 2004), which are incorporated into the filamentous structures of NSs (Struthers et al., 1984). As p44 is used by XPD for nuclear entry, the presence of NSs results in the cytoplasmic accumulation of XPD. NSs can also downregulate the levels of TFIIH subunit p62

through proteasomal degradation (Kalveram et al., 2011). Sequestering components prevents the formation of new TFIIH complexes, while p62 degradation downregulates mature TFIIH and therefore, NSs inhibits the IFN pathway through active downregulation of host mRNA transcription (Billecocq et al., 2004). RVFV utilizes the C-termini part of the protein for the degradation of multiple host targets factors (Wuert et al., 2016). For example, two motifs sequences in the NSs gene that interacts with RVFV were identified: the proline-rich motif PXXP and the ΩXaV motif which interacts with p44 and p62 subunits of the TFIIH, respectively. These motifs are located within the last 17 amino acids of the C-termini (Cyr et al., 2015; Billecocq et al 2004; Le May et al., 2004).

1.7.1.2 Suppression of IFN-β promoter and other host genes

A more direct approach to the suppession of the IFN pathway is through NSs interaction with the IFN-β promoter. NSs interacts with Sin-3A associated protein (SAP30), which associates with the Sin3A/NCoR/HDAC repressor complex (Le May et al., 2008). NSs-SAP30 directs a repressor complex to Yin-Yang-1 (YY1) transcription factor (Huang et al., 2003), which is a known regulatory element of the IFN-β promoter (Klar and Bode., 2005). The targeting of a repressor complex by NSs to the IFN-β promoter prevents its activation. The deletion of NSs's SAP30 interaction domain attenuates the virulence of RVFV, stressing the importance of directed INF-β promoter repression (Le May et al., 2008).

Large scale ChIP-on-chip experiments showed that other gene targets could be suppressed by NSs (Benferhat et al., 2012). Factors involved in the JAK-STAT signaling pathway were identified for NSs-mediated downregulation such as Tyk2 and STAT2. STAT2-dependent stimulation of genes is enhanced by a mediator complex, Med14 (Lau et al., 2003), and was also a factor subject to NSs-mediated downregulation (Benferhat et al., 2012). Restriction factors from the OAS protein family would also be negatively affected by NSs, which will prevent the antiviral response through OAS-mediated activation of RNAse L (Silverman., 1994). Finally, NSs can dysregulate several factors in the coagulation cascade by interacting with genomic regulatory elements (Benferhat et al., 2012), which might explain features of severe RVFV cases such as the hemorrhagic pathology as a result of ineffective

clotting, as well as the presentation of disseminated intravascular coagulation (DIC) (reviewed in Ikegami and Makino, 2011). NSs can interact with DNA in regions outside of regulatory elements of genes that contribute to pathogenesis. NSs binds pericentromeric γ-satellites, which has been linked to chromosomal cohesion and segregation defects (Mansuroglu et al., 2010), and is possibly the cause of the high abortion rates in RVFV infections (Daubney et al., 1931).

1.7.1.3 PKR degradation

The RNA-dependent protein kinase R (PKR) is one of the host's pattern recognition receptors (PRR) and is a key component of the innate immune system (Dzananovic et al., 2018). RVFV can prevent detection of its viral RNA and subsequent viral replication restriction through its interaction with the RNA-dependent protein serine/threonine kinase (PKR). NSs can also downregulate PKR through proteasomal degradation (Habjan et al., 2009a). NSs binds PKR and this interaction is essential for NSs-mediated PKR degradation (Kalveram et al., 2013). Furthermore, NSs can prevent eIF2α phosphorylation through PKR downregulation (Ikegami et al., 2009) and would hinder eIF2α suppression of host translation, which could inhibit viral protein synthesis.

1.8 Animal models for Rift Valley fever virus

Experiments performed to determine the host range of RVFV showed that mice, rats, and hamsters were highly susceptible. Since then, mice and rats have been the main platform to conduct RVFV pathogenicity and vaccine efficacy studies, while RVF in livestock has mostly been characterized during outbreaks with some laboratory-based experimental vaccination studies in goat and sheep (Kortekaas et al., 2013). Non-ruminants such as birds, horses, rabbits, and pigs were resistant to RVFV (Findlay, 1932). RVFV also causes diseases in other animals including goats, cattle, camels, dogs, cats, and ferrets (Shimshoni and Barzilai, 1983; reviewed in Peters and Slone, 1982;). Few studies have been conducted in non-human primate models (Morril et al., 1989).

1.8.1 Mice

Mice are one of the most widely used animal models to study RVFV pathogenesis and vaccines because they are highly susceptible, cost-effective, and the pathology in infected mice mimics the disease seen in humans and newborn lambs. Mice show severe clinical signs by 2-3 d.p.i. characterized by ruffled fur, hunched posture and lethargy, and usually succumb to fulminant hepatitis in 2-5 days post infection (p.i.) (Smith et al., 2010; Vialat et al., 2000; Bouloy et al., 2001). Occasionally, some mice that survive this stage have hind limb paralysis and succumb to encephalitis on day 8-14 d.p.i. (Gray et al., 2012; Smith et al., 2010). Clinical disease onset is correlated with viral titers in the serum, liver, and spleen and a significant decrease in blood platelets indicative of hemorrhagic disease (Gray et al., 2012; Smith et al., 2010). Despite decreases in blood platelets, mice do not exhibit extreme hemorrhagic manifestations (Ikegami and Makino 2011). The rectal temperature of infected mice is often normal or decreased to below normal (Mims et al., 1956). Furthermore, mice infected with wild type RVFV show temporal increases in pro-inflammatory cytokines that is thought to contribute to disease severity (Gray et al., 2012). In addition to viral determinants of disease, host factors are thought to play a role in influencing disease severity, especially those genes involved in regulating the activation of the Type I IFN pathway (do Vale et al., 2010).

1.8.2 Rats

Unlike mice, the susceptibility of rats to RVFV differs among rat strains (Findlay and Howard, 1952). Symptoms in susceptible strains such as Wistar-Furth are characterized by fatal hepatic disease and death as early as two days, while the more resistant Lewis strain has a significantly higher survival rate but can be more susceptible to encephalitis at later time points (Anderson and Slone, 1987). However, like mice, rats do not develop hemorrhagic manifestations in response to RVFV infection (Ikegami and Makino 2011).

1.8.3 Ruminants

Ruminants are the most applicable model for studying RVFV pathogenesis and vaccines as they are the natural host of RVFV. However, lack of large animal biocontainment facilities can limit their use in research. Despite this, RVFV infection in sheep has been studied (reviewed in Ikegami and Makino, 2011). Neonatal and newborn lambs are most susceptible to RVFV infection as demonstrated by so-called “abortion storms”, in which rapid virus transmission induces widespread abortions in herds of pregnant sheep causing up to 100% neonatal mortality (Munyua et al., 2010; Bird et al., 2008). Although RVF in neonatal and young lambs is nearly uniformly fatal, adult sheep are differentially susceptible depending on RVFV strain and sheep breed (Daubney, 1931). Other ruminants such as goats and camels are less susceptible to RVFV, though experimental and observational data show cattle can develop severe clinical disease characterized by febrile illness and high fetal mortality (Morril et al., 1997; Findlay, 1932). Interestingly, the gradual replacement of native more resistant livestock (such as Zebu cattle) with more susceptible European breeds are thought to increase RVFV outbreakes in Africa (Munyua et al., 2010).

1.8.4 Non-human primates

Although most nonhuman primates show mild clinical RVF, Rhesus macaques best demonstrate the range of symptoms seen in humans (Ross et al., 2012). In macaques infected intravascularly, symptoms range from mild febrile illness to severe disease characterized by anorexia, lassitude, vomiting and hemorrhagic manifestations (Ross et al., 2012). However, newer models need to be developed that mimic the natural extravascular inoculation route of RVFV by mosquitoes (Turrel et al., 1992) that contribute to the increase of RVFV outbreaks throughout Africa (Munyua, et al., 2010; Bird et al., 2007).

1.9 Thesis objectives

The NSs protein is the major virulence factor of RVFV that inhibits host innate antiviral defense mechanisms. Deletion of the NSs gene results in attenuation of RVFV, but less is known about the exact role of specific amino acid residues within the protein. The RVFV NSs gene encodes five conserved cysteine residues at positions 39, 40, 150, 179 and 195 (Aitken, 2008; Sall et al.,1997). These residues are conserved in all isolates of RVFV except the attenuated Clone 13, which contains a deletion of 69% of the NSs gene that includes these cysteines.

The objectives of this thesis are as follows:

1.9.1 General objective:

Investigate the effect of NSs conserved cysteine substitutions on RVFV virulence in a mouse model.

1.9.2 Specific objectives:

1. Perform cysteine-to-serine point mutations in the NSs gene of the wild type RVFV isolate SA35/74 at position 39 and 40, 149, 179 and 194.
2. Rescue recombinant wild type RVFV SA35/74 and the generated mutants from transcription cDNA plasmids (pUC57-L, -M and -S) making use of the T-7 based reverse genetics system.
3. Study the growth kinetics of the rescued viruses in interferon-competent and interferon-deficient cell lines.
4. Study the effect of the NSs mutations on the biology of RVFV by analyzing the effect on degradation of some important host proteins such as protein kinase R; the subunit p62 of the transcription factor TFIIH, and the subcellular localization of the NSs protein.
5. Analyze the pathogenesis of the individual mutations in the mouse model by comparing virological parameters, viral loads, histopathology, immunohistochemistry.
6. Analyze the cytokine gene expression profiles in the liver and spleen of mice infected with the wilt type RVFV SA35/74 and the NSs mutant viruses.

1.10 Hypothesis

Null hypothesis: Conserved cysteine residues in the NSs gene are not essential for the structure and function of the protein, thus they do not play a role in virulence.

Alternative hypothesis: Conserved cysteine residues in the NSs gene are essential for the structure and function of the NSs protein and substitution of these with serine residues will result in decreased virulence.

CHAPTER 2

2 Materials and methods

2.1 Ethics statement

This work was done in agreement with the South African National Standards for the Care and Use of Animals for Scientific Purposes (SANS 10386:2008), under permission to do research in terms of Section 20 of the Animal Disease Act issued by the Department of Agriculture, Forestry and Fisheries of the Republic of South Africa (permission no. 12/11/1/1/13), and under the provisions of the South African Genetically Modified Organisms Act No. 15 of 1997 (facility registration no. 39.2/NICD/NHLS-15/115), see Appendix 4. The procedures for inoculation of mice with RVFV and corresponding mutants were approved by the Animal Ethics Committees of the University of Pretoria and the National Health Laboratory Service (clearance certificate no V013-14 and 142/14, respectively), see Appendix 4. Blood was collected under anesthesia, and tissues were taken from exsanguinated animals as previously described (Jansen van Vuren et al., 2011).

2.2 Experimental animals

All work with infectious RVFV and inoculated animals was conducted in Biosafety Level 3 (BSL3) animal facilities at the Centre for Emerging Zoonotic and Parasitic Diseases (CEZPD), National Institute for Communicable Diseases, a division of the National Health Laboratory Service (NICD-NHLS), Sandringham, South Africa. Personal protective equipment (PPE), including a powered air purifying respirator, a Tyvek® suit, rubber boots and a double pair of gloves was used by all laboratory workers involved in the animal experiments. BALB/c mice were obtained from the South African Vaccine Producers, Sandringham, South Africa. Mice were kept in isolation cages (IVC-Bio. A.S. Vent light, EHRET), each containing 3 animals, and provided food (Epol mice cubes) and water *ad libitum*.

2.3 Viruses

The wtRVFV 35/74 was isolated during the 1974 RVF outbreak in South Africa (Woods et al., 2002). The genome sequence of this isolate was used as the backbone for the generation of plasmids pUC57-L, M and S (Kortekaas et al., 2011). These plasmids were kindly provided by Prof. Jeroen Kortekaas from the Wageningen Bioveterinary Research, Lelystad, the Netherlands, and generated as described in Kortekaas et al., 2011. The virus was isolated as described previously (Barnard et al., 1979). Briefly, the RVFV strain 35/74 was isolated from a liver of a sheep that died during the outbreak of RVFV in the Free State province of South Africa in 1974. The virus was passaged four times in mouse brain and three times in BHK-21 cells. This RVFV isolate is a virulent strain and have been used in some *in vitro* and *in vivo* studies in lambs (Wichgers Schreur et al., 2016, Oreshkiva et al., 2013).

The NSs mutants of pUC57-S used in this study were generated using the quick change II XL Site-Directed Mutagenesis Kit (Agilent Technologies, Santa Clara, USA), according to the manufacturer's instructions. Forward and reverse PCR primers to mutate the five cysteine residues at positions 39, 40, 149, 178 and 194 of the NSs protein, were designed using the web based QuickChange primer design program available online (www.agilent.com/genomics/qcpd). To induce changes in the coding region, two complimentary oligonucleotides containing the nucleotide mutations of interest, flanked by unmodified nucleotide sequences, were designed.

2.4 Cell lines

Five cell lines were used for different purposes during the experiments; a cell line of green monkey kidney cells (Vero, CCl008); baby hamster kidneys cells (BHK-21 clones 13 and clone BSR-T7/5); fibrosarcoma cells (QM5 cells) and a diploid human cell line [(Medical Research Council cell strain 5 (MRC-5)]. The cells were maintained in specific culture media, including Eagle's Minimum Essential Medium, (EMEM) (Lonza, Basel, Switzerland), Minimal Essential Medium, MEM-Earle's medium 32360034 (Gibco, Gaithersburg, USA) containing L-glutamine BE17-605E (Lonza, Basel, Switzerland), MEM eagle Non-Essential Amino Acids 11140-035 (Gibco, Gaithersburg, USA), Dulbecco's minimum essential medium (DMEM) (Gibco, Gaithersburg, USA) and Waymouth medium MB 752/1 (CE) (Thermo Fisher Scientific,

Waltham, USA). All cell media were supplemented with antibiotics (Penicillin-Streptomycin-Amphotericin B mixture 17-745E (Lonza, Basel, Switzerland) and 10% heat-inactivated fetal bovine serum (FBS) (Hyclone®, Thermo Scientific, Waltham, USA). The cells were cultured at 37ºC with 5% CO_2 in 75 cm^2 tissue culture flasks (Nunc™ EasYFlask™, Thermo Fisher Scientific, Waltham, USA) and passaged when the cell monolayer reached 90-100% confluency.

Culture of Vero cells Clone 1008

A cell line of green monkey kidney cells (Vero) clone 1008 was obtained from the CEZPD, NICD-NHLS) and maintained in a monolayer at 37ºC in 75 cm^2 tissue culture flasks (Nunc™ EasYFlask™, Thermo Fisher Scientific, Waltham, USA) with Minimal Essential Medium, MEM-Earle's medium (Gibco 32360034) containing L-glutamine (Lonza BE17-605E), MEM eagle' Non-Essential Amino Acids (NEAA, Gibco 11140-035) and supplemented with antibiotics/antimycotics (Penicillin-Streptomycin-Amphotericin B mixture (Lonza 17-745E) and 10% heat-inactivated fetal bovine serum (FBS) (Hyclone® thermo Scientific, USA). Confluent Vero cell monolayers were trypsinized and subcultured weekly. Briefly, the media was removed and the cell monolayer rinsed twice with sterile Phosphate buffered saline (1x PBS) free of Ca++ and Mg++ (Lonza, Basel, Switzerland). Trypsin- EDTA (ethylenediaminetetraacetic acid) solution at the concentration of 0.25% trypsin and 0.05% EDTA respectively was then added, and the flask incubated at 37ºC for 5 minutes. When the cells started dislodging, 10mL of MEM was added to trypsinized cells and the mixture aspirated with a sterile syringe and needle to ensure complete dislodgement and thorough mixing of the media and the cells. Subsequently, a 2mL aliquot of cell suspension was transferred into a flask containing 18mL of MEM and 10% of FBS and incubated at 37ºC in a CO_2 incubator. When the cell monolayer reached 90-100% confluency, the flasks were incubated at 28ºC or used immediately for titration of RVFV.

Culture of BHK-21 clone 13

A cell line of Baby hamster kidney cells (BHK-21), clone 13 were obtained from the (CEZPD, NICD-NHLS) and maintained in a monolayer at 37ºC in 75cm^2 tissue culture flasks supplemented with Minimal Essential Medium, MEM-Earle's medium (Gibco 32360034) containing L-glutamine (Lonza BE17-605E), MEM eagle Non-Essential

Amino Acids (NEAA, Gibco 11140-035), antibiotics, Penicillin-Streptomycin-Amphotericin B mixture (Lonza 17-745E) and 10% heat-inactivated FBS. Confluent BHK-21 cell monolayers were trypsinised and subcultured weekly. When the cell monolayer reached 90-100% confluency, the cells were subcultured into new flasks, as described for Vero cells, or used immediately for RVFV amplification.

Culture of BHK-21 clone BSR-T7/5 cells

A cell line of Baby hamster kidney cells (BHK-21), clone BSR-T7/5, which constitutively expresses the T7 RNA polymerase, were provided by Dr. Ursula Buchholz from the National Institute of Health (NIH, USA), and maintained in a monolayer at 37^{o}C in 75cm^{2} tissue culture flasks supplemented with Dulbecco's minimum essential medium (DMEM) (Gibco), antibiotics/antimycotics (Penicillin-Streptomycin-Amphotericin B mixture (Lonza 17-745E) plus 10% FBS (Hyclone® Thermo Scientific, USA). Confluent BSR-T7/5 cell monolayers were trypsinized as described above for the subculturing of Vero cells. A ratio of 1:8 to 1:12 was used for subculturing. When the cell monolayer reached 90-100% confluency, cells were split to new flasks or used immediately for transfections. At every second passage, 5% geneticin (Gibco 10131), was added to the culture as selective antibiotic.

Culture of QM5 cells

A cell line of fibrosarcoma Qm5 cells was obtained from (CEZPD, NICD-NHLS) and maintained in a monolayer at 37^{o}C in 75cm^{2} tissue culture flasks supplemented with Waymouth medium MB 752/1 (CE) (Gibco), antibiotics/antimycotics (Penicillin-Streptomycin-Amphotericin B mixture) (Lonza 17-745E) and 5% FBS (Hyclone™ Thermo Scientific, USA). QM5 monolayers were trypsinized and subcultured weekly. When the cell monolayer reached 90-100% confluency, the cells were subcultured into new flasks or used immediately for passage and for titration of the recombinant Fowl pox T7 virus.

Culture of MRC-5 cells

A cell line of MRC-5 (Medical Research Council cell strain 5), a diploid human cell culture line composed of fibroblasts, was obtained from Cellonex™, Maharashtra, India. The cells were revived from frozen cultures by thawing the plastic cryovials quickly for 1 minute in a 37^{o}C water bath. The thawed cells were transferred to a 25cm^{2} cell culture flask containing reviving media (DMEM supplemented with 20% FBS) and incubated overnight at 37^{o}C in a CO_2 incubator. The following day, the media was removed, the attached cells washed with PBS and the media replaced by the culture media (DMEM supplemented with antibiotics/antimycotics (Penicillin-Streptomycin-Amphotericin B mixture) (Lonza17-745E) and 10% heat-inactivated FBS (Hyclone™ thermo Scientific, USA)). When the monolayer reached 90-100% confluency, the cells were subcultured to a 75cm^{2} at a 1:3 ratio.

2.5 Mutagenesis of the five cysteine residues of the NSs protein

The mutations in the NSs gene of RVFV were introduced using the quick change II XL Site-Directed Mutagenesis Kit (Agilent Technologies, Santa Clara, USA), according to the manufacturer's instructions. Briefly, mutagenesis was performed in 3 steps: a) synthesis of the mutant strand, b) digestion of the parental supercoiled DNA with *Dpn*I, resulting in mutated DNA, and c) transformation of the mutated plasmid molecule into competent cells. Forward and reverse primers targeting the five cysteine residues at positions 39, 40, 149, 178 and 194 of the NSs protein coding region were designed using the web-based Quick-change primer design program available online at www.agilent.com/genomics/qcpd. Four cysteine-to-serine mutations were generated. Due to the fact that cysteines 39 and 40 are adjacent, a double mutant with substitutions at serines 39 and 40 and three single mutants with substitutions at positions 149, 178 and 194 were generated (Figure and table 2.1). The recombinant RVFV SA35/74, with the GenBank accession numbers JF784386, JF784387 and JF784388 for the L, M and S segments, respectively, was used as template. The two complimentary oligonucleotides containing the desired mutation (cysteine-to-serine substitutions), flanked by unmodified nucleotide sequence were synthesized (Inqaba Biotech, Pretoria, South Africa). The PCR amplification was done using the cycling conditions shown in Table 2.4.

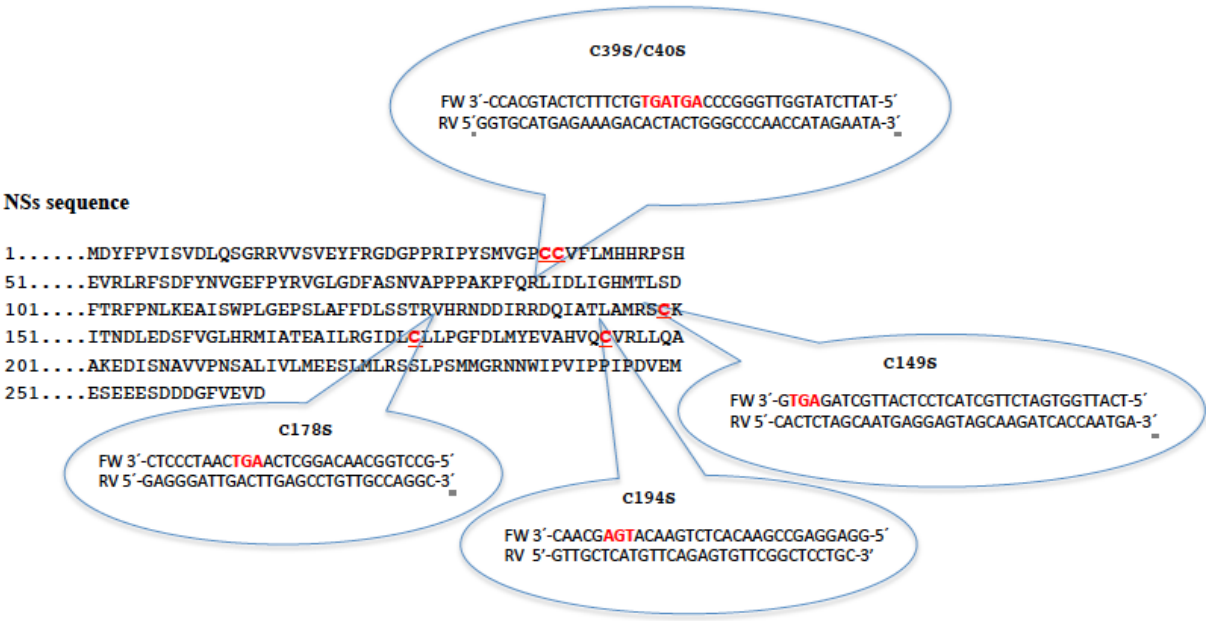

Figure 2.1. Diagram representing the primers and the position of the cysteine-to-serine mutation in the NSs gene of RVFV isolate SA35/74.

Table 2.1.Primers used for the generation of the mutant NSs viruses.

Mutants	Primer	SEQUENCE
C39S/ C40S	Fw #1	5'TATTCTATGGTTGGGCCCAGTAGTGTCTTTCTCATGCACC-3'
	Rv #1	5'GGTGCATGAGAAAGACACTACTGGGCCCAACCATAGAATA-3
C149S	Fw #2	5'TCATTGGTGATCTTGCTACTCCTCATTGCTAGAGTG- 3'
	Rv #2	5'CACTCTAGCAATGAGGAGTAGCAAGATCACCAATGA- 3'
C178S	Fw #3	5'-GCCTGGCAACAGGCTCAAGTCAATCCCTC-3'
	Rv #3	5'-GAGGGATTGACTTGAGCCTGTTGCCAGGC-3'
C194S	Fw #4	5'-GCAGGAGCCGAACACTCTGAACATGAGCAAC-3'
	Rv #4	5'-GTTGCTCATGTTCAGAGTGTTCGGCTCCTGC-3'

2.5.1 Extraction of the DNA Plasmid pUC57

For generation of the mutant strand, a pUC57 DNA plasmid containing the S segment of the isolate SA35/74 of RVFV was used as template. The plasmid was isolated from *E.coli* strain JM109, containing a resistance gene to counteract ampicillin.

2.5.1.1 Transformation of JM 109 *E. coli* bacteria

Competent JM 109 *E. coli* cells where prepared using the Mix & Go *E. coli* Transformation Kit (Zymo Research Corp, USA). Cells were grown to a cell count OD (600 nm) reading of between 0.4 and 0.6 in Luria Bertani (LB) broth medium. Fifty milliliters (50mL) of cells were collected by centrifugation at 250 rpm for 10 min at 4ºC and the pellet gently resuspended in 5mL of ice-cold wash buffer. Cells were collected by centrifugation at 250 rpm for 10 min, resuspended in 5mL ice-cold transformation buffer and dispensed into 100µl aliquots. The competent cells JM109 were stored at -70ºC. Each aliquot of competent JM109 cells was thawed on ice and 1 to 5µl of plasmid DNA was added and mixed gently for a few seconds. 50 to 100µl of the ligation mix was spread onto a pre-warmed (37°C) LB agar plate (LB with 12% bacterial agar containing 1mg/mL ampicillin).

2.5.1.2 MidiPrep plasmid purification

Midiprep plasmid DNA was extracted using the Qiagen Plasmid Midi Kit (Qiagen, Hilden, Germany). One hundred milliliters (100 mL) of LB broth was inoculated with a plate stock of the desired clone and incubated at 37ºC overnight in a shaking incubator at 250 rpm. Fifty milliliters of culture was centrifuged at 3200 x g for 25 min and the pellets were resuspended in 6mL of P1 suspension buffer. After resuspension, 6mL of P2 lysis buffer was added and incubated for 5 min at room temperature. The reaction was neutralized by adding 6mL of P3 neutralization buffer and left on ice for 5 min. The lysate was then centrifuged at 3200 x g for 25 min at 4ºC and the supernatant was transferred to a High Speed™ midi column. Prior to the addition of the supernatant, the High Speed™ column was equilibrated by applying 4mL of QBT buffer [750mM NaCl, 50 mM MOPS, (pH7.0), 15% ISOH, 15% Triton® X100]. Once the supernatant had flown through, the column was washed twice with 20ml of QC Buffer [1 M NaCl, 50 mM MOPS, (pH 7.0), 15% ISOH). The plasmid DNA was eluted with 5 mL of QF Buffer [1.25 M NaCl, 50 mM Tris-HCl, (pH 7.0), 15% ISOH] and precipitated with 3.5mL of ISOH at -80ºC for 1h. The DNA was pelleted by centrifugation at 3200 x g for 90 min at 4ºC. Two milliliters of 70% ethanol was added to the pellet and centrifuged at 3200 x g for 5 min at 4ºC. The pellet was air-dried and

resuspended in 200µl of sterile nuclease-free water. The concentration of plasmid was determined by a spectrophotometer (Nanodrop ND-1000, Thermo Fisher Scientific, Waltham, USA) at the absorbance of 260/280nm.

2.6 Synthesis of the mutant strand

The mutated strand was synthesized by replacing the wt S gene from the puC57 plasmid with the mutated S gene, making use of the quick change II XL Site-Directed Mutagenesis kit (Agilent Technologies, Santa Clara, USA). The sample reaction was set up using 10ng of the plasmid DNA and 1µl (2.5 U/ µl) of the Pfu Ultra HF DNA polymerase according to the manufacturer's instructions Four amplification reactions were performed using DNA primers targeting the mutation at positions 39/40, 149, 179 and 194. The QuickChange II XL Site-Directed Mutagenesis Kit included a control reaction consisting of 10ng of the pWhitescript 4.5-kb control plasmid. The sample reaction and PCR cycling parameters are shown in Table 2.2, 2.3 and 2.4, respectively.

Table 2.2. Sample reaction used for the mutant strand synthesis. For the control reaction, the pWhitescript 4.5-kb DNA template (provided by the kit) was used.

Reagent	**µl per 1 reaction**	**concentration stock solution**	**Final concentration**
Reaction buffer	5	10x	1x
dsDNA template (S segment From SA35/75)	1.5	(5 7.3ng/µl)	10ng
T115a primer #1	1	(100 ng/µl)]	125ng
T115b primer #2	1	(100 ng/µl)]	125 ng
[a]dNTP mix	1		
[a]QuikSolution reagent	3		
ddH2O	36.5		
***PfuUltra* HF DNA polymerase**	1	(2.5 U/µl)	2.5U
Total volume	50		

[a] The dNTP mix and the QuickSolution reagent were provided with the kit ready to use.

No concentrations were provided.

Table 2.3. Control reaction. The plasmid pWhitescript 4.5-kb DNA template (provided with the kit) was used as control along with 2 primers to amplify the gene of interest.

Reagent	**µl per 1 reaction**	**concentration stock solution**	**Final concentration**
Reaction buffer	5	10x	1x
pWhitescript 4.5-kb control plasmid (5 ng/ul)	2	(5ng/ µl)	10ng
Oligonucleotide control primer #1	1.25	(100 ng/µl)]	125ng
Oligonucleotide control primer #2	1.25	(100 ng/µl)]	125 ng
adNTP mix	1		
aQuikSolution reagent	3		
ddH2O	3.5		
PfuUltra HF DNA polymerase	1	(2.5 U/µl)	2.5U
Total volume	50		

[a] The dNTP mix and the QuickSolution reagent were provided with the kit ready to use.

No concentrations were provided.

Table 2.4. Thermal cycling parameters used for the four NSs mutant strand synthesis reactions.

Cycles	Temperature	Time
1	95°C	1 minute
18	95°C	50 seconds
	60°C	50 seconds
	68°C	2.42 minutes (Puc57=2,71kb)
1	68°C	7 minutes

2.6.1 Digestion of the parental supercoiled plasmid DNA

Following the PCR amplification, 1µl of the *Dpn*I restriction enzyme (10U/µl) (Agilent Technologies, Santa Clara, USA) was added to each 50µl amplification reaction and incubated for 1 hour at 37ºC for digestion of the parental (non-mutated) supercoiled plasmid DNA. The reaction was stopped by removing the tubes from the incubator.

2.6.2 Transformation of the mutated plasmid in ultracompetent cells

The XL10-Gold ultracompetent cells provided with the kit were gently thawed on ice. For each control and sample reaction to be transformed, 45 µl of the ultracompetent cells where aliquoted to a prechilled 14-mL BD Falcon polypropylene round-bottom tube (Thermo Fisher Scientific, Waltham, USA). A 2 µl aliquot of β-Mercaptoethanol (β-ME) mix (provided with the kit) was added to a 45 µl volume of cells, and the contents of the tube swirled gently. The mixture was incubated on ice. After 10 minutes, 2 µl of the DpnI-treated DNA from each control and sample reaction was added to separate aliquots of the ultracompetent cells. As an optional control, the transformation efficiency of the XL10-Gold ultracompetent cells was verified by adding 1 µl of 0.01 ng/µl pUC18 control plasmid (the control provided was diluted 1:10 in high-quality water) to another 45µl aliquot of cells. The transformation reactions were swirled gently to mix and incubated on ice for 30 minutes.

The tubes containing the transformation reactions were placed in a 42°C water bath for 30 seconds and incubated on ice for 2 minutes. A volume of 0.5 mL of preheated (42°C) NZY+ broth was added to each tube. The NZY+ was provided with the kit and

composed of NZ amine (casein hydrolysate), yeast extract, deionized H2O and adjusted to pH 7.5 using NaOH. Prior to use it was supplemented with MgCl2, MgSO4 and glucose. The tubes were incubated at 37°C for 1 hour with shaking at 225–250 rpm.

For the mutagenesis and transformation controls, 250 µl of each transformation reaction was then plated on LB–ampicillin agar plates and incubated at 37°C overnight. For the control transformation, 80 µg/mL X-gal and 20 mM IPTG (Promega Corporation, Madison, USA) was added to the LB-ampicilin agar plates for blue-white colony screening. While the pWhitescript 4.5-kb control plasmid was used to test the efficiency of mutant plasmid generation, the pUC18 was used to test the efficiency of transformation of XL10-gold ultracompetent cells with the generated plasmids. The pWhitescript 4.5-kb control plasmid contains a stop codon (TAA) at the position where a glutamine codon (CAA) would normally appear in the B-galactosidase gene of the pBluescript II SK(–) phagemid (corresponding to amino acid 9 of the protein). The XL10-Gold ultracompetent cells transformed with this control plasmid appear white on LB–ampicillin agar plates containing IPTG and X-gal, because β-galactosidase activity has been obliterated. In this case, the oligonucleotide control primers create a point mutation that reverts the T residue of the stop codon (TAA) in the β galactosidase gene encoded on the pWhitescript 4.5-kb control template to a C residue to produce a glutamine codon (Gln, CAA). Following transformation, colonies can be screened for β-galactosidase production (β-gal+) by virtue of a blue colony phenotype. If transformation of the pUC18 control plasmid was performed, more than 98% of the colonies must have the blue phenotype. For better results, when transformation is efficient, greater than 98% of the colonies must have the blue phenotype.

Table 2.4. Transformation reactions. Reagents used per reaction in the transformation of *DpnI*–treated DNA in XL-10 Gold ultracompetent cells.

Reactions	***DpnI*-treated DNA**	**XL-10 Gold ultracompetent cells**	**β-Mercaptoethanol**	**X-gal and IPTG added to the control LB-ampicilin agar plates (for blue-white col screening)**
RVFV S-C39S/C40S	2 µl	45µl	2 µl	-
RVFV S-C149S	2 µl	45µl	2 µl	-
RVFV S-C178S	2 µl	45µl	2 µl	-
RVFV S-C194S	2 µl	45µl	2 µl	-
***pUC18**	2 µl	45µl	2 µl	80 µg/mL X-gal and 20 mM IPTG

* Control plasmid provided with the kit

2.6.3 Extraction of mutated plasmids

A single colony was picked and inoculated into LB-ampicillin medium and incubated overnight with shaking at 250 rpm. The following day, the plasmid was extracted using the EndoFree® plasmid maxi kit (Qiagen, Hilden, Germany). The OD of the plasmid was measured using a spectrophotometer (Nanodrop ND-1000, Thermo Fisher Scientific, Waltham, USA). Subsequently, the plasmid was gel-purified using the Wizard® SV gel and PCR Clean-Up System (Promega, Madison, USA). To verify that selected clones contain the desired mutation, the purified plasmid preparations were sent for full DNA sequencing at the National Institute for Communicable Diseases (NICD) sequencing core facility according to the methodology described in section 2.5.5.

2.6.4 Viruses rescue

The wtRVFV SA35/74, RVFV NSs mutants C39S/C40S, C149S, C178S and C194S were rescued making use of transfection in mammalian cells. Briefly, semi-confluent monolayers of BSR-T7/5 cells were prepared in six-well plates (Nunc™ Thermo Fisher Scientific, Waltham, USA). For each transfection reaction, BSR-T7/5 cell monolayers in 75 cm^2 flasks were trypsinized (trypsin-EDTA) and DMEM (containing Penicillin-

Streptomycin-Amphotericin B mixture) added to seed 2x6 well plates with 2 mL per well of the cell suspension (500,000 cells/well in 2mL). Cells were incubated at 37°C in a 5% CO_2 environment for 24 hours. Five of the six well plates were then inoculated with 10^5 $TCID_{50}$ (50% tissue culture infective dose) of recombinant fowlpox-T7 virus (Das et al., 2000; Britton et al., 1996) and incubated for 1h. Subsequently, supernatant of all wells were removed and 2 mL of fresh DMEM supplemented with 2% FBS was added. The cells were subsequently transfected with the plasmids pUC57-L, pUC57-M and pUC57-S to rescue wild type SA35/74, or with the modified plasmids containing the point mutations in the NSs gene **(**C39S/C40S, C149S, C178S and C194S) (Figure 2.2 and 2.3). For each DNA plasmid, 1000ng per reaction were mixed with 150 mM NaCl in cryotubes. An equal amount of the DNA transfection reagent, JetPEI® (Polyplus, IIIkirck, France) was added to the DNA mixture, mixed gently and incubated at room temperature. After 15 – 30 minutes, 200 µl per well of the JetPEI--DNA mixture was added dropwise to the correspondent well, and plates incubated at 37°C, 5% CO_2 for 7 days. 1 mL supernatant was collected on day 4 and the remaining 1mL on day 7. Aliquots were stored in properly labeled cryotubes at -70°C. The recombinant viruses were propagated in BHK-21 cells [C13] (ATCC® CCL-10™).

Plate 1

FP-T7 35/74 S39/40 35/74 M Jetpei 35/74 L	FP-T7 35/74 S39/40 35/74 M Jetpei 35/74 L	Cell control (FP-T7 infected)
FP-T7 35/74 S149 35/74 M Jetpei 35/74 L	FP-T7 35/74 S149 35/74 M Jetpei 35/74 L	Cell control (no treatment)

Plate 2

FP-T7 35/74 S178 35/74 M Jetpei 35/74 L	FP-T7 35/74 S178 35/74 M Jetpei 35/74 L	Cell control (FP-T7 infected)
FP-T7 35/74 S194 35/74 M Jetpei 35/74 L	FP-T7 35/74 S194 35/74 M Jetpei 35/74 L	Cell control (no treatment)

Figure 2.2 Transfection plates layout. Two six-well plates were seeded with 2mL per well of the BSR-T7/5 cell suspension (500 000 cells/well in 2mL) the day before transfection. The wtRVFV 35/74 was used as backbone for the generation of the NSs plasmids and each well in duplicate was then transfected with 200µl of DNA plasmid-Jetpei mix accordingly. The reaction was incubated at 37°C, 5% CO_2 for 4-7 days.

2.6.4.1 Propagation of recombinant rescued viruses

Monolayers of BHK-21 cells in 25 cm^2 tissue flasks were infected with 1:10 dilution of supernatants from transfected cells and maintained in Eagle's minimum essential medium (EMEM) containing L-glutamine, non-essential amino acids and antibiotics (100IU penicillin, 100µg streptomycin and 0.25µg amphotericin B). The presence of virus was confirmed by microscopic observation of cytopathic effect (CPE) followed by standard microtitration ($TCID_{50}$) in Vero cells Cl008 (ATCC® CRL-1586™). Briefly, the supernatants from transfected cells were diluted 1:10 in EMEM containing L-glutamine, non-essential amino acids and antibiotics (100IU penicillin, 100µg streptomycin and 0.25µg amphotericin B). Four replicates of 100µl volumes of each

dilution (ranging from 10^{-1} – 10^{-12}) were transferred into flat bottom 96-well cell culture microplates (Nunc, Roskilde, Denmark). Equal volumes of Vero cell suspension in EMEM containing 4% fetal bovine serum (FBS) were then added. Microplates were incubated at 37ºC in a CO_2 incubator and observed microscopically for CPE up to 7 days post inoculation. On day 7, virus titers were calculated according to the Spearman-Kärber method (Kärber, 1931), expressed in $TCID_{50}$/mL and converted to PFU/mL (PFU/mL=0.7*$TCID_{50}$).

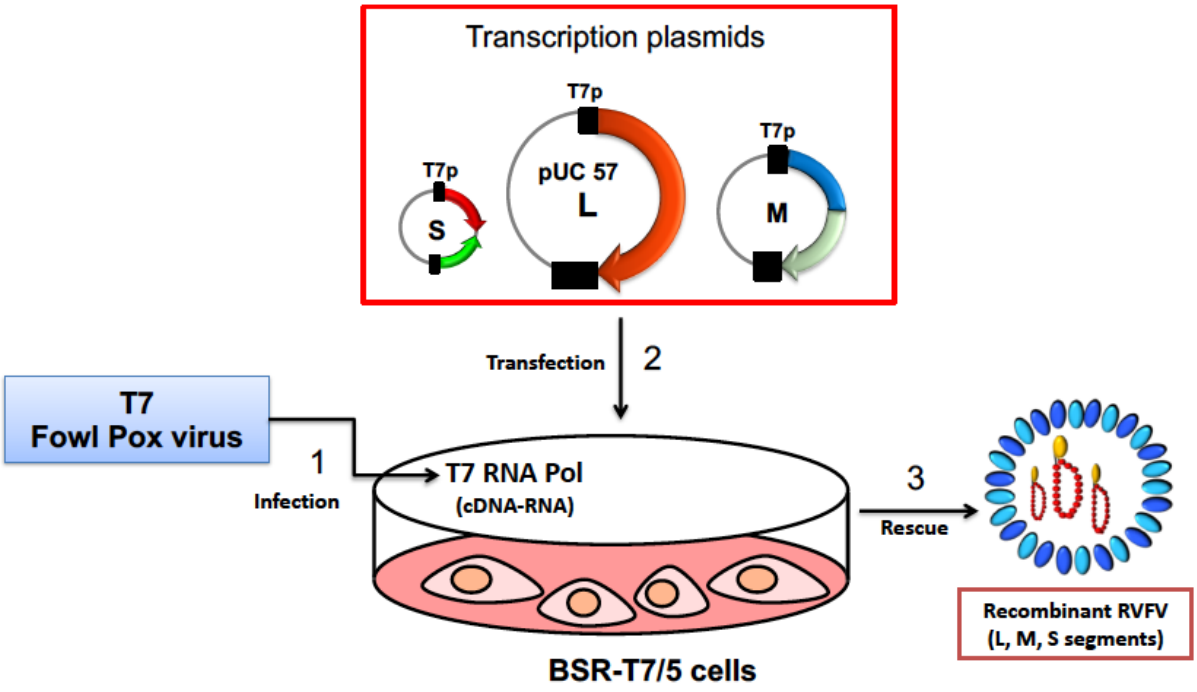

Figure 2.3 Representation of the rescue of RVFV from transcription plasmids using a three plasmid reverse genetics system. BHK-21 cells (clone BSR-T7/5) were infected with recombinant fowlpox T7 (step 1) and subsequently transfected with plasmid pUC57 encoding RVFV S, M and L segments. After four days, the culture media was collected (step 3). Transcription from the plasmids is controlled by the T7 promoter (T7p). Untranslated regions are depicted as black boxes (adapted from Kortekaas et al., 2011).

2.6.5 Sequencing analysis of the rescued viruses

RNA was extracted from supernatants of passage 2 (BHK-21) cultures infected with NSs mutants (C39S/C40S, C149S, C178S and C194S) using the QIAamp viral RNA kit (Qiagen, Hilden, Germany) according to manufacturer's instructions. RT-PCR primers designed by Bird et al., 2007a and the transcription one-step RT-PCR kit (Roche, Basel, Switzerland) were used as per manufacturer's instructions. A full genome sequencing was performed. The entire S and M segments were amplified in one piece, using the following primers: RFVS-AFwd 5'-ACACAAAGCTCCCTAGAGATAC-3' and RVFSARev 5'-ACACAAAGACCCCCTAGTG-3'; RVFVM-AFwd 5'-ACACAAAGACGGTGC-3' and RVFM-ARev 5'-ACACAAAGACCGGTGC-3'. Amplification of the L segment required two overlapping sections (LA and LB) and was amplified using RVFV-AFwd 5'-ACACAAAGGCGCCCAATC-3' and RVFL-3482Rev 5_-GGAAGCATATAGCTGCGG-3' (LA region), and RVFL-2845Fwd, 5'-GAGACAATAGCCAGGTC-3' and RVFL-ARev 5'-ACACAAAGACCGCCCAATATTG-3' (LB region). The PCR amplicons were resolved using agarose gel electrophoresis (0.7%) and purified using the Wizard® SV Gel and PCR Clean-Up System (Promega, Madison, USA). Amplicons were sent for full genome sequence at the Sequencing Core Facility of the NICD, Johannesburg, South Africa. The sequencing was carried out on the MiSeq platform (Illumina, San Diego, USA) with 300bp paired-end reads using the Nextera XT DNA library Prep kit (Illumina, San Diego, USA). Sequencing data were analyzed using the CLC Bio Genomics Workbench software version 7.5 (Qiagen, Hilden, Germany). Raw reads were trimmed and mapped to the reference sequence and the consensus for each fragment was exported to a FASTA sequence file. Sequences where aligned to reference sequences available from GenBank (accession no. JF784386, JF784387, JF784388) corresponding to the L, M and S segment, respectively (Kortekaas et al., 2011), using Molecular Evolutionary Genetics Analysis (MEGA 5.0) software (http://mega.software.informer.com/5.0/).

Table 2.5. Sequence of primers used for amplification of the three genome segments of RVFV used for full genome sequencing.

Genome segment	Primer	Length (bp)	Sequence
RVFV S	SAFwd	22	5'-ACACAAAGCTCCCTAGAGATAC-3'
	SARev	19	5'-ACACAAAGACCCCCTAGTG-3'
RVF M	MAFwd	15	5'-ACACAAAGACGGTGC-3'
	MARev	16	5'-ACACAAAGACCGGTGC-3'
RVF LA	LAFwd	17	5'-CACAAAGGCGCCCAATC-3'
	3482-LRev	18	5'-GGAAGCATATAGCTGCGG-3'
RVF LB	2845LFwd	17	5'-GAGACAATAGCCAGGTC-3'
	LARev	22	5'-ACACAAAGACCGCCCAATATTG-3'

2.7 Characterization of the rescued virus

2.7.1 Viral growth kinetics analysis

Vero cells and MRC-5 cells (ATCC® CCL-171™) in 25cm^2 flasks (Nunc™ EasYFlask™, Thermo Fisher Scientific, Waltham, USA) were inoculated with virus at a multiplicity of infection (MOI) of 0.01 for 1 hour at 37ºC, washed three times with PBS (Lonza, Basel, Switzerland) and overlaid with 10 mL of the respective culture media. The cells were inspected daily for CPE development, and cell culture supernatants were collected at 6, 12, 24, 48, 72 and 120 h.p.i. for standard ($TCID_{50}$) microtitration in Vero cells according to the methodology described in section 5.5.2. The results were converted into PFU/mL($PFU/mL=0.7*TCID_{50}$) to enable comparison with results from other studies.The points in the growth curves are shown as means ± standard deviation from three independent experiments.

2.7.2 Characterization of viral foci morphology by plaque assay

The characterization of viral foci was performed to assess if there were any phenotypical difference in between plaques formed by the wtRVFV and the mutant C39S/C40S. Vero cells in six-well plates were inoculated with a serial dilution of either wtRVFV or the mutant C39S/C40S, overlaid with 1% methylcellulose in EMEM (Lonza, Basel, Switzerland) containing 4% of FBS, and incubated for 3 days at 37ºC to allow plaque development. The cells were then fixed in 10% formaldehyde and stained with 2% crystal violet. The plaque morphology was inspected under inverted microscope.

The plaque assay described here was based on the methodology described by Baer et al. (2014). One week before the assay was run, a stock solution of 2% methyl cellulose (Sigma-Aldrich St. Louis, USA) was prepared in sterile water. The working solution of 1% methylcellulose (sigma-Aldrich St. Louis, USA) was prepared in sterile EMEM containing 4% FBS. A tenfold dilution of the viruses inocula were prepared using EMEM. Monolayers of Vero cells (10^6 cells/mL) in a 6 well tissue culture plate were inoculated with each virus dilution in duplicate and incubated for 1 hour at 37°C in a 5% CO_2 incubator. Inoculated plates containing each 500µl of the inoculum were rocked gently every 20 min to ensure even coverage by inoculum and to prevent the cell monolayer from drying. After one hour of incubation, the inoculum was removed and cells overlaid with 2mL of 1% methylcellulose, and then incubated for 3 days at 37ºC in an 5% CO_2 incubator. On day 3 post inoculation, cell monolayers were fixed with 1mL of 10% formaldehyde solution for 30 min. The formaldehyde was discarded and the semi-solid plugs of methylcellulose gently removed using running water. The cell monolayers were covered with 500µl of crystal violet solution for 15 minutes and plates rocked to ensure even coverage. The crystal violet stain was gently washed off with water and plates allowed to dry at room temperature. Once cell monolayers dried, plaques were counted in each well inoculated with different virus dilutions. The non-inoculated control wells were processed as inoculated wells, and after fixing and staining, have a uniform monolayer representing a negative reference control. The viral titer was determined as the average number of plaques multiplied by the highest virus $\log_{10}$ dilution at which plaques were still observed.

2.7.3 Western blot analysis

Vero cells were inoculated with wtRVFV or the mutant C39S/C40S at a MOI of 4 for 1 hour at 37ºC. At 4, 8, and 12 h.p.i., the supernatant of the cell culture was removed and the lysis agent, Cytobuster™ protein extraction buffer (Novagen, Madison, USA) was added. The cells were scraped and collected into a 1.5mL eppendorf tube and incubated for 30 min at 4ºC. The tube was then centrifuged (Sorvall Legend Micro 17, Thermo Scientific, Waltham, USA) at 13,800 x g for 15 minutes at 4ºC. The protein was separated using sodium dodecyl sulphate-polyacrylamide gel electrophoresis (SDS-PAGE), according to the method described by Laemmli (1970). The percentage of resolving gel was 10%. The resolving gel was then transferred to an immun-Blot® PVDF membrane (Bio-Rad, Hercules, USA), followed by incubation in Tris- buffered saline (TBS), blocking buffer containing 5% (w/v) of nonfat milk powder and 0.05% Tween-20. The membrane was then incubated with primary antibody for 1h with shaking at 60 rpm. After three washes with 0.05% TBS-Tween-20, the membrane was incubated with horseradish peroxidase-conjugate secondary antibody. After three washes, detection was performed using the Supersignal® West Pico chemiluminescent HRP substrate (Thermo Scientific, Waltham USA). The protein bands were visualized in the Molecular Imager® ChemiDoc™ XRS$^+$ and analyzed by the Image Lab™ software (Bio-Rad, Hercules, USA). The membranes were probed with primary antibodies against the following targets: (1) PKR (PRK B-10: sc-6282 monoclonal antibody, Santa Cruz Biotechnology, Dallas, USA), diluted 1:200; (2) GTF2H1 (p62 monoclonal mouse antibody 5B7 by ThermoFisher Scientific, Waltham, USA), (3) RVFV NSs (Polyclonal RVFV Rabbit Anti-NSs SY2430, diluted 1:200 (kindly provided by Dr. Benjamin Brennan, University of Glasgow, UK) and β-actin diluted 1:500 (ACTBD117: sc-81178 monoclonal antibody, Santa Cruz Biotechnology, Dallas, USA) as a loading control. Peroxidase-conjugated anti-mouse IgGk BP-HRP diluted 1:10000 (Santa Cruz Biotechnology, Dallas, USA) and the polyclonal anti-rabbit IgG dilutes 1:10000 (KPL 5210-0174) were used as secondary antibodies. All of the antibodies were diluted in the dilution buffer [1% (w/v) nonfat milk powder and 0.05% Tween-20]. As controls for western blot, Beta actin and NSs were used.

2.7.4 Immunofluorescence analysis

Subcellular localization of NSs mutant protein was detected by immunofluorescence assay of infected cells at 12 h.p.i. Vero cells were grown on coverslips to 50-70% confluency, and infected with either wtRVFV or the mutant C39S/C40S at a MOI of 2. Cells were assayed for the presence of NSs protein by immunofluorescence detection. Briefly, at 12 h.p.i., cells were fixed with 10% neutral-buffered formalin (Sigma-Aldrich St. Louis, USA) for 10 minutes, permeabilized with 0.1% triton X-100 in PBS for 10 minutes and blocked for 1 hour with PBS 0.1% triton X-100 and 3% BSA. The cells were probed with the primary antibody polyclonal rabbit anti-RVFV NSs SY2430 diluted 1:100 in the blocking buffer. After incubation at room temperature for 1 hour, the coverslips were washed 3 times with PBS 0.1% triton X-100 and incubated at room temperature for 1 hour with goat anti-rabbit coupled with fluorescein isothiocyanate conjugate (Santa Cruz Biotechnology, Dallas, USA) diluted 1:100 in blocking buffer. DAPI was used at 0.1µg/mL to counterstain the nuclei. After washing three times, coverslips were mounted on glass slides. Stained samples were sealed with transparent nail polish and examined using the scanning confocal microscope (Zeiss LSM 880, Oberkochen, Germany), magnification 400x at the Laboratory of Microscopy and Microanalysis, University of Pretoria. The photos were taken with three filters; FITC for the NSs protein, DAPI for the nucleus, and the third photomicrography merging the previous two.

2.7.5 Two-step quantitative TaqMan RT-PCR assays

Expression of IFN-β mRNA was detected in MRC-5 cells infected with the wtRVFV and the RVFV NSs mutant C39S/C40S which represents the attenuated mutant. Briefly, a monolayer of MRC-5 cells ($1x10^6$ cells/well) was infected with a multiplicity of infection (MOI) of 4 of each virus inoculum (wtRVFV SA35/74 and M39/40) and incubated for 1 hour. At specific time points (4h, 8h, 12h) the cells were washed and collected using 600µl of lysing buffer (buffer RLT, Qiagen RNeasy Mini Kit, Qiagen, Hilden, Germany) and stored at -20^{o}C. Total cellular RNA was isolated with the RNeasy Mini kit (Qiagen, Hilden, Germany) and eluted in 30µl of nuclease free water. An aliquot of 100ng RNA was then used as a template for cDNA synthesis using the SuperScript™ IV First-Strand Synthesis System (ThermoFisher Scientific, Waltham,

USA) as per manufacturer's instructions. PCR was performed using the TaqMan® Gene Expression Assay identity number Hs02621180_s1. The kit provides the assay with primers and probes and a PCR-TaqMan fast advanced mix that were used according to the manufacturer's instructions.. Two mRNA transcripts were amplified; the IFN-β1 and the GAPDH as the housekeeping reference gene. The PCR reaction was performed in a 96 well optical reaction plate. The reaction mix consisted of 18µl of the PCR reaction mix and 2 µl of the template per well. For the control reactions, 2 µl of nuclease free water was added. The ABI 7500 real time PCR instrument (Applied Biosystems, Foster City, USA) was used with the following cycling profile: polymerase activation at 95°C for 20 min, 40 cycles of 95°C for 3s and 60°C for 30 min. The cycle threshold (C_t) values were determined using the cycler software and an automated baseline adjustment (ABI 7500 software version 2.0.6, Applied Biosystems, Foster city, USA). Three replicates per experimental group per time point were analyzed and average C_t values calculated. The gene expression results were analysed by relative quantification Delta Ct method (Livak and Schmittgen 2001) and the fold induction values calculated. These values were subjected to statistical analysis using the non-parametric Wilcoxon signed-rank test at a significance of 95% (McDonald, 2014). The conversion of Ct values in fold induction is presented on appendice 1 table 2.

2.8 Study of the virulence of the mutated viruses in BALB/c mice

2.8.1 Virus inoculation in BALB/c mice and collection of samples

Seventy-eight BALB/c mice (12 weeks old) were obtained from the South African Vaccine Producers (Pty) Ltd, Sandringham, South Africa. Mice were kept in isolation cages (IVC-Bio. A.S. Vent light, EHRET), each containing 3 animals, and provided with food (Epol mice cubes) and water *ad libitum*. The mice were labelled with a permanent marker at the base of the tail (one line for mice n^o 1, two lines for mice n^o 2 and three lines for mice n^o. three).

In a pilot experiment conducted before the main experiments, three groups of BALB/c mice each containing 5 animals were inoculated subcutaneously (s.c.) with 100µl of tissue culture supernatant containing wtRVFV isolate 35/74 ($10^{6.85}$, $10^{3.85}$ or $10^{1.85}$ PFU/mL respectively) in order to determine the challenge virus dose for the main experiment. The 4th group was mock inoculated s.c. with 100µl serum free EMEM

supplemented with 100 IU/mL penicillin, 100µl/mL streptomycin and 0.25µg/mL amphotericin B and served as a control group.

The main experiment consisted of 6 experimental animal groups. The groups I-V consisted of 15 animals each, and group VI of 3 animals. Experimental groups I-V were inoculated s.c. with 100µl of tissue culture supernatants containing $10^{2.85}$ PFU/mL of wtRVFV isolate 35/74 or one of four mutants, respectively as described in Table 2.6 Mice from group VI were inoculated s.c. with 100 µl of serum free EMEM supplemented with 100 IU/mL penicillin, 100µl/mL streptomycin and 0.25µg/mL amphotericin B.

Experimental animals were monitored by observation for clinical signs such as ruffled fur, hatched posture and paralysis twice daily; weighed, and temperatures recorded. Weight was taken making use of a digital scale with the mice in a container for immobilization, and the rectal temperature was measured with an electronic thermometer. Mice scheduled for euthanasia on days 1, 3, 5, 7 and 14 post inoculation (d.p.i.) or any moribund animals were anaesthetized with an intramuscular (i.m.) injection of 5mg/kg xylazine and 35mg/kg ketamine. Whole blood was collected in Minicollect® KJEDTA 1 ml tubes (Greiner Bio-on, Austria) via cardiac puncture, and the mice exsanguinated until death, followed by full necropsy. Liver, spleen, brain, lungs, heart and kidney samples were collected aseptically and preserved in either EMEM (Lonza, Basel, Switzerland), 10% neutral-buffered formalin (Sigma-Aldrich, St. Louis, USA) or RNALater (Qiagen, Hilden, Germany) for virus titration, histopathology and gene expression studies. The 0.5mL insulin syringes and needles (15/64” x 31G) (BD Veo™) and the AVACARE™ syringes (1 ml 26Gx1/2”) were used for inoculations and for blood collection, respectively.

Table 2.6. Outline of the main experiment. BALB/c mouse experimental group I was inoculated with the parental wtRVFV isolate 35/74. Groups II to V were inoculated with the mutant viruses generated. Group VI was mock inoculated with 100µl of EMEM and served as the control group.

Experimental groups	No. of animals	Virus inoculated	Designation
Group I	15	RVFV isolate 35/74	wtRVFV
Group II	15	RVFV NSsC194S	RVFV-C194S
Group III	15	RVFV NSsC178S	RVFV-C178S
Group IV	15	RVFV NSsC149S	RVFV-C149S
Group V	15	RVFV NSsC39S/C40S	RVFV-C39S/C40S
Group VI	3	*EMEM	Mock

*Control group

2.8.1.1 Processing of tissue homogenates and sera

Samples of liver, spleen or brain tissues, preserved in RNALater, were prepared as 10% (wt/vol) suspensions in EMEM supplemented with antibiotics as described above. The organs were homogenized using a tissuelyser II and 5mm stainless steel beads (Qiagen, Hilden, Germany) as per manufacturer's instructions (8 mins at 30Hz). The tissue homogenates were clarified by centrifugation at 13,000 x g for 5 minutes and supernatants free of cells were harvested and stored at -70^{o}C until further analysis. Serum was separated from whole blood by centrifugation at 1,500 x g for 10 mins and stored at -70^{o}C until further analysis.

2.8.2 Extraction of RNA

RNA was extracted from 140µl of clarified homogenates of the liver, brain, spleen and serum by using the QIAamp® viral RNA mini kit (Qiagen, Hilden, Germany) according to the manufacturer's instructions. Briefly, 140 µl of sample was added to 560 µl of viral lysis buffer (AVL buffer, provided with the kit), containing 5.6 µl carrier RNA (provided with the kit), in a 1.5 mL microcentrifuge tube. The mixture was then submitted to pulse vortexing and incubated for 10 minutes at room temperature to allow for lysis to occur. The mixture was then briefly centrifuged to remove any droplets from the sides of the tube. A volume of 560µl of 96% ethanol was added to the sample, mixed by pulse-vortexing and centrifuged to remove droplets. The mixture was then

applied to the QIAamp spin column in a 2 mL collection tube and centrifuged at 6000 x *g* for 1 minute. After transferring the QIAamp spin column to a new collection tube, 500 µl of washing buffer AW1 (provided with the kit) was added and the tube centrifuged at 6000 x *g* for 1 minute. This was followed by adding 500 µl washing buffer AW2 (provided with the kit) to the QIAamp spin column in a new 2 mL collection tube, and centrifugation at 20 000 x *g* for 3 minutes. The QIAamp spin column was then transferred to a clean 1.5 mL microcentrifuge tube. The elution buffer AVE (provided with the kit) was then added to the QIAamp spin column, incubated at room temperature for 1 minute followed by centrifugation at 6000 x *g* for 1 minute. The QIAamp spin column was then discarded and the eluted viral RNA was stored at -20°C or used immediately.

2.8.3 Viral loads

Quantitative real-time reverse-transcription PCR (Q-RT-PCR) was performed using the Qiagen OneStep RT-PCR Kit (Qiagen, Hilden, Germany) and the Roche LightCycler® 480 real time PCR instrument (Roche, Basel, Switzerland). Amplifications were carried out in 25µl reaction mixes containing 5µl of target virus RNA, 1µM of each sense and antisense primer, 0.2µM of the probe, 12.5mM $MgCl_2$ and 0.4mM deoxyribonucleotide triphosphates (dNTPs). Cycling profiles, primers and a TaqMan probe targeting a region of the M segment were used as described by Drosten et al (Drosten et al., 2002). Standard curves were prepared using RNA of RVFV Ar 20368 mosquito isolate 1981 SA containing the target region of the primers and probe. Tenfold serial dilutions of the RNA standard in RNA free water containing carrier RNA was prepared starting from 10^8 to 10^1 copies per mL. The standard of 10^7 was used for this experiment. Samples with cycle threshold values ≤ 40 were regarded as positive. Sample reaction and amplification parameters are shown in Tables 2.7 and 2.8, respectively.

Table 2.7. Sample reaction for the amplification of the M segment of RVFV using One step RT-PCR kit from Qiagen. The Ar 20368 mosquito isolate 1981 SA was used as control and for the generation of a standard curve. Primers were designed by Drosten et al., 2002.

Reagent	µl per reaction	Concentration stock solution	Final concentration
5x QIAGEN OneStep RT-PCR Buffer	5.0	5x	1x
dNTP Mix	1.0	10 mM	0.4 mM
Primer RVS	2.5	10 µM	1 µM
Primer RVAs	2.5	10 µM	1 µM
Probe RVP	0.5	10 µM	0.2 µM
Bovine serum albumin (BSA)	0.8	1000 µg/mL	32 µg/mL
QIAGEN OneStep RT-PCR Enzyme Mix	2.0		
Water, nuclease free	5.7		
Total volume Mastermix	20		
Template RNA added as the final step:	5		
Total volume	25		

Table 2.8. Thermal cycling parameters used for RT-PCR. Lightcycler 480 (Roche).

	Reverse transcription	Hotstart Taq activation	Amplification Signal analysis F1	Amplification Signal analysis F2	Cooling
Cycles	1	1	45		1
Analysis Mode	none	none	Quantification		none
Temperature Targets	1	1	1	2	1
Target Temperature	50°C	95°C	95°C	57°C	30°C
Incubation time (h:min:sec)	0:30:00	0:15:00	0:00:05	0:00:35	0:00:30
Temperature Transition Rate	20°C/s	20°C/s	20°C/s	20°C/s	20°C/s
Secondary Target Temperature	0	0	0	0	0
Step Size	0	0	0	0	0
Step Delay (Cycles)	0	0	0	0	0
Acquisition Mode	none	none	none	Single	none

2.9 Sequencing analysis of the virus extracted from infected organs

The RNA was extracted from the livers of infected mice on day 3 p.i. and amplified by RT-PCR using primers for amplification of the full genomes (S,M, LA and LB (Table 2.5), designed by Bird et al., (2007a). PCR products were purified from a 0.7% agarose gel, followed by sequencing to confirm the stability of the mutant viruses. Analysis of the sequencing data was performed as described previously in section 2.6.4.

2.10 Histopathology examination

Liver, spleen, kidney, lung, heart and brain tissues collected on 3 and 5 d.p.i. were fixed in 10% neutral-buffered formalin (Sigma-Aldrich St. Louis, USA) for 24 hours and dehydrated through increased ethanol concentrations. Subsequently, the tissues were cleared with two changes of xylene (Sigma-Aldrich St. Louis, USA), embedded in paraffin wax (Sigma-Aldrich St. Louis, USA) and sent to the Pathology laboratory at the Faculty of Veterinary Sciences, University of Pretoria for further processing. Embedded tissues were sectioned at a 4µm thickness, mounted on microscope slides and incubated for 20 minutes at 60°C. Tissue sections were then deparaffinized with two changes of xylene, rehydrated through decreased ethanol baths to distilled water, and then stained with hematoxylin and eosin (Thermo Fisher Scientific, Waltham, U.S.A). The sections were then dehydrated through increased ethanol baths, cleared in two changes of xylene, mounted using Entellan® (Thermo Fisher Scientific, Waltham, USA) and then coverslipped. The sections were inspected under a routine light microscope. Liver and spleen histopathology was scored for lesion severity on a semi-quantitative scale from 0–3 with a score of 0 indicating no lesions attributable to infection with RVFV and a score of 1–3 indicating progressively and more severe histopathology (Table 2.9 and 2.10). All microscopic images were captured with a DP25 camera (Olympus, Tokyo, Japan) on a BX46 light microscope (Olympus, Tokyo, Japan) using the program CellSens Standard Version 1.12 (Olympus, Tokyo, Japan), magnification 100x, 200x and 400x. The photomycrograpies were taken at magnification 200x and 400x, Bar=50x and 100x .

Table 2.9. Description of liver histopathology scoring in BALB/c mice experimentally infected with wtRVFV and the NSs mutants.

Histopathology score	Description
0	No significant histopathology.
1	Multifocal hepatocyte apoptosis involving single cells or groups of 2-5 cells accompanied by a low number of infiltrating neutrophils and lymphocytes with Kupffer cell hyperplasia. Less than 10% of the liver parenchyma affected.
2	Multifocal hepatocyte necrosis involving up to 50% of the liver parenchyma with scattered hepatocyte apoptosis and a mild to moderate inflammatory cell infiltrate as recorded less than 1 above.
3	As for category 2 above, but with hepatocyte necrosis involving more than 50% of the hepatic parenchyma and accompanied by multifocal hemorrhages.

Table 2.10. Description of spleen histopathology scoring in BALB/c mice experimentally infected with wtRVFV and the NSs mutants.

Histopathology score	Description
0	No significant histopathology.
1	Mild to moderate white pulp expansion with occasional coalescence of white pulp foci. Occasional lymphocyte apoptosis involving up to 10 cells per follicular germinal center associated with tingible body macrophages.
2	As for category 1 above but with increased expansion and coalescence of the white pulp with apoptosis of up to 50% of lymphocytes in follicular germinal centers associated with tingible body macrophages. Multifocal mild to moderate red pulp atrophy (characterized by reticulosclerosis and depletion of cells compared to control mice).
3	As for category 2 above but with apoptosis of more than 50% of lymphocytes in lymphoid follicles. Severe diffuse red pulp atrophy (described under 2 above).

2.11 Immunohistochemistry examination

Immunohistochemical staining (IHC) for the detection of RVFV antigen was performed on duplicate tissue sections using a polyclonal hyperimmune mouse serum and an avidin-biotinylated peroxidase complex (ABC) immunodetection technique as previously described (Odendaal et al., 2014). Briefly, the standard immunoperoxidase method included routine deparaffination with two changes of xylene, rehydration through graded alcohol baths to distilled water, and incubation with 3% hydrogen peroxide for 15 minutes. This was followed by heat-induced epitope retrieval (HIER) via microwave in citrate buffer solution at a pH of 6, , followed by blocking of non-specific epitopes by pre-incubation with normal horse serum (Sigma-Aldrich, St Louis, USA catalogue no. H0146) diluted 1:10 in PBS/BSA, pH 7.6. Epitopes were blocked for 20 minutes in a moist chamber at room temperature. Following blocking, the serum was replaced with the polyclonal hyperimmune mouse ascitic fluid to RVFV, diluted 1:500 in PBS/BSA buffer, and incubated for 1 hour in a moist chamber at room temperature. The ascitic fluid was prepared by the NICD in 1996 as previously described (Van Der Lugt et al., 1996; Swanepoel et al., 1986; Sartorelli et al., 1966). Sections were sequentially incubated with the antigen biotinylated rabbit anti-mouse secondary antibody (Dakocytomation, Glostrup, Denmark, catalogue no. E0432) diluted 1:500 in PBS/BSA buffer. The incubation with the secondary antibody was performed at room temperature in a moist chamber for 30 minutes followed by rinsing with distilled water and then PBS/BSA buffer. Peroxidase-conjugated avidin (Vectastain ABC kit, Elite PK6100 Standard, Vector Laboratories, Burlingame, USA) was applied as per manufacturer's instructions and incubated for 30 minutes at room temperature in a moist chamber. Sections were immerged in the NovaRED substrate (Vector Laboratories, Burlingame, USA, catalogue no. SK-4800) using a droplet method for approximately 1-2 minutes at room temperature in a moist chamber. Sections were subsequently rinsed in a distilled water bath and counterstained with Mayer's hematoxylin for 3-4 minutes and rinsed with tap water for 10 minutes to remove excess substrate. The sections were then dehydrated though increasing ethanol concentrations and xylol, mounted using Entellan® and then coverslipped. Slides were examined for positive labelling, typified as fine diffuse to coarse granular cytoplasmic labelling, using a light microscope. Liver and spleen immunolabelling was

scored on a semi-quantitative scale from 0–3 with a score of 0 indicating no signal specific to the presence of RVFV antigen and a score of 1–3 indicating a progressively increasing quality of signal pertaining to the presence of RVFV antigen (Table 2.7). All microscopic images were captured with a DP25 camera (Olympus, Tokyo, Japan) on a BX46 light microscope (Olympus, Tokyo, Japan) using the program CellSens Standard Version 1.12 (Olympus, Tokyo, Japan), magnification 100x, 200x and 400x, Bar=50x and 100x .

Table 2.11. Description of liver and spleen immunolabelling scoring in tissues of BALB/c mice experimentally infected with wtRVFV and the NSs mutants.

Score	Description
0	No signal
1	Minimal positive signal detected in up to 10% of organ parenchyma and involving single cells or multifocal groups of 2 to 5 cells
2	Multifocal positive signal detected in up to 50% of organ parenchyma
3	Widespread positive signal involving more than 50% of organ parenchyma.

2.11.1 Inflammatory cytokines and receptors and Type-I inflammatory response

Quantitative mRNA expression analysis of 84 chemokines and their receptors and 84 Type-I interferon and response genes were performed in the livers and spleens of mice using the RNA profiling RT^2 profiler array "Inflammatory cytokines and receptors" (SABioscience, Qiagen catalogue No. 330231 PAMM 016ZA) and the "Type-I IFN response" (SABioscience Qiagen catalogue No. 330523 PAMM 011ZA). The list of transcripts targeted, fold changes and *P*-values are shown in appendix 3, and Tables A1 and A2.

The RNA was isolated from the liver and spleen of mice infected with the wtRVFV SA35/74 and the mutant C39S/C40S. Approximately 30mg of liver and spleen preserved in RNAlater (Qiagen, Hilden, Germany) was added to 500µl lysis buffer (RLT, Qiagen, Hilden, Germany) and homogenized in a TissueLyser (Qiagen, Hilden, Germany) as described in the section 2.7.1.1. Homogenates were clarified and the supernatants stored at -70°C until further processing. RNA was extracted from homogenized livers and spleens of control and infected mice (collected at 3 and 5 d.p.i.) using the RNeasy mini kit (Qiagen, Hilden, Germany) and diluted to 125ng/µl in nuclease free water. Complementary DNA (cDNA) was prepared from the RNA using the RT^2 first strand kit (SABiosciences, Qiagen, Hilden, Germany) as per manufacturer's instructions. Briefly, a total of 1µg of each RNA preparation was mixed with 5x genomic DNA elimination buffer and the reaction incubated at 42^{o}C for 5 min (total volume 10µl). After the incubation, the reactions were immediately placed on ice and an equal volume of RT-cocktail mix (5x RT buffer, primers and external control mix, RT-enzime mix and RNase-free water) was added. These reactions were then incubated at 45°C for 15 min followed by inactivation at 95°C for 5 minutes. The resultant cDNA of each preparation was diluted 1:10 in nuclease-free water, mixed with 2x master mix, containing dNTPs, $MgCl_2$, and DNA polymerase (SABioscience RT^2qPCR SYBR Green Mastermix, Qiagen, Hilden, Germany). Reactions were made up to 25µl with nuclease free water and aliquoted onto the PCR array plates containing primer sets for the arrays PAMM-016Z, and PAMM-011Z SABiosciences, Qiagen, Germany. The plates were run on an ABI 7500 real time PCR instrument (Applied Biosystems, Foster city, USA), using the following cycling program: 95°C for 10 min, 40 cycles of 95°C for 15 s and 60°C for 1 min. The cycle threshold (C_t) values

were determined using the cycler software and an automated baseline adjustment (ABI 7500 software version 2.0.6, Applied Biosystems, Foster city, USA).

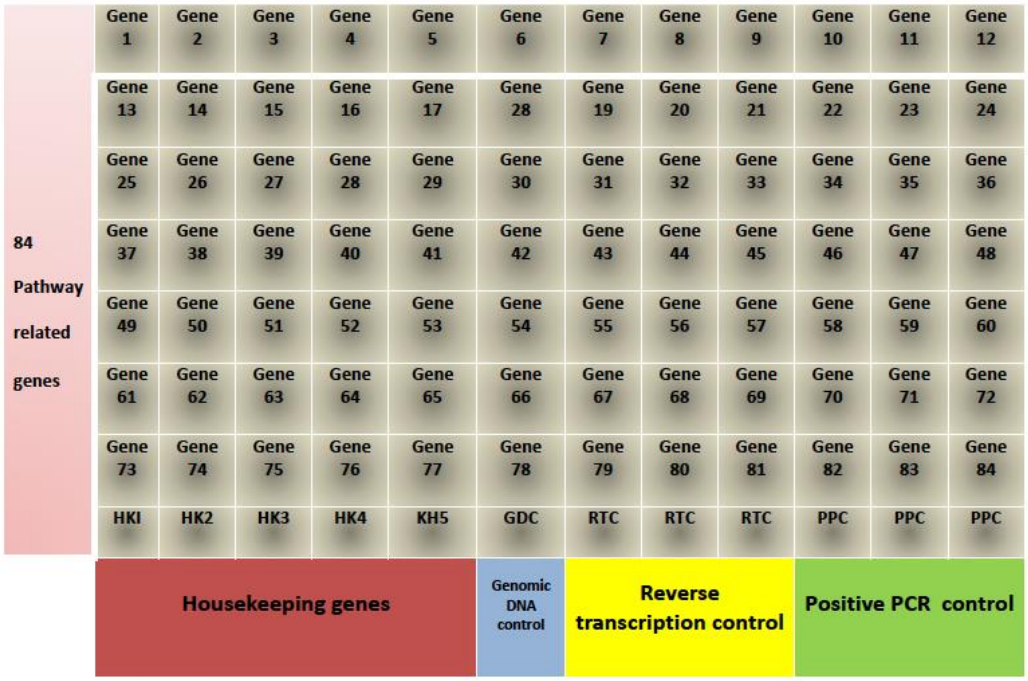

Figure 2.4. RT^2 PCR Array format for 96 wells. Each well comes with primers for amplification of a specific gene. One plate was used for one sample and three replicates of each sample.

2.12 Relative quantification data analysis

Three mice per group per time point were analyzed and average values calculated. Calculation of fold change values obtained by the SABiosciences quantification PCR array makes use of the $2^{-\Delta\Delta CT}$ method except for the use of the five housekeeping genes (Actin beta (Actb), Beta-2 microglobulin (B2M), Glyceraldehyde-3-phosphate dehydrogenase (GAPDH), glucuronidase beta (Gusb) and heat shock protein 90 alpha (cytosolic), class B member 1 (Hsp90ab1) for normalization of data.

2.13 Statistical analysis

Statistical significances in viral load levels and viral growth curves were calculated by the Kruskal-Wallis rank test at 95% confidence using the statistic program STATA version 13 (College Station, TX: StataCorp LP, College Station, USA). Statistical significances in weight and temperature between experimental groups were determined by a paired t-test two-sample analysis. The SABioscience PCR Array Data Analysis Template Excel Utility includes calculation of a *P*-value based on a Student's t-test of the replicate $2^{-\Delta CT}$ values for each gene in the control group and treatment groups. The calculations were done using the SABiosciences PCR Array Data Analysis Template Excel Utility, version 4.0 (http://sabiosciences.com/pcrarraydataanalysis.php). The formula used to calculate the relative gene expression level is: ΔCT=CT(GOI)-Avr(CT(HKG)) where GOI is each gene of interest and HKG are the housekeeping genes chosen. Genes were only regarded as upregulated with fold changes ≥ 2.0 and downregulated with fold changes ≤ -2.0 (table A1, appendice 4). Fold changes with *P*-values less or equal to 0.05 ($p \leq 0.05$) were considered statistically significant. Three biological replicates were used at all experimental time points in all groups.

CHAPTER 3

3 Rescue and characterization of wtRVFV and NSs mutants

3.1 Introduction

The success in viral infection is mediated by virulence factors, including viral attachment proteins and nonstructural proteins. Their contribution to infection and disease have been delineated by reverse genetics that enables experimental production of recombinant and reassortant viruses from cloned cDNA. Through reverse genetics, scientists have developed a deeper understanding of virulence factors key to causing disease, thereby enabling development of live attenuated vaccines and antiviral therapeutics (Walpita and Flick, 2005).

Reverse genetics is an approach with which the expression of a gene can be disrupted either by mutating the DNA sequence of the gene or knocking down the gene expression using RNA interference. With the classical (forward) genetics, mutant phenotypes are known long before these genes have been identified. Organisms such as bacteria were treated with a mutagen and screened offspring for a particular phenotype of interest. In the post-genomic era, the classical problem has been reversed. All the genes in an organism are known, but the exact function of many of them are unknown. In addition, it is not known what phenotypes are caused by mutation in the predicted genes. The site directed mutagenesis technique is a reverse genetic approach used to make a specific change at an exact nucleotide in the gene of interest and requires that the gene of interest be cloned into plasmids. Mutagenesis is performed *in vitro* on the cloned gene in bacteria, followed by insertion of the mutated gene into the host genome in a transposable element vector. Briefly, the DNA is denatured by heating, cooled in the presence of two complementary primers, and the plasmid is replicated *in vitro* with non-standard-displacing polymerase. Methylated parental DNA is digested with DpnI enzyme, resulting in *in vitro* synthesized DNA. The mutated plasmid is then transformed into bacteria and replicated. Finally, DNA sequencing is performed to ensure proper nucleotide changes (Wan et al., 2012, Walker, 2016).

In recent years, different groups have developed several reverse genetics systems for the rescue of RVFV from cDNA constructs. Systems using the Pol-I promoter were traditionally used to rescue viruses that replicate in the nucleus. Pol-I based reverse genetics systems were recently also shown to be suitable for the rescue of RNA viruses that replicate in the cytoplasm, such as the bunyaviruses (Billecocq et al., 2008; Habjan et al., 2008). The T7 promoter, recognized by the phage T7 polymerase has also been used extensively to rescue RVFV (Kortekaas et al., 2011; Habjan et al., 2008; Ikegami et al., 2006). The Pol-I system, however, requires co-transfection with helper plasmids expressing the nucleocapsid and polymerase proteins whereas the T7 system does not. T7-based reverse genetics systems (Habjan et al., 2008b; Gerrard et al., 2007; Ikegami et al., 2006) either make use of stable cell lines expressing T7 polymerase (BSR.T7/5 cells or BHK-T7/9 cells) and/or recombinant poxviruses (Vaccinia virus or fowlpox virus) providing the T7 polymerase (Kortekaas et al., 2011). Indeed, the availability of reverse-genetics systems for negative-strand RNA viruses has facilitated the elucidation of virulence factors as well as the development of efficient vaccines. The fact that one rescues a virus population from a single known cDNA clone eliminates the disadvantage of virus subpopulations that are inherently found in clinical isolates, which could introduce unwanted variation in results (Freiberg et al., 2008a).

When a virus infects a host cell, it hijacks the biosynthetic capacity of the cell to produce virus progeny, a process that may take less than an hour or more than a week. The overall time required for a virus to reproduce depends collectively on the rates of multiple steps in the infection process, including initial binding of the virus particle to the surface of the cell, virus internalization and release of the viral genome within the cell, decoding of the genome to make viral proteins, replication of the genome, assembly of progeny virus particles, and release of these particles into the extracellular environment. For a large number of virus types, much has been learned about the molecular mechanisms and rates of the various steps (Yin and Redovich, 2018). The growth kinetics of RVFV has been studied in experimental designs where mutations are introduced in the RVFV genome (Won et al., 2006, Lokugamage and Ikegami, 2017) and also in reassortment studies (Ly et al., 2017).

The NSs protein is the most extensively studied phlebovirus virulence factor due to its ability to counteract the host immune response early in infection. There are three major ways that the NSs can affect the host innate immune response; 1) Degradation of PKR via proteasome, preventing eif2a phosphorylation and thereby preventing translation shut-off; 2) Interaction with SAP30/YY1 (Sin3A complex) on the IFN-b promoter, thus preventing transcription of this gene; 3) Degradation of p62 and sequestering p44/xPB, preventing general host transcription (Kalveran et al., 2011, 2013). Mutation of conserved cysteine residues in the NSs gene may have an impact on the biology of the protein.

This chapter describes the rescue and characterization of the recombinant wtRVFV isolate 35/74 and four NSs mutants with cysteine-to-serine substitutions at positions 39/40, 149, 178 and 194 of the NSs protein of RVFV. It also describes the effect of mutations on the biological characteristics of the rescued virus such as the growth kinetics, plaque formation, subcellular localization, interferon antagonism and degradation of host proteins such as PKR and the subunit p62 of the transcription factor II Human (TFIIH).

3.2 Results

3.2.1 Rescue of recombinant RVFV from transcription plasmids

To investigate the effect of cysteine-to-serine substitutions at the five target cysteines, known to be conserved in all known isolates of RVFV to date (Aitken et al., 2008; Sall et al., 1997), on RVFV virulence, four mutants with cysteine-to-serine substitutions at residues 39/40, 149, 178 and 194 of the NSs gene, were included in the rescue assay. The rescue assay was based on the reverse genetics T7 polymerase system, and was performed by transfecting BSR-T7/5 cells, which constitutively express the T7 RNA polymerase. The wtRVFV isolate 35/74 and the NSs mutants C39S/C40s, C149S, C178S and C194S were rescued efficiently form transcription plasmids with titers ranging from $10^{4.9}$ to $10^{4.2}$ PFU/mL. The titer of the rescued virus where $10^{4.9}$, $10^{4.9}$, $10^{4.2}$, $10^{4.2}$ and $10^{4.2}$ PFU/mL for the wtRVFV and the mutants C39S/C40s, C149S, C178S and C194S, respectively. The sequences of the rescued mutants were aligned with the corresponding NSs sequence of wtRVFV and were shown to carry the introduced mutations (Appendix 2).

3.2.2 Characterization of the rescued virus

3.2.2.1 Replication kinetics of cysteine-to-serine mutants in MRC-5 and Vero cell lines

In order to assess the effects of the cysteine-to-serine mutations on virus replication kinetics, IFN-competent MRC-5 cells and IFN-deficient Vero cells were infected with wtRVFV or the mutants at a MOI of 0.01 and the titers determined at 6, 12, 24, 48, 72 and 120 h.p.i. The two viruses replicated to equivalent levels in Vero cells but not in MRC-5 cells. There was a statistical difference ($*p < 0.05$) in the replication kinetics of the wtRVFV and the mutant C39S/C40S. The mutant C39S/C40S replicated less efficiently in IFN-competent cells when compared to the growth of the wtRVFV. There were significant differences in terms of development of cytopathic effect (CPE) and the titers of the viruses at different time points (Figure 3.2). In Vero cells, exponential growth started at 6 h.p.i. and the average titer reached 10^3 PFU/mL at 12 h.p.i., while in MRC-5 cells, exponential growth started 12 h.p.i. with a hundred times difference in virus titer when compared to those recorded in Vero cells (Figure 3.2A). Interestingly, early in infection, all mutants, with the exception of mutant C194S, replicated more

efficiently than wtRVFV in Vero cells. However, over a period of 72 hrs, mutant C39S/C40S replicated the least efficiently in IFN-competent MRC-5 cells, followed by mutant C149S. Mutants C178S and C194S as well as wtRVFV replicated efficiently in MRC-5 cells, reaching an average of 10^7 PFU/mL after 48 h.p.i., differing by an order of approximately 2 logs from mutant C39S/C40S (Figure 3.2B). Based on the fact that the mutant C39S/C40S replicated less efficiently in IFN-competent cells (MRC-5 cells) when compared to the wtRVFV ($p < 0.05$), further analysis of certain biological properties of the NSs protein, comparing the wtRVFV and the mutant C39S/C40S, were performed.

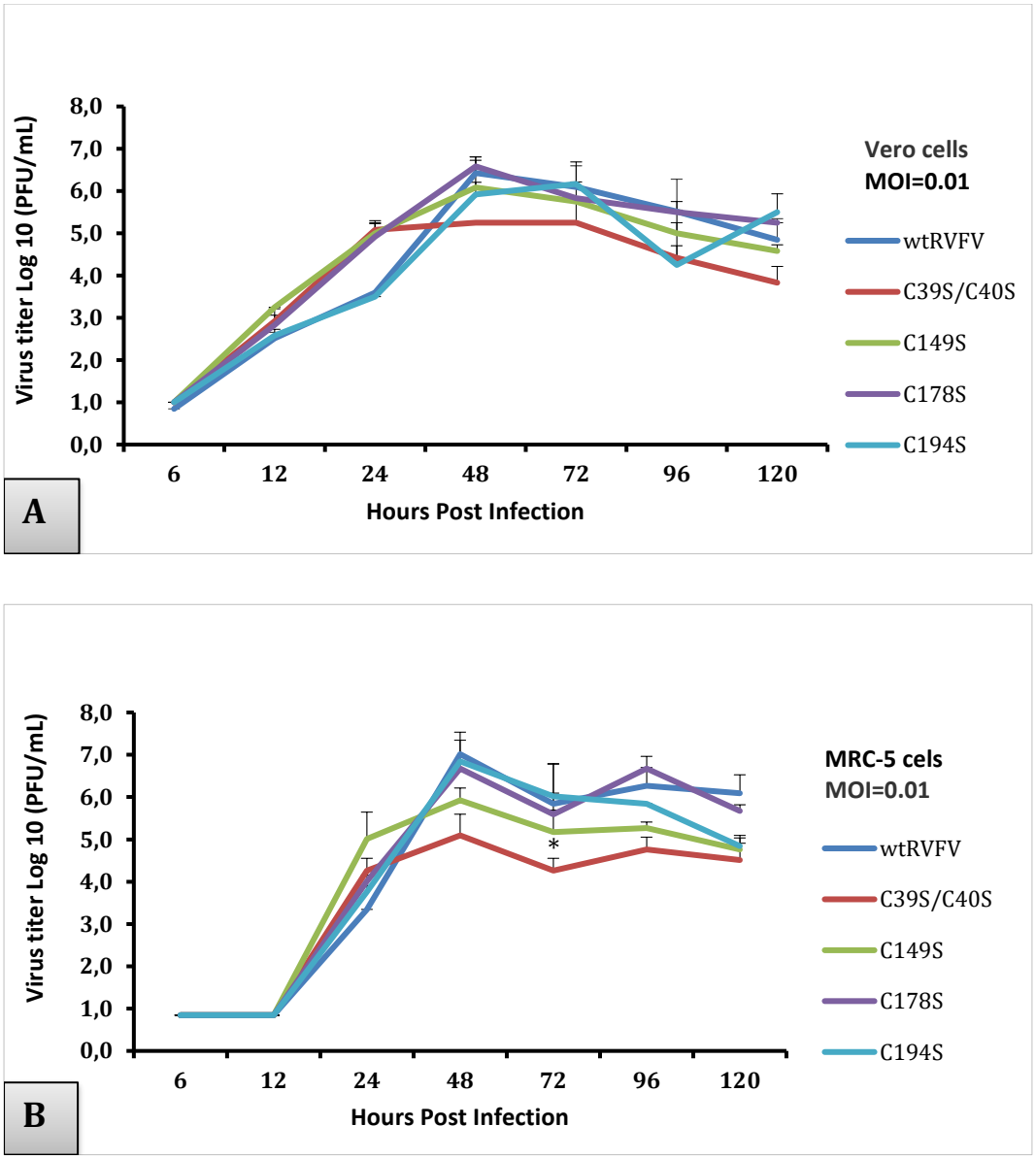

Figure 3.1. RVFV replication kinetics in IFN-competent and IFN-deficient cells. Replication kinetics of wtRVFV and the mutants RVFV-C39S/C40S, -C149S, -C178S and -C194S in Vero cells (A) and MRC-5 cells (B). The points in the growth curves are shown as means +/- standard deviation from nine replicates. Asterisk (*) indicates statistically significant differences (Kruskal-Wallis test; $p < 0.05$).

3.2.2.2 Biological properties of the NSs attenuated mutant C39S/C40S

The growth kinetics of mutant C39S/C40S differed from the single mutants, and more specifically did not replicate efficiently in IFN-competent cells. In order to understand the mechanisms underlying this attenuation, certain well-known biological properties of the NSs protein such as the plaque morphology, the ability to suppress the type-I IFN response, the trafficking of the protein to the nucleus and the degradation of some important host proteins such as PKR and p62 were analyzed.

No significant differences in plaque sizes and morphology were detected among the wtRVFV and the mutant C39S/C40S in Vero cells (Figure 3.3).There was a significant upregulation ($p \leq 0.05$) of IFN-β mRNA gene expression in the lysates of cells infected with the mutant C39S/C40S, while IFN-β mRNA levels were suppressed in wtRVFV infected cells. This result suggests that the C39S/C40S mutations compromise the IFN antagonizing property of NSs (Figure 3.4).

Lysates of Vero cells infected with the wtRVFV or the mutant C39S/C40S collected 4, 8 and 12 h.p.i. were probed with the anti-RVFV NSs, anti-PKR, anti-p62 and anti-β actin in a western blot assay. The NSs proteins of both wtRVFV and the mutant C39S/C40S were detected in cell lysates collected at 8 and 12 h.p.i., although expression of the mutant NSs protein was relatively lower at 8 h.p.i. (Figure 3.5).

Immunofluorescence microscopy demonstrated that both wtRVFV and the C39S/C40S NSs mutant enters the nucleus where it forms filaments, although the mutant C39S/C40S appeared less efficient in forming these structures compared to the wild type (Figure 3.6).

As the NSs protein was previously described to promote degradation of protein kinase R (PKR) (Kalveram et al., 2013), it was investigated whether this function of NSs is compromised by the C39S/C40S mutations. Western blot analysis demonstrated that infection of Vero cells with wtRVFV resulted in the degradation of PKR between 8 and 12 h.p.i., whereas PKR levels were maintained in cells infected with mutant C39S/C40S (Figure 3.5). Related to this, the p62 was equally degraded by the mutant C39S-C40S as observed in the wtRVFV.

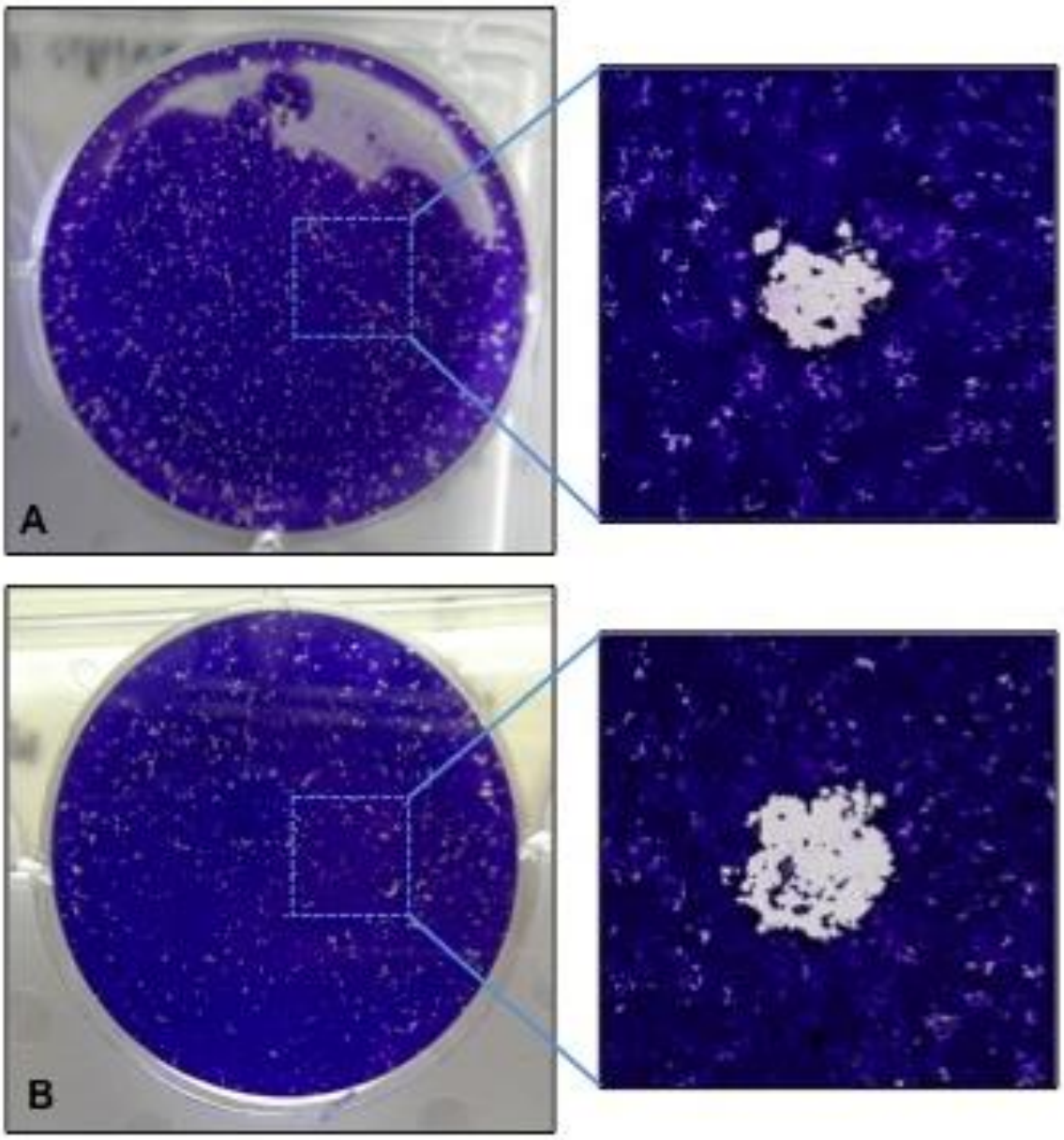

Figure 3.2 Plaque morphology. Morphology of plaques produced by (A) wtRVFV and (B) the mutant C39S/C40S. No differences were observed in the morphology and size of plaques produced in Vero cells infected with the wtRVFV and the attenuated mutant C39S/C40S. The cells were fixed in 10% neutral-buffered formalin and stained with 2% crystal violet. Plaques were inspected and measured under inverted microscope, Olympus CellSens Dimension 1x53Camera SC30, 40x magnification.

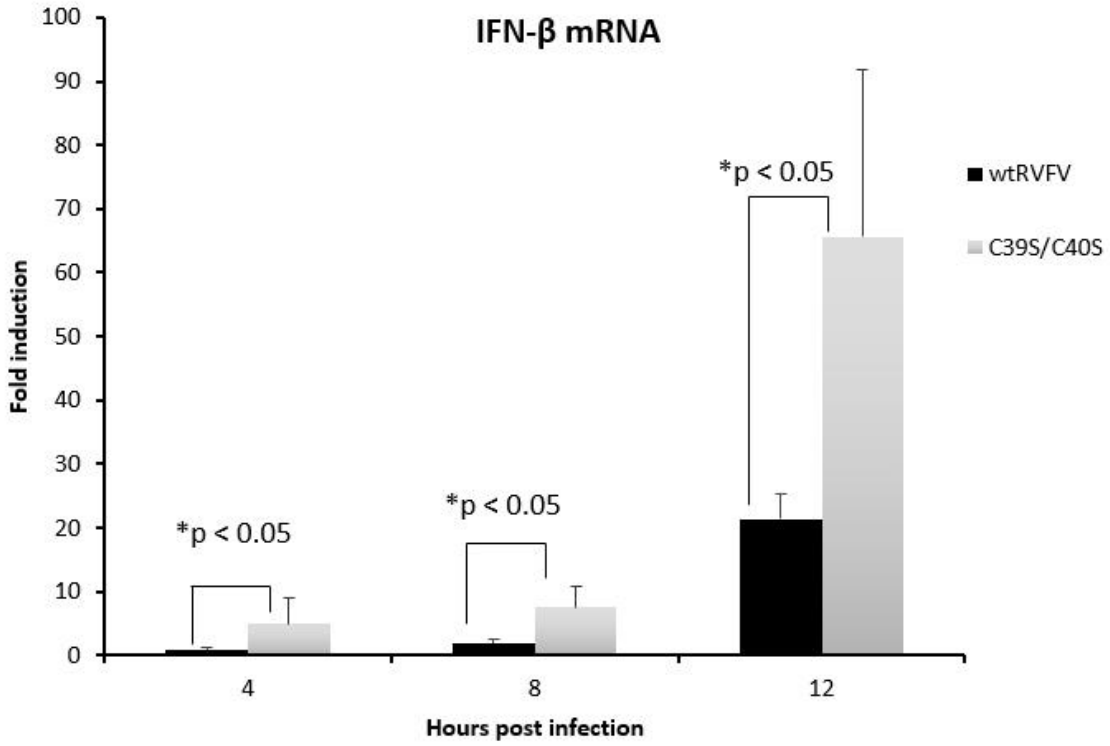

Figure 3.3 Induction of IFN-β gene transcription in RVFV infected cells. At indicated time points post infection, total RNA was extracted from MRC-5 cells infected with either wtRVFV, the mutant C39S/C40S or mock infected. cDNA was amplified using specific primers for human IFN-β and GAPDH. (TaqMan gene expression, ThermoScientific, Waltham, USA). Data represents mean and SD of three replicates. (*) indicates statistical significance (student's t-test $p < 0.05$).

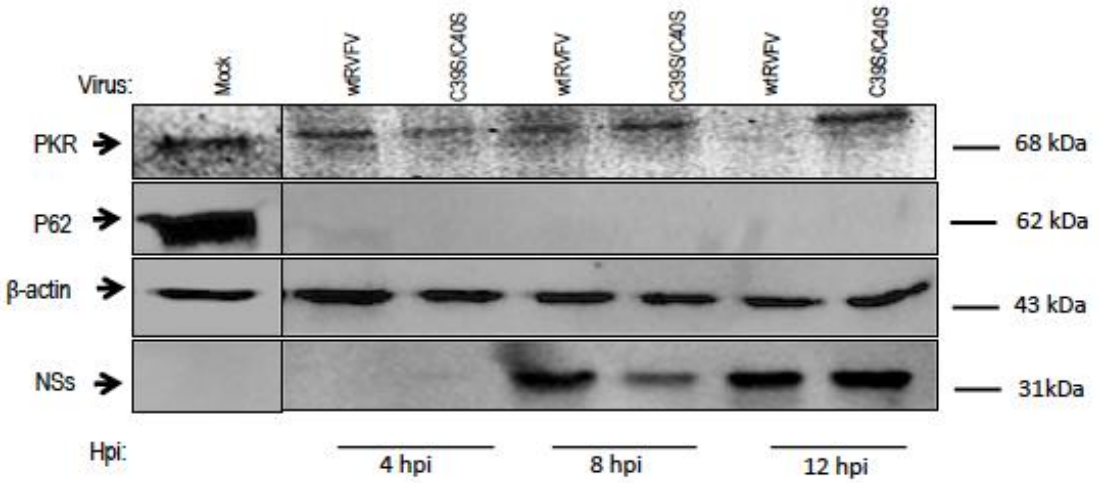

Figure 3.4 Western blot detection of NSs and host proteins PKR, p62 in infected vero cells. Vero cells were seeded in 75cm^2 cell culture flasks and infected with wtRVFV or the mutant C39S/C40S at an MOI of 4. After 4, 8 and 12 h.p.i., cell lysates were prepared and subjected to western blot analysis for dettection of NSs, PKR and p62, as described in the material and methods. ß-actin was used as cell lysate control. Infection with wtRVFV resulted in degradation of PKR between 8 and 12 h.p.i while p62 was equally degraded by the wtRVFV and the mutact C39S/C40S. The NSs protein was detected in both wtRVFV and the mutant C39S/C40S from 8 h.p.i.

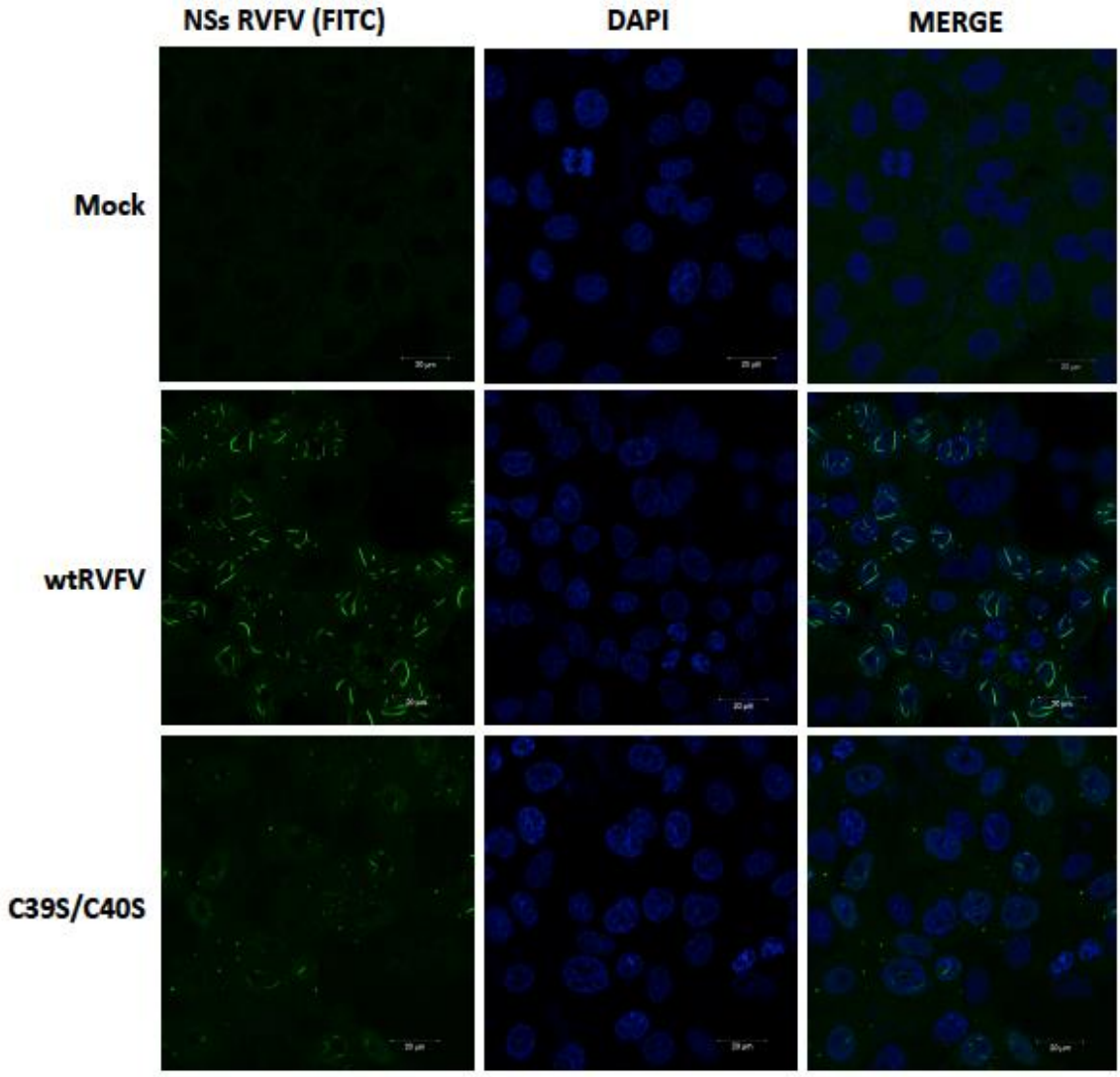

Figure 3.5 Subcellular localization and filament formation of wtRVFV and mutant C39S/C40S NSs proteins. Monolayers of Vero cells on coverslips were infected either with wtRVFV or the mutant C39S/C40S at a MOI of 2. Cells were fixed at 12 h.p.i. and stained with NSs-specific antibodies for the detection of infected cells by immunofluorescence analysis. The left panels show distribution of the nonstructural NSs protein detected with anti-NSs rabbit polyclonal antibody stained with FITC (green), the middle panels show counterstain of the nucleus with DAPI (blue) and the merged image of NSs and DAPI are shown in the right panels. Bars = 20µm.

3.3 Discussion

This study reports the rescue of recombinant wtRVFV and four NSs mutants carrying cysteine-to-serine mutations at positions 39/40, 149, 179 and 194. Since these cysteines are highly conserved and the NSs protein is the major virulence factor, it was hypothesized that substitutions of these amino acids would affect the virulence of the mutant viruses generated. The cytopathic effect observed in the transfected wells suggested that infectious virus was successfully recovered. This was further confirmed by the results of the microtitration, followed by the sequencing results which showed that the recovered virus carried the introduced mutations and lacked other mutations in the NSs gene. The results of this study further show that mutating highly conserved cysteine residues of the RVFV NSs protein results in differential replication kinetics in IFN-competent and IFN-deficient cells. The mutations were found to be stably maintained during serial passages in cell culture. The mutant C39S/C40S was not able to replicate efficiently in IFN-competent cells early in the infection while the other mutants C149S, C178S and C194S replicated efficiently in IFN-competent cells (similar to wtRVFV). During the first 24 to 48 hours, the viral growth was exponential. After 48 hours,the growth was maintained at that level and individual viruses showed differences in growth kinetics, with mutant C39S/C40S replicating less efficiently in IFN-competent cells. These findings demonstrate that the mutant C39S/C40S is not efficient on counteracting the host IFN response induced by virus infection. Similar results were observed with Clone 13 and other RVFV virus lacking the entire NSs gene (McElroy and Nichol, 2012). Indeed, this finding was further confirmed in gene expression studies where upregulation of IFN-β mRNA transcripts was observed in cells infected with the mutant C39S/C40S, suggesting that its attenuated phenotype is explained by a compromised IFN-antagonistic function of NSs. Interestingly, there were no significant differences of the plaque size and morphology between the wtRVFV and the attenuated mutant C39S/C40S. It was expected that the attenuated mutant would cause less cytopathic effect and consequently minor plaques compared to the wtRVFV plaques.

Another function of NSs, which is independent of its IFN-antagonistic function, is its ability to promote PKR degradation (Kalveram et al., 2013). Indeed, western blot analysis showed decreasing levels of PKR between 8 and 12 h.p.i. in cells infected

with wtRVFV, whereas PKR levels in cells infected with the mutant C39S/C40S were not affected. This finding shows that the high pathogenicity of RVFV is also related to its ability to degrade PKR (Habjan et al., 2009a). The NSs protein of both wtRVFV and mutant C39S/C40S was detected between at 8 and 12 h.p.i., although expression of the mutant NSs protein was relatively lower at 8 h.p.i. NSs protein is expressed early in the infection. This relatively late detection can be explained by the fact that the amount of protein accumulated might not have been enough to be detected earlier. If cells were collected between 4 and 8 hours, the NSs would probably be detected in that interval.

A characteristic feature of RVFV pathogenesis is the formation of filamentous structures in the nucleus of infected cells (Barski et al., 2017; Benferhat et al., 2012). Although the replication of RVFV takes place in the cytoplasm, the NSs protein has the ability to traffic to the nucleus where it interacts with specific host proteins and forms filamentous structures. The most dramatic consequence of nuclear localization of NSs is the degradation of p62, which results in the disruption of the TFIIH complex, followed by host transcription shut-off (Cyr et al., 2015). Interestingly, this work shows that mutant C39S/C40S is still capable of entering the nucleus and that it efficiently degrades p62. The mutant also formed nuclear filaments, although this formation seemed much less efficient than that of wild type NSs. Apart from the ability of NSs to downregulate general host transcription, NSs also directly interacts with SAP30, which is part of a Sin3A/NCoR/HDACs repressor complex. NSs recruits this repressor complex to the IFN-β promotor through YY1, inhibiting the production of IFN-β mRNA (Le May et al., 2008). Considering the findings of this study, it is conceivable that the C39S/C40S mutations compromise the interaction of NSs with this repressor complex.

CHAPTER 4

4 Virulence study in BALB/c mice

4.1 Introduction

RVFV is the causative agent of RVF, which causes clinical disease in humans and animals. The clinical manifestation ranges from moderate fever to fatal illness, suggesting that the host immune response determines disease severity. The RVFV infection in laboratory rodents mimics many aspects of the pathology in humans (Lorenzo et al., 2014; Ross et al., 2012). In particular, BALB/c mice are known to be susceptible to RVFV with lesions such as hepatitis and encephalitis, nearly equivalent to those observed in human disease (Smith et al., 2010).

Various animal models have been used to study RVFV pathogenesis and virulence, including inbred rat strains (Ritter et al., 2000; Anderson et al., 1987, Peters and Slone., 1982); specific mouse strains (do Valle et al., 2010), non-human primates (Morrill et al., 1989) and sheep (Kortekaas et al., 2012; Busquets et al., 2010). Differences in susceptibility to infection with RVFV have been shown in those different hosts. Different inbred rat strains have been shown to have variable susceptibility to RVFV infection. Wistar-Furth rats from an American breeding colony were found to be highly susceptible to infection with a RVFV isolated from a fatal hemorrhagic case of RVF (named ZH-501), whereas Lewis rats from the same American breeder were slightly resistant (Anderson et al., 1987). However, Wistar-Furth rats from a European breeder were shown to be slightly resistant to infection with the ZH-548 isolate, which was isolated from a febrile patient with uncomplicated illness. Lewis rats from the same European breeder were highly susceptible to ZH-548 (Ritter et al., 2000). These varying results are possibly explained by differences in host genetic backgrounds or differences in the RVFV isolates. Interestingly, there also seems to be a difference in virulence of viruses isolated from different geographic locations. Wistar-Furth rats that were highly susceptible to infection with the Egyptian ZH-501 isolate were shown to be relatively resistant to infection with RVF viruses isolated from fatal cases occurring during sub-Saharan African outbreaks. RVFV isolates that cause fatal infection in

Wistar-Furth rats and those that are less virulent differ in some generally conserved amino acids (Anderson et al., 1989).

In both animals and humans, the primary site of replication and the dominant target of RVFV pathology is the liver, where the virus replicates to high titers and causes necrosis and extensive damage of the hepatocytes via apoptosis (Anderson et al., 1987). The virus is also able to cross the blood-brain barrier and cause meningoencephalitis and retinitis (Anderson et al., 1987). Apart from these organs, the tropism of RVFV includes spleen, lymph nodes, heart, kidney, lung, pancreas and the adrenal glands (Smith et al., 2010). The disease is more severe in domestic ruminants than in other animal species and is particularly severe in pregnant animals where up to 90% of infected ruminants abort their fetuses. The very high level of viremia increases the chances of transmission to humans that handle infected tissues (Flick and Bouloy., 2005; Woods et al., 2002;). In the mouse model, the pathogenesis of RVFV in the liver and brain is mostly associated with chemokine and pro-inflammatory cytokine responses (Gray et al., 2012, McElroy et al., 2012). Specific host genetic factors seem to play an important role in the severity of disease caused by RVFV as shown by different responses to infection in different strains of inbred rats (Peters et al., 1989; Anderson et al., 1987).

The NSs protein of wtRVFV has been shown to have type-I IFN antagonist activity while this property is lacking in the NSs mutant viruses, including the Clone 13 which has an in frame deletion in the NSs gene (Billecocq et al., 2004; Bouloy et al., 2001). Studies using virus reassortants between the ZH548 strain of RVFV and the Clone 13 (Muller et al., 1995) suggested that RVFV mouse virulence is controlled by the S segment (Vialat et al., 2000). The importance of NSs for virulence was confirmed by using wtRVFV lacking the entire NSs gene (Bird et al., 2008).

The NSs protein contains five highly conserved cysteine residues at positions 39, 40, 149, 178 and 194. Cysteine is a highly reactive hydrophobic amino acid, capable of forming bridges between each other via covalent disulphide bonds, which stabilizes the tertiary and quaternary structure of proteins. Consequently, point mutations leading to substitutions of these amino acids may potentially affect the pathogenicity

of RVFV. In order to assess the role of these cysteines, the virulence of four NSs cysteine-to-serine mutants was studied in the BALB/c mouse model.

This chapter describes the evaluation of clinical, virological and histopathological responses of BALB/c mice to subcutaneous inoculation with the wtRVFV isolate 35/74 and the cysteine-to-serine mutants generated (C39S/C40S, C149S, C178S, C194S). Clinical signs were monitored daily until the end of the experiment (day 14). Full necropsy and sample collection was performed at scheduled time points or when mice were found moribund. The double mutant RVFV-C39S/C40S virus was highly attenuated with no clinical disease observed in mice. Clinical signs in mice infected with viruses containing cysteine-to-serine substitutions at either position 178 or 194 were similar to those occurring in mice infected with wtRVFV, while a mutant containing a substitution at position 149 caused mild, non-fatal disease.

4.2 Results

4.2.1 Evaluation of RVFV virulence in BALB/c mice

To study the role of conserved cysteines of the NSs protein in virulence, the clinical response to the cysteine mutants was compared with the parental wtRVFV. Before this study was initiated, the optimal dose to be used was first determined. Based on those results, the dose of $10^{2.85}$ PFU/mL, intermediary between the dose of $10^{3.85}$ and $10^{1.85}$ PFU/mL, was selected as the challenge dose for each of the mutant viruses used in this study (Figure 4.1).

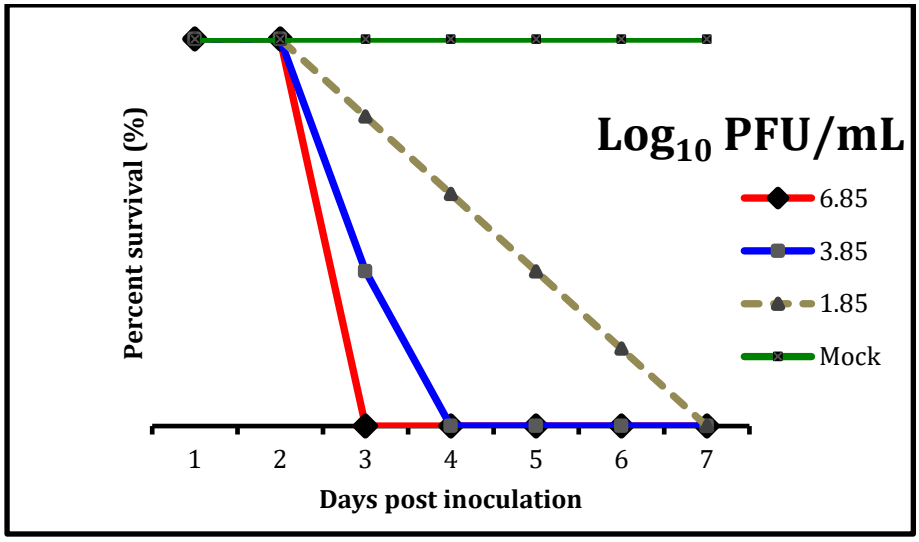

Figure 4.1 Clinical responses in BALB/c mice inoculated with different doses of wtRVFV. Three groups of BALB/c mice each containing five animals were inoculated subcutaneously (s.c.) with 100µl of tissue culture supernatant containing wtRVFV isolate 35/74 ($10^{6.85}$, $10^{3.85}$, or $10^{1.85}$ PFU/mL, respectively). The fourth group was mock inoculated s.c. with 100µl culture media serum free EMEM.

4.2.2 Survival of mice

In the main experiment, five experimental animal groups consisting of 15 BALB/c mice were inoculated s.c. with 100µl of tissue culture supernatants containing $10^{2.85}$ PFU/mL of wtRVFV isolate 35/74 or one of four mutants accordingly. Mice from group six were mock inoculated with culture medium. Experimental animals were monitored for clinical signs twice daily, weighed and temperatures recorded. Mice were scheduled for euthanasia on days 1, 3, 5, 7 and 14 p.i. After inoculation of mice with each of the mutants, some animals lost more weight than others but no statistically significant changes in body weights were observed between the experimental groups, as determined by paired t-test two-sample analysis (STATA version 13 (College Station, TX: StataCorp LP, College Station, USA). No significant differences were observed in the temperatures between the five experimental groups during the course of the experiment, the temperatures dropped below normal after the onset of clinical disease and none of the mice became febrile (results not shown).

Mock inoculated animals and animals infected with RVFV-C39S/C40S did not show any signs of clinical disease during the course of the experiment. Over half of the animals from the RVFV-C149S group showed signs of illness from day 3 to 5 p.i. (ruffled fur) but all started to recover from day 6 p.i., apart from one mouse that developed neurological disease noticeable on day 12 p.i. This mouse was euthanized on day 14 p.i. due to paralysis and excessive weight loss. Mice infected with RVFV-C178S and RVFV-C194S developed acute fatal disease clinically indistinguishable from that observed in mice infected with the wtRVFV. Animals from these experimental groups started showing signs of illness (i.e. ruffled fur and hunched posture) on day 2 p.i., and all succumbed to disease one to three days after onset of clinical signs (Figure 4.2).

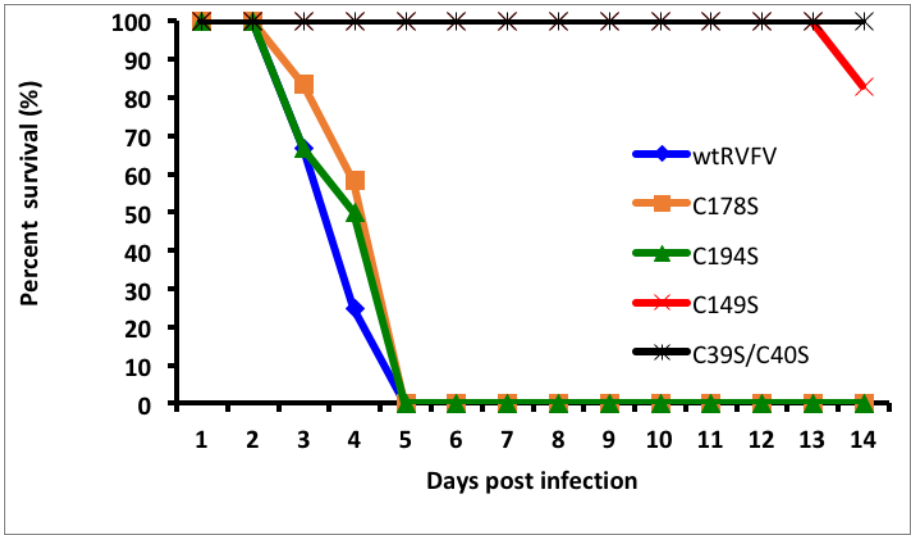

Figure 4.2 BALB/c mice survival following subcutaneous inoculation with 100µl of inoculum containing 102.85 PFU/mL wtRVFV isolate SA35/74 and the NSs mutants: RVFV-C194S, RVFV-C178S, RVFV-C149S and RVFV-C39S/C40S. The drop in the percentage of survival on the RVFV-C149S, day 14, is due to the death of a mouse with neurological disease, euthanized on day 14 p.i. Each experimental group consisted of 15 animals.

4.2.3 Detection of viral RNA by Q-RT-PCR in infected mice

The viral loads (RNA copies/mL) are shown in Figure 4.3. The values shown in the figure represent the average of 3 animals scheduled to be euthanized on each day. In few cases more than 3 mice were sampled due to the death of mice out of the scheduled time point. In other cases, less than 3 animals were sampled specifically in the case of serum samples when mice died before blood was collected. For example, on day 3 p.i. serum was taken from only two animals in the wtRVFV and RVFV-C178S groups due to death of the other mice scheduled for sampling before blood could be collected. On day 5 p.i., serum was taken from two animals in the RVFV-C178S and C194S groups and on day 14 p.i. serum was taken from only one mouse in the RVFV-C149S group that had to be euthanized after reaching a humane endpoint.

Replication of the wtRVFV and the mutant viruses was detected in all tissues tested (Figure 4.3). By day 5 p.i., all mice from the wtRVFV, RVFV-C194S and RVFV-C178S groups had succumbed to infection, therefore no data is shown for those groups on day 7 and 14 p.i. (Figure 4.3). In general, the brains had lower viral loads compared to the livers, spleens and sera. There were no significant differences ($p > 0.05$) between virus titers in the brain on day 3 and 5 p.i. in the different experimental groups.

The highest titer was detected in the brain of the mouse that developed neurological disease. There were significant differences ($p < 0.05$) between the virus titers of the wtRVFV group and the RVFV-C39S/C40S groups pertaining to liver, spleen, serum and brain samples, but no significant differences were observed in virus titers between the wtRVFV and the RVFV-C149S, RVFV-C194S and RVFV-C178S groups (Figure 4.3).

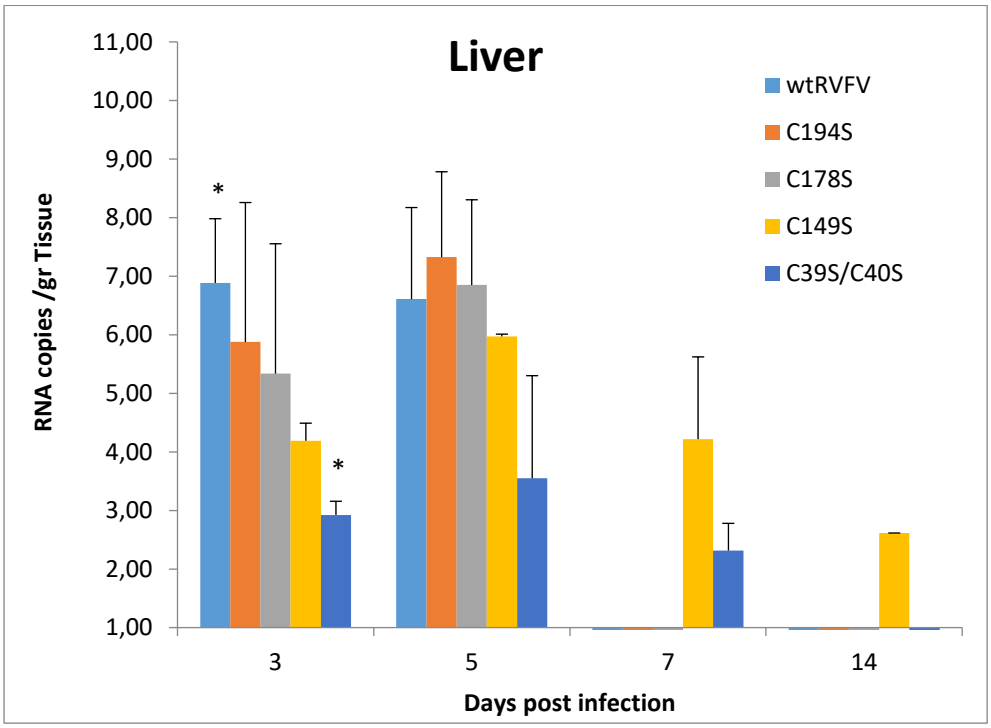

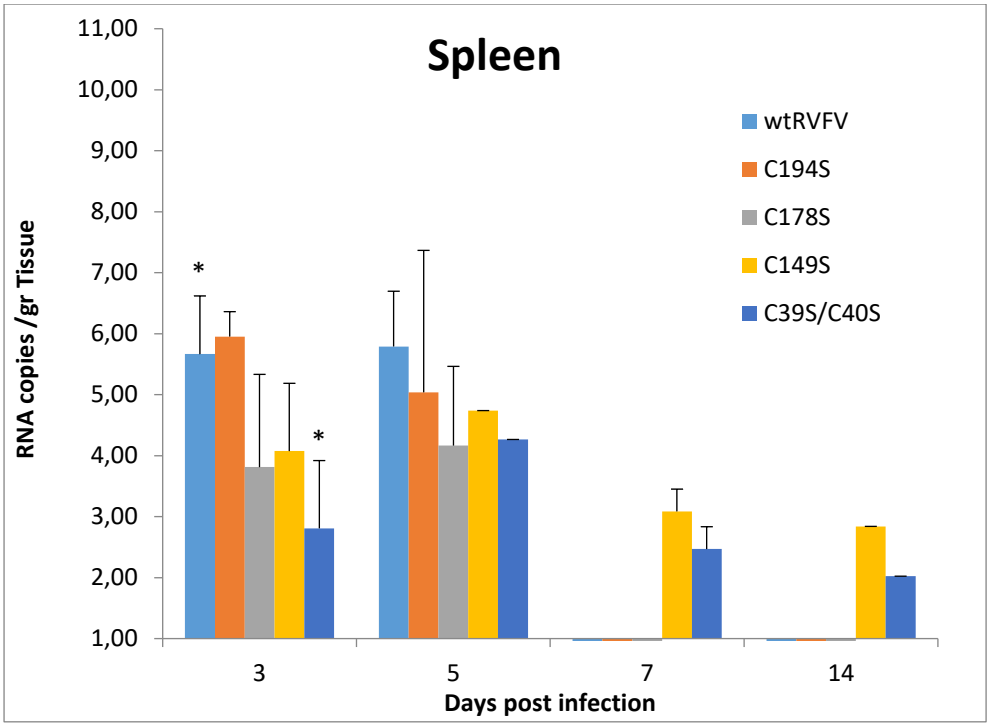
Spleen
RNA copies /gr Tissue
11,00
10,00
9,00
8,00
7,00
6,00
5,00
4,00
3,00
2,00
1,00
*
*
3
5
7
14
Days post infection
wtRVFV
C194S
C178S
C149S
C39S/C40S

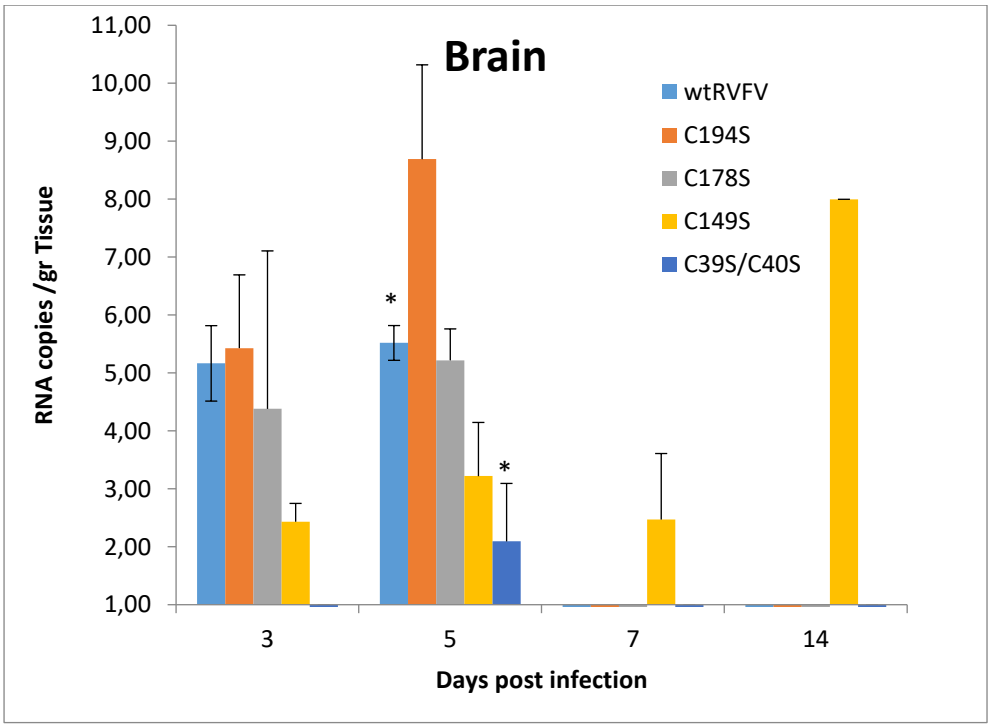
Brain
RNA copies /gr Tissue
11,00
10,00
9,00
8,00
7,00
6,00
5,00
4,00
3,00
2,00
1,00
*
*
3
5
7
14
Days post infection
wtRVFV
C194S
C178S
C149S
C39S/C40S

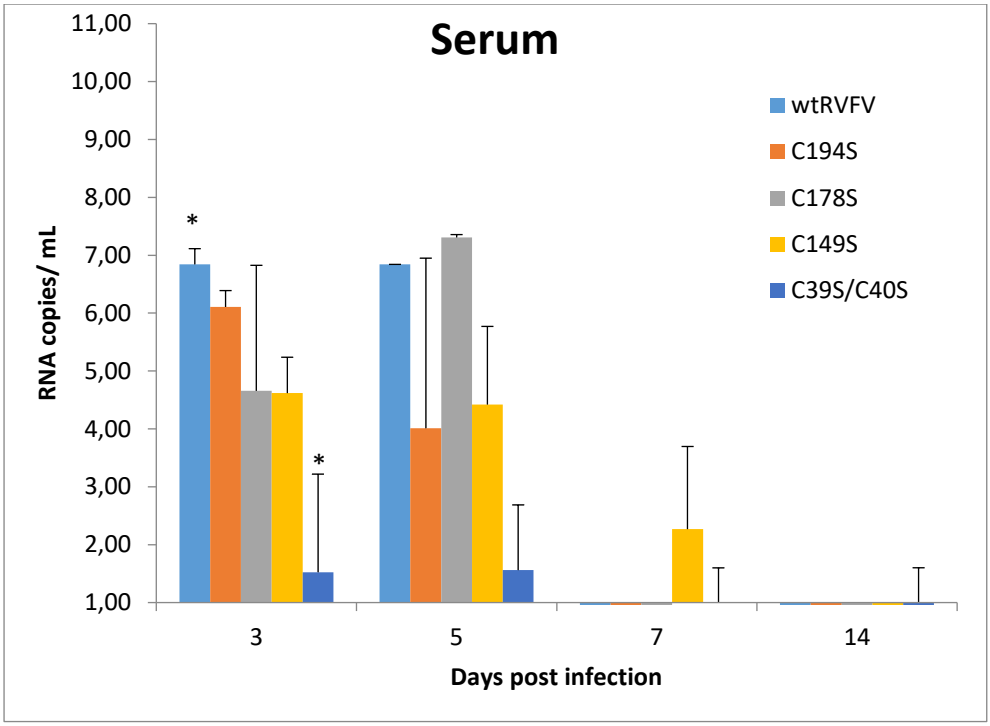

Figure 4.3 RVFV viral loads in tissues and sera of BALB/c mice infected with wtRVFV isolate 35/74 and the RVFV mutants (C194S, C178S, C149S and C39S/C40S). Samples collected on day 3 and 5 p.i. from mice infected with wtRVFV or mutants RVFV-C194S and RVFV-C178S and on day 3, 5, 7 and 14 p.i. for the RVFV-C178S and RVFV-C178S. Each bar represents the mean of RNA copies/g tissue or per mL of serum of mice in each of the experimental groups. The error bars represent the standard deviation. (*) indicates statistically significant differences (Kruskal-Wallis test $p < 0.05$).

4.2.4 Histopathology

To better understand the pathogenesis of the generated mutant viruses, we performed histopathological and IHC analysis of various organs of mice inoculated s.c. with $10^{2.85}$ PFU/mL of the wtRVFV and the mutant viruses. Hepatic and splenic histopathology scores and immunohistochemistry (IHC) findings are summarized in Table 4.1. Significant differences were observed in the severity of the histopathology between different experimental groups. The average histopathology scores of RVFV-infected liver (shown in Table 4.1) ranged from 2.8 (wtRVFV and RVFV-C178S) to 0.16 (RVFV-C39S/C40S), and in RVF-infected spleen it ranged from 2.4 (RVFV-C178S) to 0.6 (RVFV-C39S/C40S). The RVFV-C39S/C40S group was the least affected with only scattered single hepatocytes with morphological features of apoptosis observed in 1/6 cases examined, while no significant histopathology was observed in the remaining five cases (Figure 4.4-A). Lesion severity varied in the RVFV-C149S and RVFV-

C194S mutant groups from single cell morphological features of apoptosis (affecting only a few hepatocytes in 3/10 cases examined) to diffuse hepatic necrosis with hemorrhage in 4 other cases (Figure 4.4-B). Over half of the mice (9/11) in the wtRVFV and RVFV-C178S experimental groups had widespread hepatocyte necrosis involving most of the hepatic parenchyma, and was accompanied by hemorrhage and mild inflammation characterized by histiocytes with fewer degenerate and viable neutrophils. The portal tracts were preserved, with small groups of surviving limiting plate hepatocytes showing moderate to severe hydropic degeneration. One mouse in each of the wtRVFV and RVFV-C178S experimental groups exhibited moderate hepatic lesions with necrosis of up to 50% of the hepatic parenchyma (Figure 4.4-C). The remaining three cases in the mutant RVFV-C149S and RVFV-C194S groups exhibited moderate hepatic pathology characterized by necrosis of up to 50% of the hepatic parenchyma.

The spleens in all the experimentally infected mice exhibited varying degrees of lymphoid hyperplasia with coalescence of white pulp foci. Mice from the mutant RVFV-C39S/C40S group were least affected with 3/6 mice examined exhibiting no appreciable histopathology and the remaining three showing hyperplasia of the white pulp and scarce apoptotic lymphocytes within the follicular germinal centres (Figure 4.4-G). On average, splenic lesions were more severe in the wtRVFV, RVFV-C178S, RVFV-C194S and RVFV-C149S groups with most cases (10/19) exhibiting moderate hyperplasia with coalescence of the white pulp (Figure 4.4-H) and apoptosis of up to 50% of lymphocytes in follicular germinal centres (Figure 4.4-I). Some spleen specimens (5/19) exhibited apoptosis of more than 50% of the lymphocytes in the follicular germinal centres accompanied by marked diffuse red pulp atrophy. Red pulp atrophy was characterized by reticulosclerosis and a decrease in the number of lymphocytes, macrophages and extramedullary hematopoietic (EMH) cells as compared with the control mice (Figure 4.4-I). The spleen was normal in 1/4 cases in the wtRVFV, RVFV-C178S, RVFV-C194S and RVFV-C149S groups while the three other cases had mild white pulp hyperplasia and occasional lymphocytolysis within the follicular germinal centres.

In addition, nine mice, from the wtRVFV, RVFV-C178S, RVFV-C194S, and RVFV-C149S experimental groups exhibited mild pulmonary lesions including alveolar and

bronchiolar hemorrhages occasionally accompanied by variable alveolar and interstitial pulmonary edema. Myocardial hemorrhages were detected in one mouse from each mutant RVFV-C149S and RVFV-C194S group. No remarkable lesions were detected in the brain or kidneys from any of the mice examined. Mice in the mutant RVFV-C39/40S group had no lesions attributed to RVFV infection in any of the organs examined, including the lungs and heart.

4.3 Immunohistochemistry

The average immunohistochemistry (IHC) scores of RVFV-infected liver (Table 4.1) ranged from 3 (wtRVFV, RVFV-C178S) to 0.33 (RVFV-C39S/C40S), and from 1 (RVFV-C178S) to 0.2 (RVFV-C39S/C40S) in RVF-infected spleens. In the RVFV-C39S/C40S group, 4/6 cases were negative by IHC for the presence of viral antigen with only scarce single cells exhibiting positive labelling in the other two cases (Table 4.1). In the latter two cases, the labelled cells appeared histologically unaffected (Figure. 4.4-D). All the mice from the wtRVFV and RVFV-C178S experimental groups exhibited widespread fine diffuse to coarse granular immunolabelling in the cytoplasm of necrotic hepatocytes (Figure 4.4-E). Immunolabelling was less consistent in mice from the RVFV-C149S and RVFV-C194S groups with results varying from widespread labelling in four cases, to multifocal labelling of up to 50% of necrotic hepatocyte in two mice and sparse labelling of single cells or small groups of hepatocytes in the remaining four cases. Positively labelled cytoplasmic fragments were frequently detected within hepatic sinusoids and central veins of these mice and dissolution of viral antigens seemed to occur within necrotic foci with labelling tending to be pale and diffuse or completely cleared from some areas (Figure 4.4-F). Lymphocytes (whether apoptotic or not) did not stain for RVFV antigen in any of the organ samples, including the spleen.

Table 4.1. Histopathology (HP) and immunohistochemistry (IHC) scoring of mouse tissues infected with wtRVFV and the NSs mutants. Experimental groups are arranged according to the severity of the lesions.

Mouse number	Experimental group/Virus strain	Days post inoculation	HP score		IHC score	
			Liver	Spleen	Liver	Spleen
I/wtRVFV						
4		3	3	2	3	0
6		3	2	1	3	0
7		3	3	2	3	1
9		5	3	2	3	0
15		3	3	2	3	1
Group average			2.8	1.8	3	0.4
III/RVFV-C178S						
49		3	2	2	3	1
52		3	3	3	3	1
53		5	3	2	3	1
56		5	3	3	3	1
57		5	3	2	3	1
58		5	3	2	3	1
Group average			2.8	2.4	3	1
II/RVFV-C194S						
64		3	1	2	2	1
65		3	2	ns	3	ns
66		3	1	1	2	0
70		3	3	3	3	1
72		5	3	3	3	1
Group average			2	2.3	3	1
IV/RVFV-C149S						
34		3	2	ns	1	ns
36		3	1	0	1	0
37		5	3	3	1	0
38		5	2	1	1	0
39		5	3	2	3	1
Group average			2.2	1.5	1.4	0.25
V/RVFV-C39S/C40S						
19		3	0	0		0

20		3	0	0		0
21		3	0	ns		1
22		5	0	1		0
23		5	0	1		0
24		5	1	1		1
Group average			0.16	0.6	0.3	0.2
VI/Control						
77		14	0	0		0
78		14	0	0		0
Group average			0	0	0	0

HP and IHC scores refer to are the assigned histopathology and immunohistochemistry scores as described in Table 2.5, 2.6 and 2.7.

ns - tissue not sampled.

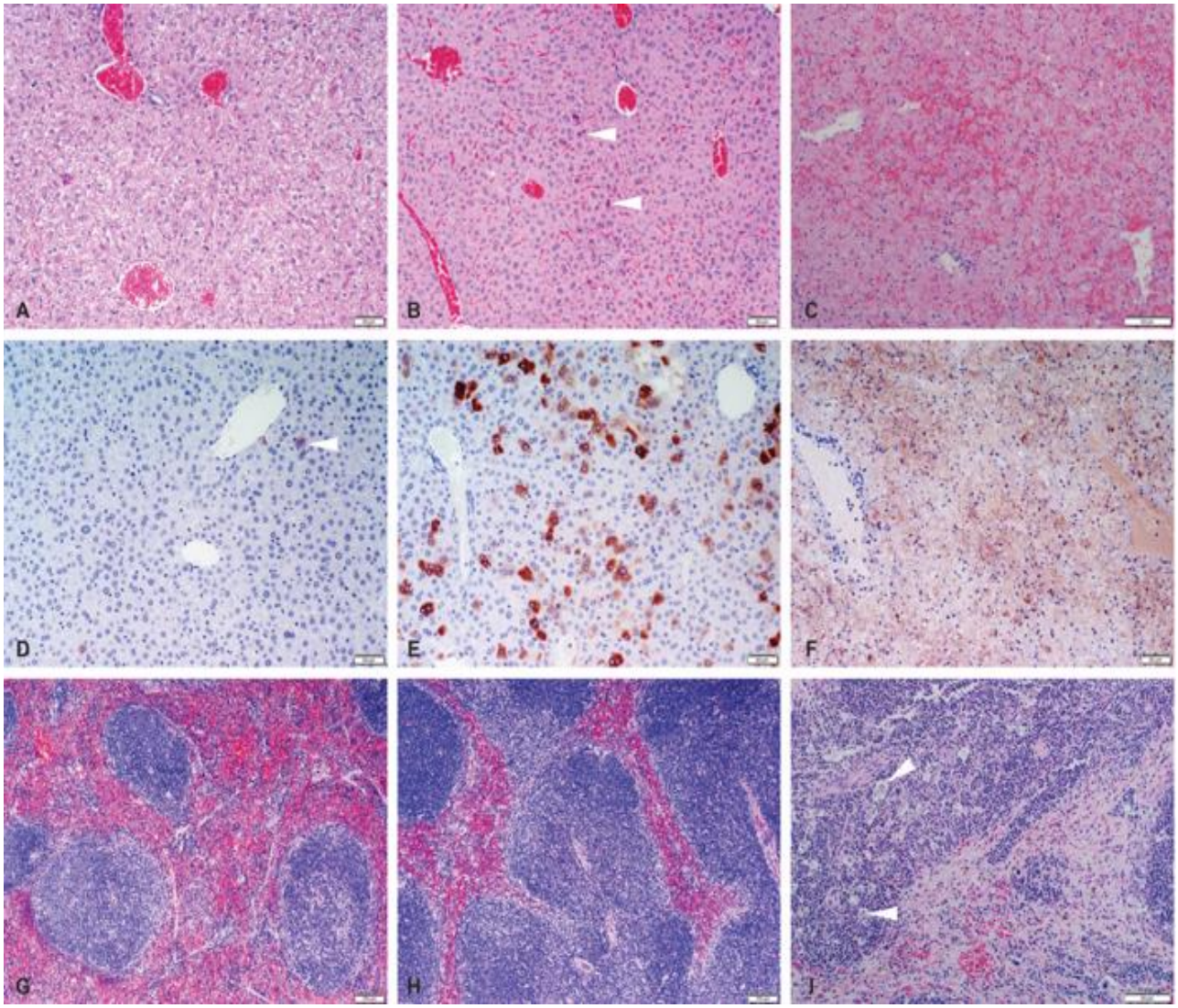

Figure 4.4 (A-I) Liver and spleen histopathological and immunohistochemical findings in BALB/c mice experimentally infected with wtRVFV and NSs mutants. Samples in panels A, B, C, G, H and I were stained with hematoxylin and eosin. Antigens in samples depicted in panels D, E and F were detected by immunoperoxidase methods with NovaRED chromogen and hematoxylin counterstain. Polyclonal hyperimmune mouse serum was used as the primary antibody and a rabbit anti-mouse antibody as the secondary antibody. Scale bars represent 100µm and 50µm resolution. A: Moderate hepatocellular hydropic change (histopathology score 0) in mouse 21 infected with RVFV-C39S/C40S. B: Multifocal hepatocyte apoptosis (arrowheads) involving single cells to small groups of 2-5 cells (histopathology score 1) in mouse 66 infected with RVFV-C194S. C: Severe diffuse hepatocyte necrosis (histopathology score 3) in mouse 9 infected with wtRVFV. D: Fine diffuse granular cytoplasmic immunolabelling of a few normal hepatocytes (arrowhead) in mouse 21 from the RVFV-C39S/C40S group. E: RVFV-specific positive labelling in multifocal hepatocytes in mouse 66 from the RVFV-C194S group. F: Diffuse intracytoplasmic RVFV-specific positive signal within necrotic foci in mouse 9 from the wtRVFV group. G: Normal spleen showing the ratio of white pulp to red pulp approaching 1:1.5 in control mouse 78. H: Prominent expansion and coalescence of the white pulp (histopathology score 1) in mouse 24 infected with RVFV-C39S/C40S. I: Prominent lymphocyte apoptosis associated with tingible body macrophages (arrowheads) and severe diffuse red pulp atrophy (histopathology score 2) in mouse 56 infected with RVFV-C178S.

4.4 Discussion

The results of this study show that mutating specific highly conserved cysteine residues of the RVFV NSs protein results in differential outcomes of RVFV infection in mice. The RVFV infection in laboratory rodents mimics many aspects of pathology in humans. Mice are highly susceptible to infection with RVFV by subcutaneous or intraperitoneal infection leading to fulminant acute hepatitis and and a late developing encephalitis. Lymphoid tissues are also affected and the mais lymphoid lesion is lymphocite apoptosis. Substitutions of conserved cysteine residues at positions 39 and 40 in the NSs gene of RVFV resulted in significant attenuation of the virus as evidenced by clinical, virological, histopathological examination. Mice infected with the RVFV-C39S/C40S mutant virus were most likely able to control virus replication by the early innate immune response, which allowed them to survive long enough to elicit an adaptive immune response. The RVFV-C39S/C40S infected mice showed no RVFV-specific pathology, with only scattered single cells hepatocellular apoptosis in 50% of the samples. An interesting finding was the fact that mice inoculated with the RVFV-C149S virus manifested mild disease from day 2 p.i., but all mice recovered except for one that developed a neurological manifestation of the disease by day 12 p.i. However, all remaining animals were euthanized at the scheduled end-point of day 14 p.i. which might have prevented the observation of a similar biphasic disease in the rest of the animals from this group. It was previously described that animals that survive the initial hepatitis effectively clear the virus from the liver and blood, but exhibit neuroinvasion and develop neurological disease (Smith at al., 2010). This observation was confirmed in this study by the results of viral loads showing a decrease of viral loads in the liver, spleen and brain, and an increase in the brain fom day 7 to 14 p.i. In contrast, viruses with cysteine-to-serine substitutions of conserved cysteines at positions 178 and 194 for serines were phenotypically similar to the wtRVFV, causing an acute fatal disease in BALB/c mice. All mutations remained stable after experimental infection of mice, therefore the virulence of RVFV-C179S and RVFV-C194S viruses cannot be attributed to reversion of the serines back to cysteines at these two positions. The mice in the wtRVFV, RVFV-C149S, RVFV-C179S and RVFV-C194S experimental groups exhibited different degrees of hepatic histopathology ranging from severe widespread hepatocyte necrosis and hemorrhage to moderate hepatic lesions with necrosis of up

to 50% of the hepatic parenchyma. These lesions are characteristic of RVFV infection and were observed in previous studies (Gray et al., 2012). The pathogenesis of RVFV in mice is associated with loss of liver function due to liver necrosis and hepatitis. In addition to the liver lesions, prominent lymphocyte apoptosis was observed in the spleens of the wtRVFV, RVFV-C149S, RVFV-C178S and RVFV-C194S infected mice. The histopathology and immunohistochemical findings were associated with high viral loads in target organs. The RVFV-C39S/C40S was highly attenuated in mice as evidenced by the absence of clinical signs of disease and the low titers of virus in different organs. Histopathological lesions characteristic of RVFV infection were not observed in the livers or other organs in the RVFV-C39S/C40S group. Similar results have been reported previously for Clone 13 and MP-12 (Muller et al., 1995).

The high level of attenuation of mutant C39S/C40S *in vivo* was expected considering its ability to replicate less efficiently in IFN-competent cells *in vitro*. This suggests that its attenuated phenotype may be due to a compromised IFN-antagonistic function. Another function of NSs, which is independent of its IFN-antagonistic function, is its ability to promote PKR degradation (Kalveram et al., 2013). Indeed, western blot analysis showed decreasing levels of PKR between 8 and 12 h.p.i. in cells infected with wtRVFV, whereas PKR levels in cells infected with the mutant C39S/C40S were unaffected. This finding provides further evidence that the high pathogenicity of RVFV is related to its ability to degrade PKR (Habjan et al., 2009a). The molecular evaluation of the basis of virulence attenuation is discussed in chapter 5.

CHAPTER 5

5 Cytokine gene expression studies

5.1 Introduction

Cytokines are small soluble molecules with pleiotropic functions, produced by different cell types as part of a gene expression pattern. They are capable of influencing and regulating the functioning of the immune system. Interferons are a family of cytokines produced in response to infection with pathogens and play a pivotal role in immunity against viruses. The type-I IFNs are produced by virus-infected cells. IFN-α and INF-β subsets, which are produced by neutrophils and helper T cells, activate the transcription of hundreds of IFN-stimulated genes (ISGs) (Schneider et al., 2014). Most of the products of the ISG exert antiviral activity at every step of the viral replication cycle and also possess antiproliferative and immunomodulatory functions (Wuerth and Weber, 2016). The function of the well characterized ISGs have been reviewed in MacMicking., 2012 and Schneider et al., 2014. IFN-inducible transmembrane protein (IFITM) interferes with fusion of the viral envelope at the plasma membrane (IFITM1) or in the endosomal pathway (IFITM2,3) and consequently, the release of viral RNPs into the cytoplasm of infected cells. In addition, the family of dynamin-like GTPases are capable of restricting a wide range of viruses via trapping of incoming viral RNPs (Haller et al., 2015). Expression of the transcription factor IRF7 is also enhanced by IFN signaling. In addition to the direct antiviral effects of ISGs and the positive feedback loop via IRF7, type-I IFN signaling also induces the production of a range of cytokines and chemokines, pro- and anti-apoptotic factors, and affects multiple other signaling pathways. Through modulation of the differentiation and function of dendritic cells, T cells, natural killer (NK) cells and B cells, type-I IFNs modulate antiviral immunity beyond the initial innate immune response (McNab et al., 2015; Schneider et al., 2014; MacMicking et al., 2012).

The NSs protein of RVFV is an IFN-antagonist and this feature is manifested by different mechanisms. Comparative studies using the naturally-attenuated RVFV strain Clone 13 and the virulent RVFV isolate ZH548, as well as reassortants between these two viruses, showed that the S segment carries the determinant for attenuation

and interference with IFN-α/β production in the murine model (Bouloy et al., 2001; Vialat et al., 2000).

The pathogenic effects of RVFV infection is correlated with the host immune response to infection (Gray et al., 2012). In order to access the state of the immune response during RVFV infection, this chapter describes the analysis of expression levels of cytokine gene transcripts in two major organs; liver and spleen of BALB/c mice, 3 and 5 days after s.c. inoculation with the cysteine-to-serine mutant C39S/C40S and the wtRVFV isolate 35/74. These organs were chosen because they have been associated with RVFV pathogenicity (Odendaal et al., 2018; Anderson et al., 1987). Two panels of PCR arrays were analyzed; the “type-I IFN response” and the “inflammatory cytokines and receptors” pathways, making use of the RT^2 profiler pathway “signature” PCR array and the Cyber Green master mix which contain the hot start polymerase, dNTPs, MgCl2 and reaction buffers at optimal concentrations ready to use. The RT^2 profiler pathway “signature” PCR array combines the real time PCR performance and the ability of microarrays to detect the expression of many genes simultaneously. These PCR arrays are designed to analyze a panel of genes related to a biological pathway and determines intracellular status of pathway activity. The array along with the participating algorithm indicates whether the pathway is activated, repressed or activity remains unchanged in experimental samples as compared to control samples. The 96 plate format of the RT^2 profiler pathway PCR array contains primer sets for 84 pathway focused genes, including a set of genes empirically determined to predict the change in activity of pathway, plus five housekeeping genes, three reverse transcription controls and three PCR controls are included in the last row of the plate. The results showed that the pattern of up- or downregulation of some type-I IFN and inflammatory cytokine gene transcripts were not identical in both groups.

5.2 Results

5.2.1 Cytokine gene expression in RVFV infected mice

Two panels of gene arrays each targeting 84 genes encoding proteins involved in inflammation and the type-I IFN response (Qiagen, Hilden, Germany), were used to determine the levels of transcripts in the livers and spleens of mice inoculated with wtRVFV and RVFV-C39S/C40S. A mock inoculated control group was used to normalize the data. These two groups were specially selected based on the different outcomes of infection in BALB/c mice as demonstrated by clinical signs, viral loads and histopathology lesions. The number of transcripts significantly up- or downregulated ($p < 0.05$) are summarized in Table 5.1.

Table 5.1. Number of transcripts up- and downregulated in the livers and spleens of mutant NSsC39S/C40S and wtRVFV. Samples were collected on day 3 and 5 p.i.

			Type-I interferon response (PAMM-016ZA Qiagen)		Inflammatory cytokines (PAMM-011ZA Qiagen)	
RVFV Virus strain	Days p.i.	Organs	No of genes significantly upregulated	No of genes significantly downegulated	No of genes significantly upregulated	No of genes significantly downegulated
wtRVFV	3	Liver	35	3	8	0
		Spleen	1	1	12	13
	5	Liver	31	2	22	0
		Spleen	5	1	16	17
RVFV-C39S/C40S	3	Liver	0	0	0	3
		Spleen	0	0	0	1
	5	Liver	0	0	0	3
		Spleen	0	0	2	6

5.2.1.1 Inflammatory cytokine and receptor array.

The pattern of up- or downregulation, or no change, was not identical between liver and spleen tissues within the same experimental groups except for transcripts for the genes CCCL12, CCLl2, CCL3, CCL7, CXCLl1, CXCL11, CXCL19, IL11, IL7b, IL4, LTA and OSM, which were upregulated in both liver and spleen samples of wtRVFV infected mice. Transcripts for the genes CCR10, CXCL1, IL17b, IL4, LTa and LTb,

were similarly up- or downregulated in the livers or spleens from mice infected with wtRVFV or RVFV-C39S/C40S. The transcripts of the genes BMP2, CCCL11, CCL12, CCL2, CC22, CCL24, CCL24, CCL3, CCL4, CcCL5, CCL7, CCR1, CCR2, CCR3, CCR4, CCR6, CCR8, CD40Lg, CSF1, CXCL1, CXCL11, CXCL19, CXCR3, FASL, IL10Rb, IL11, IL1a, IL27, IL2Rg, IL33, IL6Ra, IL7, IL16, NAMPT, SPP1, TNF, TNFRSF11 and TNFSF13 were differently up- or downregulated in livers or spleens of wtRVFV and RVFV-C39S/C40S. The relative expression levels of the rest of the gene transcripts in the array were either unchanged, or changes were not statistically significant in livers and spleens from both experimental groups (Table A.1 in Appendix 3).

5.2.1.2 The type-I IFN response array.

The pattern of up- or downregulation, or no change, was variable between liver and spleen tissues within the same experimental groups. The gene transcripts for IFI30, MX1, MX2 and TAP1 were similarly upregulated in the livers and spleens of the mice inoculated with wtRVFV. There was no similarity on up- or downregulation of transcripts from the two experimental groups. The gene transcripts ADAR, BST2, CASP1, CCL2, CCL4, CCL5, CD69, CD86, CD86, CDKN1b, CRP, DDX58, EIF2ak2, GBP2b, H2-KL, H2-M3, IFI204, IFI30, IFIh1, IFIT1, IFIT2, IFIT3, IFITM1, IIFITM3, IFNA2, IFNA4, IFNB1, IFNZ, IL10, IL6, IRF7, IRF9, ISG15, ISG20, JAK1, JAK2, MAL, MET, MX1, MX2, OAS1a, OAS1b, PML, PSME2, STAT1, STAT2, STAT3, TAP1, TIMP1, TLR3, TLR8, TLR9 and TRAF3 were significantly either up- or downregulated in livers or spleens of one of the experimental groups, but unchanged in the other group. The relative expression levels of the rest of the gene transcripts in the array in liver and spleen of both experimental groups were either unchanged or changes where not statistically significant (Table A.2 in Appendix 4).

The up- and downregulated transcripts that reached statistical significance were grouped in categories according to their role in the antiviral immune response as follows: (1) IFNs; (2) IFN signaling pathways, (3) IFN-induced proteins (restriction factors), (4) IFN biosynthetic process and (5) antigen presentation. The fold changes in expression of those gene transcripts are presented in Figure 5.1, showing an overall state of mostly upregulation of gene transcription in wtRVFV infected mice, while in

the C39S/C40S-infected mice, few gene transcripts were downregulated and the majority were unchanged.

In the IFN category, IFNB1 gene transcripts were upregulated the highest by 2537.38-fold in wtRVFV-infected mice, followed by IFNA4 and IFNA2 with 202.5- and 104.12-fold increases, respectively. The IFNZ and IIFNE transcripts in the liver of wtRVFV-infected mice increased with fold changes of 2.58 and 11.47, respectively.

In the spleen, the IFNB1 transcript was the upregulated the highest with a 6.97-fold increase, followed by IIFNA4 transcripts that increased by 3.22-fold. The levels of IFNA2 transcripts were unaffected. The IFNZ and IFNE transcripts were downregulated. Conversely, in the group of RVFV-C39S/C40S infected mice, these genes were expressed at normal levels in the liver on day 3 p.i. and downregulated on day 5 p.i. except for the IFNA2 transcript that was downregulated on day 3 p.i. and reached normal levels on day 5 p.i. In the spleen samples, no changes were detected. The transcripts were all regulated at normal levels either on day 3 or 5 p.i. In the group of IFN signaling pathways, the most notable gene transcripts that were up- or downregulated were IRF7, IRF9, JAK1, JAK2, STAT1, STAT2, STAT3 and TAP1. Within this group, the TLR9 transcript was the only transcript upregulated in the liver of both experimental groups, while the JAK1, STAT2 and TAP1 transcripts were upregulated in the spleen of both experimental groups.

In the group of IFN induced gene expression (restriction factors), the gene transcripts ADAR, EIF2ak2/PKR, IFIT2, IFIT1, IFIT2, IFIT3, IFITM1, IFITM3, ISG15 and ISG20 were most notably upregulated in the livers and spleens of the wtRVFV infected group, but were unchanged in the RVFV-C39S/C40S group. The IFIH1, MX1 and OAS1b transcripts were upregulated in the livers of both experimental groups, and OAS1a transcripts were upregulated in the spleens of both experimental groups. In the category of IFN biosynthetic process, DDX58/RIG-I and TLR8 were upregulated in the wtRVFV group, while TLR9 was upregulated in the livers of both experimental groups. In all the categories, either in the liver or spleen samples, the fold increase was higher in the wtRVFV experimental group as compared to the RFFV-C39S/C40S.

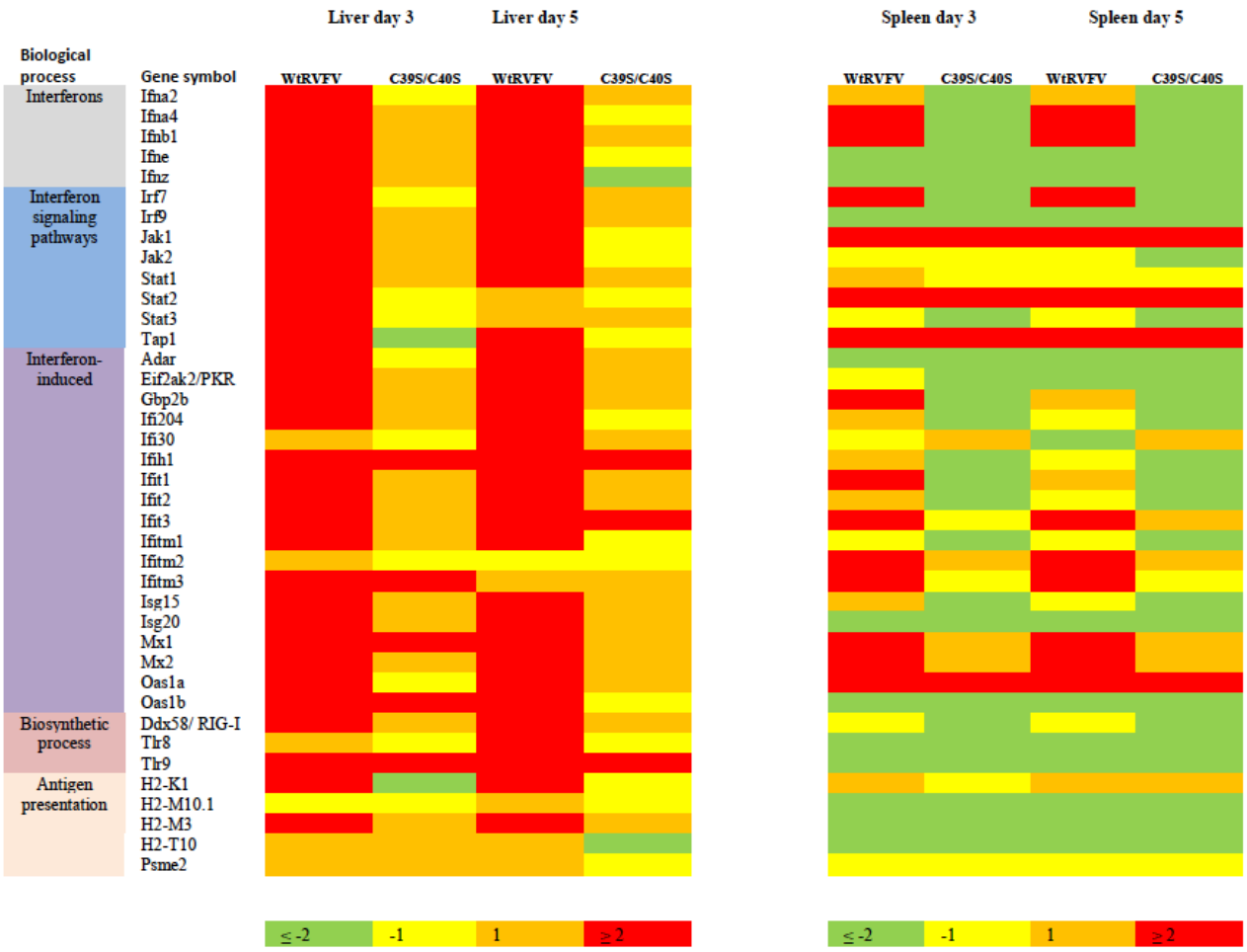

Figure 5.1 Heat map showing relative levels of RVFV-responsive gene trancripts related to the type-I IFN response. Expression profiles show significant up- or downregulation of gene transcripts in the livers and spleens of mice inoculated with wtRVFV and RVFV-C39S/C40S, on days 3 and 5 p.i. Green and red squares represent reduced and induced levels, respectively. Yellow squares indicate no changes in expression levels. The color scale at the bottom indicates the magnitude of change. Data from three biological replicates are shown for each experimental condition. Please refer to appendix 3 for the description of gene names corresponding to the symbols in the picture.

5.3 Discussion

The innate immune response to infection with the wtRVFV was associated with increased expression of most inflammatory cytokines and receptor genes in the liver and spleen samples. This was in direct contrast to the mice inoculated with the RVFV-C39S/C40S whereby no such upregulation was observed. Furthermore, the expression of different IFNs and interferon-induced proteins followed the very same pattern, with the majority of transcripts upregulated in the wtRVFV infected mice. Transcripts of the CCL4 gene, which encodes the chemokine ligand 4, also known as Macrophage inflammatory protein-1β, was highly expressed in wtRVFV infected mice, (42-45 fold upregulated in the liver and 6-12-fold in the spleen), compared to slightly lower than normal levels (± 2-fold downregulated) in RVFV-C39S/C40S-infected mice. This protein serves as a chemoattractant for neutrophils that produce other pro-inflammatory cytokines such as IL-1, IL-6 and TNF-α. Indeed, transcripts for TNF-α were also highly upregulated (165-205 fold) in wtRVFV-infected mice, but were normally expressed in RVFV-C39S/C40S mice. The upregulation of transcripts encoding the pro-inflammatory cytokines CCL2, CCL4, CSF1, and CXCL10 along with the upregulation of transcripts for the pro-apoptotic cytokine TNF-α and the chemokines CCR1, CCR2, CCR2 and CXCR3 are indicative of a strong inflammatory response and probably contributed to the liver damage observed in wtRVFV-infected animals. These transcripts were detected at normal levels in RVFV-C39S/C40S-infected animals, where no RVFV-specific liver pathology was observed.

The transcription levels for the pro-apoptotic TNF-α and the pro-inflammatory cytokine genes CCL2, CCL4, CSF1 and CXCL10 were normal or downregulated in RVFV-C39S/C40S-infected mice. This suggests that by the time of sampling (day 3 and 5 p.i.), the mice infected with RVFV-C39S/C40S had already sufficiently responded with innate immune mechanisms to control virus replication. It is thus likely that due to the mutations C39S/C40S in the NSs gene, the protein was not able to counteract very early IFN responses in the mice, resulting in decreased replication and a subsequent non-fatal outcome. Interestingly, in a previous study by McElroy et al., it was demonstrated that wtRVFV infection in human monocyte-derived macrophages lead to a productive infection and inhibition of the innate immune response via decreased expression of IFNα2, IFBβ and TFN-α. Using a recombinant virus lacking the NSs

protein, their results showed that this effect was mediated by the viral NSs protein (McElroy et al., 2012). Interestingly, previous studies involving other hemorrhagic fever viruses such as Ebola virus and Crimean Congo Hemorrhagic Fever virus demonstrated that release of pro-inflammatory cytokines in *in vitro* cell culture and animal models were associated with a pro-inflammatory response and increased fatality when examining clinical specimens (Connolly-Anderson et al., 2009, Hutchinson and Rollin 2007).

Infection with the wtRVFV virus resulted in downregulation of expression of the gene encoding Proteasome activator complex subunit 2 (PSME2), compared to normal expression levels in RVFV-C39S/C40S infected mice. This suggests a counteraction of the proteasome activity in wtRVFV infected mice. The proteasome plays an important role in the adaptive immune response by processing viral antigens to generate immunogenic peptides which are in turn displayed by major histocompatibility complex class I proteins on the surface of virus infected cells as well as antigen presenting cells (dendritic cells) to stimulate antiviral cytotoxic T cell responses. Therefore, wtRVFV infected mice would not be able to develop an efficient adaptive response to assist in viral clearance. There was activation of expression of pro-apoptotic genes (ADAR, CASP1, CCL2, CCL5-RANTES, PRKCZ, PML, STAT1, BAG3, IL10) in wtRVFV-infected mice but not in the RVFV-C39S/C40S infected mice. This probably contributed to hepatic damage, an important pathologic feature of RVFV infection.

CHAPTER 6

6 Conclusions and future directions

The NSs protein of RVFV is an important virulence factor that inhibits type-I IFN responses. This thesis brings the first insights on the effects of RVFV NSs cysteine-to-serine mutations in virulence. Compared to wtRVFV, significant differences were observed in clinical, virological, histopathological responses and host gene expression levels following infection of BALB/c mice with the RVFV-C39S/C40S mutant, but not with the mutant viruses having cysteine-to-serine mutations at positions 149, 178 and 194. While wtRVFV causes acute fatal disease marked by the upregulation of pro-inflammatory cytokines and upregulation of type-I IFN-stimulated gene transcripts in the liver, mutant RVFV-C39S/C40S was highly attenuated in mice and no such upregulations were observed. These findings show an association between a pro-inflammatory response and death of mice. Interestingly, out of five conserved cysteines, only the mutation of a pair of adjacent cysteines resulted in attenuation, while individual mutations of the other three cysteine residues had variable effects ranging from partial to no attenuation at all. Considering the importance of cysteines in protein folding, it is intriguing that the virus tolerates the loss of some highly conserved cysteines in the NSs protein. The fact that the mutant C39S/C40S replicated less efficiently in IFN-competent cells *in vitro* suggests that the IFN-antagonistic function of this NSs mutant is significantly compromised, whereas the results from western blot analysis suggest that its attenuated phenotype is explained by an inability to promote the degradation of PKR. The attenuated phenotype of the mutant C39S/C40S was correlated with a compromised ability to degrade PKR and a reduced ability to downregulate IFN-β mRNA transcription.

Since only mutants containing mutations at residues 39 and 40 showed phenotypic attenuated virulence and cysteines 149, 178 and 194 can be removed without affecting the RVFV virulence in mice, cysteines 39 and 40 may be the most crucial of the five cysteines for disulphide link stabilization. It was also interesting to note that mutants having the mutation at cysteine 149 caused mild non-fatal disease in mice. It would be of value to study the biological properties of this particular mutant. Cysteines form disulphide bonds between each other and the effect of individual mutation at cysteines

39 and 40 along with other combinations of mutations including the mutations at positions 178 and 194 in RVFV virulence would be worthy of further study.

Studies of virus dissociation and assembly have implicated disulphide bonds in the stabilization of the viral capsid. Although RVFV NSs structural studies are rare, RVFV NSs crystallography studies were carried out but information regarding the NSs disulphide bonds and folding are not available. Also, specific positions of cysteines and its interactions have not been established for phleboviruses. Future research on RVFV NSs using crystallography will help to elucidate the structure of the mutant NSs proteins and determine whether cysteines 39/40 form disulphide bonds with each other and whether the other combinations of cysteine mutations can lead to attenuated virulence, a question that this study did not answer.

7 References

AITKEN, S.C., 2008. Variation in the S segment of Rift Valley fever virus with special reference to the nonstructural NSs coding region. *MSc dissertation. University of Witwatersrand,* pp. 18-40.

AL-HAZMI, M., AYOOLA, E.A., ABDURAHMAN, M., BANZAL, S. et al. 2003. Epidemic Rift Valley fever in Saudi Arabia: a clinical study of severe illness in humans. *Clinical infectious diseases: an official publication of the Infectious Diseases Society of America,* **36**(3), pp. 245-252.

ALBARINO, C.G., BIRD, B.H. and NICHOL, S.T., 2007. A shared transcription termination signal on negative and ambisense RNA genome segments of Rift Valley fever, sandfly fever Sicilian, and Toscana viruses. *Journal of Virology,* **81**(10), pp. 5246-5256.

ANDERSON, G.W., JR and SMITH, J.F., 1987. Immunoelectron microscopy of Rift Valley fever viral morphogenesis in primary rat hepatocytes. *Virology,* **161**(1), pp. 91-100.

ANDERSON, G.W.,JR, SALUZZO, J.F., KSIAZEK, T.G., SMITH, J.F., ENNIS, W., THUREEN, D., PETERS, C.J. and DIGOUTTE, J.P., 1989. Comparison of *in vitro* and *in vivo* systems for propagation of Rift Valley fever virus from clinical specimens. *Research in Virology,* **140**(2), pp. 129-138.

ANDERSON, G.W.,JR, SLONE, T.W.,JR and PETERS, C.J., 1987. Pathogenesis of Rift Valley fever virus (RVFV) in inbred rats. *Microbial Pathogenesis,* **2**(4), pp. 283-293.

ANDRIAMANDIMBY, S.F., RANDRIANARIVO-SOLOFONIAINA, A.E., JEANMAIRE, E.M. et al. 2010. Rift Valley fever during rainy seasons, Madagascar, 2008 and 2009. *Emerging infectious diseases,* **16**(6), pp. 963-970.

ARCHER, B.N., WEYER, J., PAWESKA, J., NKOSI, D., LEMAN, P., TINT, K.S. and BLUMBERG, L., 2011. Outbreak of Rift Valley fever affecting veterinarians and farmers in South Africa, 2008. *South African medical journal = Suid-Afrikaanse tydskrif vir geneeskunde,* **101**(4), pp. 263-266.

ATASHEVA, S., AKHRYMUK, M., FROLOVA, E.I. and FROLOV, I., 2012. New PARP gene with an anti-alphavirus function. *Journal of Virology,* **86**(15), pp. 8147-8160.

BAER, A., KEHN-HALL, K., 2014. Viral concentration determination through plaque assays: using traditional and novel overlay systems. *Journal of Visualized Experiments*, **93**, e52065.

BALKHY, H.H. and MEMISH, Z.A., 2003. Rift Valley fever: an uninvited zoonosis in the Arabian peninsula. *International Journal of Antimicrobial Agents,* **21**(2), pp. 153-157.

BARNARD, B. J. 1979. Rift Valley fever vaccine—antibody and immune response in cattle to a live and an inactivated vaccine. *Journal of South African Veterinary. Association,* **50**, pp. 155–157.

BARSKI, M., BRENNAN, B., MILLER, O.K., POTTER, J.A., VIJAYAKRISHNAN, S., BHELLA, D., NAISMITH, J.H., ELLIOTT, R.M. and SCHWARZ-LINEK, U., 2017. Rift Valley fever phlebovirus NSs protein core domain structure suggests molecular basis for nuclear filaments. *eLife,* **6**, pp. 10.7554/eLife.29236.

BATTLES, J.K. and DALRYMPLE, J.M., 1988. Genetic variation among geographic isolates of Rift Valley fever virus. *The American Journal of Tropical Medicine and Hygiene,* **39**(6), pp. 617-631.

BENFERHAT, R., JOSSE, T., ALBAUD, B., GENTIEN, D., MANSUROGLU, Z., MARCATO, V., SOUES, S., LE BONNIEC, B., BOULOY, M. and BONNEFOY, E., 2012. Large-scale chromatin immunoprecipitation with promoter sequence microarray analysis of the interaction of the NSs protein of Rift Valley fever virus with regulatory DNA regions of the host genome. *Journal of Virology,* **86**(20), pp. 11333-11344.

BENTE, D.A., ALIMONTI, J.B., SHIEH, W.J., CAMUS, G., STROHER, U., ZAKI, S. and JONES, S.M., 2010. Pathogenesis and immune response of Crimean-Congo hemorrhagic fever virus in a STAT-1 knockout mouse model. *Journal of Virology,* **84**(21), pp. 11089-11100.

BERECZKY, S., LINDEGREN, G., KARLBERG, H., AKERSTROM, S., KLINGSTROM, J. MIRAZIMI, A. 2010. Crimean-Congo hemorrhagic fever virus infection is lethal for Adult type I interferon receptor-knockout mice. *Journal of General Virology*, **91**, pp. 1473-1477.

BESSELAAR, T.G. and BLACKBURN, N.K., 1992. The synergistic neutralization of Rift Valley fever virus by monoclonal antibodies to the envelope glycoproteins. *Archives of Virology,* **125**(1-4), pp. 239-250.

BILLECOCQ, A., et al. 2008. RNA polymerase I-mediated expression of viral RNA for the rescue of infectious virulent and avirulent Rift Valley fever viruses. *Virology*, **378**(2), pp. 377-84.

BILLECOCQ, A., GAULIARD, N., LE MAY, N., ELLIOTT, R.M., FLICK, R. and BOULOY, M., 2008. RNA polymerase I-mediated expression of viral RNA for the rescue of infectious virulent and avirulent Rift Valley fever viruses. *Virology,* **378**(2), pp. 377-384.

BILLECOCQ, A., SPIEGEL, M., VIALAT, P., KOHL, A., WEBER, F., BOULOY, M. and HALLER, O., 2004. NSs protein of Rift Valley fever virus blocks interferon production by inhibiting host gene transcription. *Journal of Virology,* **78**(18), pp. 9798-9806.

BIRD, B.H., ALBARINO, C.G. and NICHOL, S.T., 2007a. Rift Valley fever virus lacking NSm proteins retains high virulence *in vivo* and may provide a model of human delayed onset neurologic disease. *Virology,* **362**(1), pp. 10-15.

BIRD, B.H., ALBARINO, C.G., HARTMAN, A.L., ERICKSON, B.R., KSIAZEK, T.G. and NICHOL, S.T., 2008. Rift Valley fever virus lacking the NSs and NSm genes is highly attenuated, confers protective immunity from virulent virus challenge, and allows for differential identification of infected and vaccinated animals. *Journal of Virology,* **82**(6), pp. 2681-2691.

BIRD, B.H., KHRISTOVA, M.L., ROLLIN, P.E., KSIAZEK, T.G. and NICHOL, S.T., 2007b. Complete genome analysis of 33 ecologically and biologically diverse Rift Valley fever virus strains reveals widespread virus movement and low genetic diversity due to recent common ancestry. *Journal of Virology,* **81**(6), pp. 2805-2816.

BLAKQORI, G. AND F. WEBER. 2005. Efficient cDNA-based rescue of La Crosse bunyaviruses expressing or lacking the nonstructural protein NSs. *Journal of Virology*, **79**(16), pp. 10420-8.

BLAKQORI, G., et al. 2003. Functional L polymerase of La Crosse virus allows *in vivo* reconstitution of recombinant nucleocapsids. *Journal of General Virology*, **84**(Pt 5), pp. 1207-14.

BOSHRA, H., LORENZO, G., RODRIGUEZ, F., BRUN, A. 2011. A DNA vaccine encoding ubiquitinated Rift Valley fever virus nucleoprotein provides consistent immunity and protects IFNAR-/- mice upon lethal vírus challenge. *Vaccine*. **29**, pp. 4469-4465.

BOULOY, M. and WEBER, F. 2010. Molecular Biology of Rift Valley fever virus. *The Open Virology Journal*. **4**, pp. 8-14.

BOULOY, M., JANZEN, C., VIALAT, P., KHUN, H., PAVLOVIC, J., HUERRE, M. and HALLER, O., 2001. Genetic evidence for an interferon-antagonistic function of Rift Valley fever virus nonstructural protein NSs. *Journal of Virology,* **75**(3), pp. 1371-1377.

BRAY, M. 2001. The role of the type I interferon response in the resistance of mice to filovirus infection. *Journal of General Virology*, **82**, pp. 1365-1373.

BRIDGEN, A. 2012. Introduction, in Reverse Genetics of RNA Viruses: Applications and Perspectives, A. Bridgen, Editor., John Wiley & Sons ed.

BRIDGEN, A. AND R.M. ELLIOTT.1996. Rescue of a segmented negative-strand RNA virus entirely from cloned complementary DNAs. *Proceedings of National Academy of Sciences U S A*, **93**(26), pp. 15400-4.

BRIESE, T., ALKHOVSKY, S., BEER, M., CALISHER, C.H. et al. ICTV Taxonomic proposal 2016.030a-vM.A.vA. v6. Bunyavirales. Create the order Bunyavirales, including eight new families, and one renamed family. http://www.ictv.global/proposals-16/2016.030a-vM.A.v6.Bunyavirales.pdf. Acesses 22 August 2017.

BRITTON P., GREEN P., KOTTIER S., MAWDITT K.L., PENZES Z., CAVANAGH D., et al. 1996. Expression of bacteriophage T7 RNA polymerase in avian and mammalian cells by a recombinant fowlpox virus. *Journal of General Virology,* **77**(577(5), pp. 963-967.

BUSQUETS, N., XAVIER, F., MARTIN-FOLGAR, R., LORENZO, G., GALINDO-CARDIEL, I., DEL VAL, B.P., RIVAS, R., IGLESIAS, J., RODRIGUEZ, F., SOLANES, D., DOMINGO, M. and BRUN, A., 2010. Experimental infection of young adult European breed sheep with Rift Valley fever virus field isolates. *Vector Borne and Zoonotic Diseases (Larchmont, N.Y.),* **10**(7), pp. 689-696.

CARMENES, R.S., FREIJE, J.P., MOLINA, M.M. and MARTIN, J.M., 1989. Predict7, a program for protein structure prediction. *Biochemical and Biophysical Research Communications,* **159**(2), pp. 687-693.

CETRE-SOSSAH, C., ZELLER, H., GRANDADAM, M., CARO, V., PETTINELLI, F., BOULOY, M., CARDINALE, E. and ALBINA, E., 2012. Genome analysis of Rift Valley fever virus, Mayotte. *Emerging Infectious Diseases,* **18**(6), pp. 969-971.

CONNOLLY-ANDERSEN, A.M., DOUAGI, I., KRAUS, A.A., MIRAZIMI, A., 2009. Crimean-Congo hemorrhagic fever virus infects human monocyte-derived dendritic cells. *Virology*, **390**, pp. 157–162.

CYR, N., DE LA FUENTE, C., LECOQ, L., GUENDEL, I., CHABOT, P.R., KEHN-HALL, K. and OMICHINSKI, J.G., 2015. A OmegaXaV motif in the Rift Valley fever virus NSs protein is essential for degrading p62, forming nuclear filaments and virulence. *Proceedings of the National Academy of Sciences of the United States of America,* **112**(19), pp. 6021-6026.

DANZETTA M.L., BRUNO R., SAURO F., SAVINI L., CALISTRI P. 2016. Rift Valley fever transmission dynamics described by compartmental models. *Preventive Veterinary Medicine,* **1**(134), pp. 197-210.

DAS S.C., BARON M.D., SKINNER M.A., BARRETT T. 2000. Improved technique for transient expression and negative strand virus rescue using fowlpox T7 recombinant virus in mammalian cells. *Journal of Virological Methods*, **89**(1–2), pp. 119-127.

DAUBNEY R., HUDSON J.R., GAMHAM P.C. 1931. Enzootic hepatitis of Rift Valley fever: an undescribed virus disease of sheep, cattle and man from East Africa. *The Journal of Pathology and Bacteriology,* **34**, pp. 545-549.

DAVIS, M.E. and GACK, M.U., 2015. Ubiquitination in the antiviral immune response. *Virology,* **479-480**, pp. 52-65.

DE BOER, SM, et al. 2012. Heparan sulphate facilitates Rift Valley fever virus entry into the cell. *Journal of Virology*, **86**(24), pp. 13767-71.

DO VALLE, T.Z., BILLECOCQ, A., GUILLEMOT, L., ALBERTS, R., GOMMET, C., GEFFERS, R., CALABRESE, K., SCHUGHART, K., BOULOY, M., MONTAGUTELLI, X. and PANTHIER, J.J., 2010. A new mouse model reveals a critical role for host innate immunity in resistance to Rift Valley fever. *Journal of Immunology (Baltimore, Md.: 1950),* **185**(10), pp. 6146-6156.

DONNELLY, R.P. and KOTENKO, S.V., 2010. Interferon-lambda: a new addition to an old family. Journal of interferon & cytokine research : the official journal of the International Society for Interferon and Cytokine Research, **30**(8), pp. 555-564.

DROSTEN, C., PANNING, M., GUENTHER, S., SCHMITZ, H., 2002. False-negative results of PCR assay with plasma of patients with severe viral hemorrhagic fever. *Journal of Clinical Microbiology*, **40**(11), pp. 4394-4395.

DZANANOVIC, E., Mckenna, S.A., Patel, T.R. 2018. Viral proteins targeting host protein kinase R to evade an innate immune response: a mini review. *Biotechnology & Genetic Engineering Review*, **34**(4),1-27.

ELLIOT, R.M., 1990. Molecular biology of the bunyaviridae. *Journal of General Virology*, **71**, pp. 501-522.

ERMLER, M.E., YERUKHIM, E., SCHRIEWER, J., SCHATTGEN, S., TRAYLOR, Z., WESPISER, A.R., CAFFREY, D.R., CHEN, Z.J., KING, C.H., GALE, M.,JR, COLONNA, M., FITZGERALD, K.A., BULLER, R.M. and HISE, A.G., 2013. RNA helicase signaling is critical for type i interferon production and protection against Rift Valley fever virus during mucosal challenge. *Journal of Virology,* **87**(9), pp. 4846-4860.

EVANS, A., GAKUYA, F., PAWESKA, J.T., ROSTAL, M., AKOOLO, L., VAN VUREN, P.J., MANYIBE, T., MACHARIA, J.M., KSIAZEK, T.G., FEIKIN, D.R., BREIMAN, R.F. and KARIUKI NJENGA, M., 2008. Prevalence of antibodies against Rift Valley fever virus in Kenyan wildlife. *Epidemiology and Infection,* **136**(9), pp. 1261-1269.

FERRON, F., LI, Z., DANEK, E. I., LUO, D., WONG, Y., COUTARD, B., LANTEZ, V., CHARREL, R., CANARD, B., WALZ, T., LESCAR, J., 2011. The hexamer structure of the Rift Valley fever virus nucleoprotein suggests a Mechanism for its assembly into ribonucleoprotein complexes. *PloS Pathogens*, **7**, pp. e1002030.

FINDLAY GM. 1932. Rift Valley fever or enzootic hepatitis. *Trans R. Soc. Trop Med Hyg* **25**, pp. 229-265.

FLICK, R. and BOULOY, M., 2005. Rift Valley fever virus. *Current Molecular Medicine,* **5**(8), pp. 827-834.

FLICK, R., ET AL. 2003. Reverse genetics for Crimean-Congo hemorrhagic fever virus. *Journal of Virology*, **77**(10), pp. 5997-6006.

FONTANA, J., LÓPEZ-MONTEIRO, N., ELLIOTT, R.M., FERNÁNDEZ, J.J., RISCO, C., 2008. The unique arquitecture of Bunyamwera virus factories around the Golgi complex. *Cellular Microbiology*, **10**, pp. 2012-2018.

FREIBERG, A. DOLORES, L.K., ENTERLEIN S., FLICK, R. 2008a. Establishment and characterization of minigenome rescue system for Nipah virus: RNA polymerase I-and T7-catalized generation of functional paramyxoviral RNA. *Virology*, **370**(1), pp 33-34.

FREIBERG, A.N., SHERMAN, M.B., MORAIS, M.C., HOLBROOK, M.R. and WATOWICH, S.J., 2008. Three-dimensional organization of Rift Valley fever virus revealed by cryoelectron tomography. *Journal of Virology,* **82**(21), pp. 10341-10348.

GARCIN, D., LEZZI, M., DOBBS, M., ELLIOTT, R.M., SCHMALJOHN, C., KANG, C.Y. and KOLAKOFSKY, D., 1995. The 5' ends of Hantaan virus (Bunyaviridae) RNAs suggest a prime-and-realign mechanism for the initiation of RNA synthesis. *Journal of Virology,* **69**(9), pp. 5754-5762.

GAULIARD, N., BILLECOCQ, A., FLICK, R. and BOULOY, M., 2006. Rift Valley fever virus noncoding regions of L, M and S segments regulate RNA synthesis. *Virology,* **351**(1), pp. 170-179.

GAULIARD, N., ET AL., 2006. Rift Valley fever virus noncoding regions of L, M and S Segments regulate RNA synthesis. *Virology*, **351**(1), pp. 170-9.

GERRARD, S.R. and NICHOL, S.T., 2007. Synthesis, proteolytic processing and complex formation of N-terminally nested precursor proteins of the Rift Valley fever virus glycoproteins. *Virology,* **357**(2), pp. 124-133.

GIORGI, C., ACCARDI, L., NICOLETTI, L., GRO, M.C., TAKEHARA, K., HILDITCH, C., MORIKAWA, S. and BISHOP, D.H., 1991. Sequences and coding strategies of the S RNAs of Toscana and Rift Valley fever viruses compared to those of Punta Toro, Sicilian Sandfly fever, and Uukuniemi viruses. *Virology,* **180**(2), pp. 738-753.

GOUBAU, D., DEDDOUCHE, S. and REIS E SOUSA, C., 2013. Cytosolic sensing of viruses. *Immunity,* **38**(5), pp. 855-869.

GOWEN, B.B., HOOPES, J.D., WONG, M.H., JUNG, K.H., ISAKSON, K.C., ALEXOPOULOU, L., FLAVELL, R.A. and SIDWELL, R.W., 2006. TLR3 deletion limits mortality and disease severity due to Phlebovirus infection. *Journal of Immunology (Baltimore, Md.: 1950),* **177**(9), pp. 6301-6307.

GOWEN, B.B., WONG, M.H., JUNG, K.H., SANDERS, A.B., MITCHELL, W.M., ALEXOPOULOU, L., FLAVELL, R.A. and SIDWELL, R.W., 2007. TLR3 is essential for the induction of protective immunity against Punta Toro Virus infection by the double-stranded RNA (dsRNA), poly(I:C12U), but not Poly(I:C): differential recognition of synthetic dsRNA molecules. *Journal of Immunology (Baltimore, Md.: 1950),* **178**(8), pp. 5200-5208.

GRAY, K.K., WORTHY, M.N., JUELICH, T.L., AGAR, S.L., POUSSARD, A., RAGLAND, D., FREIBERG, A.N. and HOLBROOK, M.R., 2012. Chemotactic and inflammatory responses in the liver and brain are associated with pathogenesis of Rift Valley fever virus infection in the mouse. *PLoS Neglected Tropical Diseases,* **6**(2), pp. e1529.

GROBBELAAR, A.A., WEYER, J., LEMAN, P.A., KEMP, A., PAWESKA, J.T. and SWANEPOEL, R., 2011. Molecular epidemiology of Rift Valley fever virus. *Emerging Infectious Diseases,* **17**(12), pp. 2270-2276.

HABJAN, M., ANDERSSON, I., KLINGSTROM, J., SCHUMANN, M. et al. 2008a. Processing of genome 5' termini as a strategy of negative-strand RNA viruses to avoid RIG-I-dependent interferon induction. *PloS one,* **3**(4), pp. e2032.

HABJAN, M., PENSKI, N., SPIEGEL, M. and WEBER, F., 2008. T7 RNA polymerase-dependent and -indepenent systems for cDNA-based rescue of Rift Valley fever virus. *The Journal of General Virology,* **89**(Pt 9), pp. 2157-2166.

HABJAN, M., PENSKI, N., WAGNER, V., SPIEGEL, M., OVERBY, A.K., KOCHS, G., HUISKONEN, J.T. and WEBER, F., 2009. Efficient production of Rift Valley fever virus-like particles: The antiviral protein MxA can inhibit primary transcription of bunyaviruses. *Virology,* **385**(2), pp. 400-408.

HABJAN, M., PICHLMAIR, A., ELLIOTT, R.M., OVERBY, A.K., GLATTER, T., GSTAIGER, M., SUPERTI-FURGA, G., UNGER, H. and WEBER, F., 2009a. NSs protein of Rift Valley fever virus induces the specific degradation of the double-stranded RNA-dependent protein kinase. *Journal of Virology,* **83**(9), pp. 4365-4375.

HALLDORSSON, S., LI, S., LI, M., HARLOS, K., BOWDEN, T.A. and HUISKONEN, J.T., 2018. Shielding and activation of a viral membrane fusion protein. *Nature Communications,* **9**(1), pp. 349-017-02789-2.

HALLER, O. & KOCHS, G. 2002. Interferon induced Mx protein: Dynamin-like GTPases with Antiviral activity. *Traffic*, **3**, pp. 710-717.

HALLER, O., STAEHELI, P., SCHEWEMMLE, M. 2015. Mx GTPases: Dynamin-like antiviral machines of innate immunity. *Trends in Microbiology*, **23**(3) pp. 154-63.

HUANG, N.E., LIN, C.H., LIN, Y.S. and YU, W.C., 2003. Modulation of YY1 activity by SAP30. *Biochemical and Biophysical Research Communications,* **306**(1), pp. 267-275.

HUISKONEN, J.T., OVERBY, A.K., WEBER, F. and GRUNEWALD, K., 2009. Electron cryo-microscopy and single-particle averaging of Rift Valley fever virus: evidence for GN-GC glycoprotein heterodimers. *Journal of Virology,* **83**(8), pp. 3762-3769.

HUTCHINSON, K.L., ROLLIN, P.E., 2007. Cytokine and chemokine expression in humans infected with Sudan Ebola virus. *Journal of Infectious Disease*. **196**(2), pp. S357–S363.

IKEGAMI T., WON S., PETERS C.J., MAKINO, S. 2006. Rescue of infectious Rift Valley Fever Virus entirely from cDNA, analysis of virus lacking the NSs gene, and expression of a foreign gene. *Journal of Virology*, **80**(6), pp. 2933-40.

IKEGAMI, T. and MAKINO, S., 2011. The pathogenesis of Rift Valley fever. *Viruses,* **3**(5), pp. 493-519.

IKEGAMI, T., C.J. PETERS, AND S. MAKINO. 2005. Rift valley fever virus nonstructural protein NSs promotes viral RNA replication and transcription in a minigenome system. *Journal of Virology*, **79**(9), pp. 5606-15.

IKEGAMI, T., NARAYANAN, K., WON, S., KAMITANI, W., PETERS, C.J. and MAKINO, S., 2009. Rift Valley fever virus NSs protein promotes post-transcriptional downregulation of protein kinase PKR and inhibits eIF2alpha phosphorylation. *PLoS pathogens,* **5**(2), pp. e1000287.

IKEGAMI, T., WON, S., PETERS, C.J. and MAKINO, S., 2005. Rift Valley fever virus NSs mRNA is transcribed from an incoming anti-viral-sense S RNA segment. *Journal of Virology,* **79**(18), pp. 12106-12111.

JANSEN VAN VUREN, P., TIEMESSEN, C.T., PAWESKA, J.T., 2011. Anti-nucleocapsid protein immune responses counteract pathogenic effects of Rift Valley fever virus infection in mice. PLoS One **6**(9):e25027.JUPP, P.G., KEMP, A., GROBBELAAR, A., LEMA, P., BURT, F.J., ALAHMED, A.M., AL MUJALLI, D., AL KHAMEES, M. and SWANEPOEL, R., 2002. The 2000 epidemic of Rift Valley fever in Saudi Arabia: mosquito vector studies. *Medical and Veterinary Entomology,* **16**(3), pp. 245-252.

KALVERAM, B., LIHORADOVA, O. and IKEGAMI, T., 2011. NSs protein of Rift Valley fever virus promotes posttranslational downregulation of the TFIIH subunit p62. *Journal of Virology,* **85**(13), pp. 6234-6243.

KALVERAM, B., LIHORADOVA, O., INDRAN, S.V., LOKUGAMAGE, N., HEAD, J.A. and IKEGAMI, T., 2013. Rift Valley fever virus NSs inhibits host transcription independently of the degradation of dsRNA-dependent protein kinase PKR. *Virology,* **435**(2), pp. 415-424.

KÄRBER G., 1931. Beitrag zur Kollektiven Behandlung pharmakologie her Reihens versuche. *Archives for Experimentelle Pathologie and Pharmakologie*, **162**, pp. 480-483.

KATO, H., TAKEUCHI, O., SATO, S., YONEYAMA, M. Et al. 2006. Differential roles of MDA5 and RIG-I helicases in the recognition of RNA viruses. *Nature,* **441**(7089), pp. 101-105.

KLAR, M. and BODE, J., 2005. Enhanceossoome formation over the beta interferon promoter underlies a remote-control mechanism mediated by YY1 and YY2. *Molecular and Cellular Biology,* **25**(22), pp. 10159-10170.

KOCHS, G., JANZEN, C., HOHENBERG, H. and HALLER, O., 2002. Antivirally active MxA protein sequesters La Crosse virus nucleocapsid protein into perinuclear complexes. *Proceedings of the National Academy of Sciences of the United States of America,* **99**(5), pp. 3153-3158.

KOHL, A., et al. 2004. A bunyamwera virus minireplicon system in mosquito cells. *Journal of Virology*, **78**(11), pp. 5679-85.

KOLAKOFSKY, D. and HACKER, D., 1991. Bunyavirus RNA synthesis: genome transcription and replication. *Current Topics in Microbiology and Immunology,* **169**, pp. 143-159.

KOLOKOLTSOVA, O.A., YUN, N.E., POUSSARD, A.L., SMITH, J.K. et al. 2010. Mice lacking alpha/beta and gamma interferon receptors are susceptible to junin virus infection. *Journal of Virology,* **84**(24), pp. 13063-13067.

KORTEKAAS, J., ANTONIS, A.F., KANT, J., VLOET, R.P., VOGEL, A., ORESHKOVA, N., DE BOER, S.M., BOSCH, B.J. and MOORMANN, R.J., 2012. Efficacy of three candidate Rift Valley fever vaccines in sheep. *Vaccine,* **30**(23), pp. 3423-3429.

KORTEKAAS, J., ORESHKOVA, N., COBOS-JIMENEZ, V., VLOET, R.P., POTGIETER, C.A. and MOORMANN, R.J., 2011. Creation of a nonspreading Rift Valley fever virus. *Journal of Virology,* **85**(23), pp. 12622-12630.

KOTENKO, S. V. 2011. IFN-λs. *Current Opinion in Virology,* **23**, pp. 583–590.

LAEMMLI, U.K. 1970. Cleavage of structural proteins during the assembly of the head of bacteriophage T4. *Nature*, **227**(5259), pp. 680-685.

LATHAN, R., SIMON-CHAZOTTES, D., JOUVION, G., GODON, O., MALISSEN, M., FLAMAND, M., BRUHNS, P. and PANTHIER, J.J., 2017. Innate Immune Basis for Rift Valley Fever Susceptibility in Mouse Models. *Scientific reports,* **7**(1), pp. 7096-017-07543-8.

LAU, J.F., NUSINZON, I., BURAKOV, D., FREEDMAN, L.P, HORVATH,C.M.HORVATH, C.M., 2003. Role of Metazoan mediator proteins in interferon-responsive transcription. *Molecular and Cellular Biology*, **23**, pp. 620-628.

LE MAY, N., DUBAELE, S., PROIETTI DE SANTIS, L., BILLECOCQ, A., BOULOY, M. and EGLY, J.M., 2004. TFIIH transcription factor, a target for the Rift Valley hemorrhagic fever virus. *Cell,* **116**(4), pp. 541-550.

LE MAY, N., GAULIARD, N., BILLECOCQ, A. and BOULOY, M., 2005. The N terminus of Rift Valley fever virus nucleoprotein is essential for dimerization. *Journal of Virology,* **79**(18), pp. 11974-11980.

LE MAY, N., MANSUROGLU, Z., LEGER, P., JOSSE, T., BLOT, G., BILLECOCQ, A., FLICK, R., JACOB, Y., BONNEFOY, E. and BOULOY, M., 2008. A SAP30 complex inhibits IFN-beta expression in Rift Valley fever virus infected cells. *PLoS Pathogens,* **4**(1), pp. e13.

LÉGER P., LOZACH P.Y. 2015. Bunyaviruses: from transmission by arthropods to virus entry in the mammalian host first target cells. *Future Virology*. **10**, pp. 859-881.

LÉGER P., TETARD M, YOUNESS B, et al. 2016. Differential use of the C-Type Lectins L-SIGN and DC-SIGN for phlebovirus endocytosis. *Traffic*, **17**, pp. 639-656.

LERNOUT, T., CARDINALE, E., JEGO, M., DESPRES, P., COLLET, L., ZUMBO, B., TILLARD, E., GIRARD, S. and FILLEUL, L., 2013. Rift Valley fever in humans and animals in Mayotte, an endemic situation? *PloS one,* **8**(9), pp. e74192.

LEVY, D. E., MARIÉ, I. J., AND DURBIN, J. E. (2011). Induction and function of type I and III interferon in response to viral infection. *Current Opinion in Virology***, 1**, pp. 476–486.

LINTHICUM, K.J., DAVIES, F.G., KAIRO, A. and BAILEY, C.L., 1985. Rift Valley fever virus (family Bunyaviridae, genus Phlebovirus). Isolations from Diptera collected during an inter-epizootic period in Kenya. *The Journal of hygiene,* **95**(1), pp. 197-209.

LIU, L., CELMA, C.C. and ROY, P., 2008. Rift Valley fever virus structural proteins: expression, characterization and assembly of recombinant proteins. *Virology journal,* **5**, pp. 82-422X-5-82.

LIVAK, K. J., SCHMITTGEN, T. D. 2001. Analysis of relative gene expression data using real-time quantitative PCR and the 2(-Delta Delta C(T)) method. *Methods.* 2001.25(4), pp. 402-8.

LOFTS, L.L., IBRAHIM, M.S., NEGLEY, D.L., HEVEY, M.C. and SCHMALJOHN, A.L., 2007. Genomic differences between guinea pig lethal and nonlethal Marburg virus variants. *The Journal of Infectious Diseases,* **196** (2), pp. 305-12.

LOKUGAMAGE N., IKEGAMI T. 2017. Genetic stability of Rift Valley fever virus MP-12 vaccine during serial passages in culture cells. *npj Vaccines 2*(20), pp. e10.1038

LOPEZ, N., MULLER, R., PREHAUD, C. & BOULOY, M. 1995. The L protein of Rift Valley fever virus can rescue viral Ribonucleoproteins and transcribe synthetic genome-like RNA molecules. *Journal of Virology.* **69**(7), pp. 3972–9

LORENZO, G., RODRIGUEZ-PULIDO, M., LOPEZ-GIL, E., SOBRINO, F., BORREGO, B., SAIZ, M. and BRUN, A., 2014. Protection against Rift Valley fever virus infection in mice upon administration of interferon-inducing RNA transcripts from the FMDV genome. *Antiviral Research,* **109**, pp. 64-67.

LOWEN, A.C., et al. 2004. Efficient bunyavirus rescue from cloned cDNA. *Virology*. **330**(2), pp. 493-500.

LOZACH, P., MANCINI, R., BITTO, D., MEIER, R., OESTEREICH, L., OVERBY, A.K., PETTERSSON, R.F., HELENIUS, A., 2010. Entry of Bunyaviruses into mammalian cells. *Cell Host & Microbe*, **7**, pp. 488-499.

LY HJ, LOKUGAMAGE N, NISHIYAMA S, IKEGAMI T. 2017. Risk analysis of inter-species reassortment through a Rift Valley fever phlebovirus PM-12 vaccine strain. *PLoS One*.**12**(9), pp. e0185194.

MAcMICKING, J.D., 2012. Interferon-inducible effector mechanisms in cell-autonomous immunity. *Nature Reviews Immunology***, 12,** pp. 367-382.

Maes, P., ALKHOVSKY, S.V., BÀO, Y. et al., 2018. Taxonomy of the family Arenaviridae and the order Bunyavirales: updated 2018. *Archives of Virology*, **163**, pp. 2295-2310.

MAGURANO, F. and NICOLETTI, L., 1999. Humoral response in Toscana virus acute neurologic disease investigated by viral-protein-specific immunoassays. *Clinical and Diagnostic Laboratory Immunology,* **6**(1), pp. 55-60.

MANSUROGLU, Z., JOSSE, T., GILLERON, J., BILLECOCQ, A., LEGER, P., BOULOY, M. and BONNEFOY, E., 2010. Nonstructural NSs protein of Rift Valley fever virus interacts with pericentromeric DNA sequences of the host cell, inducing chromosome cohesion and segregation defects. *Journal of Virology,* **84**(2), pp. 928-939.

MATEO M., CARBONNELLE C., REYNARD O., KOLESNIKOVA L., et al. 2011. VP24 is a molecular determinant of Ebola virus virulence in Guinea pigs. *Journal of Infectious Diseases*. **204**, pp.1011-1020.

McDONALD, J.H. 2014. Handbook of Biological Statistics (3rd ed). Sparky House Publishing, Baltimore, Maryland, pp 186-189. Accessed at http://www.biostathandbook.com/Wilcoxonsignedrank.html on 3rd August 2015.

McELROY, A.K., NICHOL, S.T. 2012. Rift Valley fever virus inhibits a pro-inflammatory response in experimentally infectes human monocytes derived macrophages and a pro-inflamatory cytokine response may be associated with patient survival during natural infection. *Virology*, 422(1), pp.6-12.

McNAB, F., MAYER-BARBER, K., SHER, A., WACK, A., O'GARRA, A., 2015. Type I interferons in infection disease. *Nature Reviews Immunology,* **15,** pp 87-103.

MEEGAN J.M., BAILEY C.L. Rift Valley fever. In: Nonath TP. ed. 1988. *The Arboviruses Epidemiology and Ecology*; **4**, pp. 51-76.

MENDENHALL, M., WONG, M.H., SKIRPSTUNAS, R., MORREY, J.D. and GOWEN, B.B., 2009. Punta Toro virus (Bunyaviridae, Phlebovirus) infection in mice: strain differences in pathogenesis and host interferon response. *Virology,* **395**(1), pp. 143-151.

METRAS, R., PORPHYRE, T., PFEIFFER, D.U., KEMP, A., THOMPSON, P.N., COLLINS, L.M. and WHITE, R.G., 2012. Exploratory space-time analyses of Rift Valley Fever in South Africa in 2008-2011. *PLoS Neglected Tropical Diseases,* **6**(8), pp. e1808.

MEYER, O. 2009. Interferons and autoimmune disorders. *Joint Bone Spine*, **76**, pp. 464-473.

MIMS CAC. 1956. Rift Valley fever virus in mice. I. General features of the infection. *British Journal of Experimental Pathology*, **37**, pp. 110–119.

MIR, M.A., DURAN, W.A., HJELLE, B.L., YE, C., PANGANIBAN, A.T. 2008. Storage of cellular 5´mRNA caps in P bodies for bodies for viral cap-snatching. *Proceedings of the National Academy of Sciences*, **105**, pp. 19294-19299.

MIR, M.A., SHEE,A, S., HASEEB, A., HAQUE, A., 2010. Hantavirus nucleocapsid protein has distinct m7G Cap- and RNA-binding sites. *Journal of Biological Chemistry*, **285**, pp. 11357-11368.

MOGENSEN, T.H., 2009. Pathogen recognition and inflammatory signaling in innate immune defenses. *Clinical Microbiology Reviews,* **22**(2), pp. 240-73.

MOHAMED, M., MOSHA, F., MGHAMBA, J., ZAKI, S.R., SHIEH, W.J., et al. 2010. Epidemiologic and clinical aspects of a Rift Valley fever outbreak in humans in Tanzania, 2007. *The American Journal of Tropical Medicine and Hygiene,* **83**(2), pp. 22-27.

MORRILL, J.C., KNAUERT, F.K., KSIAZEK, T.G., MEEGAN, J.M. and PETERS, C.J., 1989. Rift Valley fever infection of rhesus monkeys: Implications for rapid diagnosis of human disease. *Research in Virology,* **140**, pp. 139-146.

MOUTAILLER, S., KRIDA, G., SCHAFFNER, F., VAZEILLE, M., FAILLOUX, A. B., 2008. Potential vectors of Rift Valley fever virus in the Mediterranean region. *Vector-Borne and zoonotic Diseases*, **8**, pp. 749-753.

MOUTAILLER, S., ROCHE, B., THIBERGE, J.M., CARO, V., ROUGEON, F. and FAILLOUX, A.B., 2011. Host alternation is necessary to maintain the genome stability of Rift Valley fever virus. *PLoS Neglected Tropical Diseases,* **5**(5), pp. e1156.

MUDHASANI, R., TRAN, J.P., RETTERER, C., RADOSHITZKY, S.R., KOTA, et al. 2013. IFITM-2 and IFITM-3 but not IFITM-1 restrict Rift Valley fever virus. *Journal of Virology,* **87**(15), pp. 8451-8464.

MULLER, R., SALUZZO, J.F., LOPEZ, N., DREIER, T., TURELL, M., SMITH, J. and BOULOY, M., 1995. Characterization of clone 13, a naturally attenuated avirulent isolate of Rift Valley fever virus, which is altered in the small segment. *American Journal of Tropical Medicine and Hygiene,* **53**, pp. 405-411.

MUNDEL, B., GEAR, J., 1951. Rift Valley fever: The occurrence of human cases in Johannesburg. *South African Medical Journal,* 3, **25**(44), pp. 797-800.

MUNYUA, P., MURITHI, R.M., WAINWRIGHT, S et al. 2010. Rift Valley fever outbreak in livestock in Kenya, 2006-2007. *The American Society of Tropical Medicine and Hygiene*, **83**(S2), pp. 58-64.

NARAYANAN, A., POPOVA, T., TURELL, M., KIDD, J., CHERTOW, J., POPOV, S.G., BAILEY, C., KACHANCHI, F., KEHN-HALL, K. 2011. Alteration in superoxide dismutase 1 causes oxidative stress and p38 MAPK activation following RVFV infection. *Plos ONE*, **6**, pp. e20354.

NGUKU, P.M., SHARIF, S.K., MUTONGA, D., AMWAYI, S., et al. 2010. An investigation of a major outbreak of Rift Valley fever in Kenya: 2006-2007. *The American Journal of Tropical Medicine and Hygiene,* **83**(2), pp. 5-13.

ODENDAAL L, CLIFT SJ, FOSGATE GT, DAVIS AS. 2018. Lesions and cellular tropism of Natural Rift Valley fever virus infection in adult sheep. *Veterinary Pathology,* pp*. 1-17*.

ODENDAAL L, FOSGATE GT, ROMITO M, COETZER JA, CLIFT SJ., 2014. Sensitivity and specificity of real-time reverse transcription polymerase chain reaction, histopathology, and immunohistochemical labeling for the detection of Rift Valley fever virus in naturally infected cattle and sheep. *Journal of Veterinary Diagnostic Investigation*, **26**(1), pp. 49-60.

OGAWA, Y., et al. 2007. Rescue of Akabane virus (family Bunyaviridae) entirely from cloned cDNAs by using RNA polymerase I. *Journal of General Virology*, **88**(Pt 12), pp. 3385-90.

OVERBY, A.K., PETTERSSON, R.F., GRUNEWALD, K. and HUISKONEN, J.T., 2008. Insights into bunyavirus architecture from electron cryotomography of Uukuniemi virus. *Proceedings of the National Academy of Sciences of the United States of America,* **105**(7), pp. 2375-2379.

PERROTTA, A.T. AND M.D. BEEN. 1991. A pseudoknot-like structure required for efficient self-cleavage of hepatitis delta virus RNA. *Nature*, **350**(6317), pp. 434-6.

PERRY, S. T., BUCK, M.D., LADA, S.M, SCHINDLER, C., SHRESTA, S., 2011. STAT2 mediates innate immunity to Dengue Virus in the absence of STAT 1 via the type I interferon receptor. *PloS Pathogens*, **7**, pp. e1001297.

PESTKA, S., KRAUSE, C.D., WALTER, M.R., 2004. Interferons, interferon-like cytokines, and their receptors. *Immunology Review,* **202**, pp. 8-32.

PETERS C.J. & MEEGAN J.M. 1981. Rift Valley fever. In: Beran G (ed). CRC handbook series in zoonoses, sect. B1 403-419. Boca Raton, Florida: CRC press, Inc.

PETERS, C.J. and SLONE, T.W., 1982. Inbred rat strains mimic the disparate human response to Rift Valley fever virus infection. *Journal of Medical Virology,* **10**(1), pp. 45-54.

PETERS, C.J., LIU, C.T., ANDERSON, G.W.,JR, MORRILL, J.C. and JAHRLING, P.B., 1989. Pathogenesis of viral hemorrhagic fevers: Rift Valley fever and Lassa fever contrasted. *Reviews of Infectious Diseases,* **11**(4), pp. S743-9.

PETERS, C.J., REYNOLDS, J.A., SLONE, T.W., JONES, D.E. and STEPHEN, E.L., 1986. Prophylaxis of Rift Valley fever with antiviral drugs, immune serum, an interferon inducer, and a macrophage activator. *Antiviral Research,* **6**(5), pp. 285-297.

PICHLMAIR, A., LASSNIG, C., EBERLE, C.A., GORNA, M.W., BAUMANN, C.L., BURKARD, T.R., BURCKSTUMMER, T., STEFANOVIC, A., KRIEGER, S., BENNETT, K.L., RULICKE, T., WEBER, F., COLINGE, J., MULLER, M. and SUPERTI-FURGA, G., 2011. IFIT1 is an antiviral protein that recognizes 5'-triphosphate RNA. *Nature immunology,* **12**(7), pp. 624-630.

PICHLMAIR, A., SCHULZ, O., TAN, C.P., REHWINKEL, J., KATO, H., TAKEUCHI, O., AKIRA, S., WAY, M., SCHIAVO, G. and REIS E SOUSA, C., 2009. Activation of MDA5 requires higher-order RNA structures generated during virus infection. *Journal of Virology,* **83**(20), pp. 10761-10769.

PIFAT, D.Y. and SMITH, J.F., 1987. Punta Toro virus infection of C57BL/6J mice: a model for phlebovirus-induced disease. *Microbial Pathogenesis,* **3**(6), pp. 409-422.

PIPER, M.E., SORENSON, D.R., GERRARD, S.R., 2011. Efficient cellular release of Rift Valley fever virus requires genomic RNA. *PloS one*, **6**, pp. e18070.

POTGIETER, A. C., et al. 2009. Improved strategies for sequence-independent amplification and sequencing of viral double-stranded RNA genomes. *Journal of General Virology*, **90**, pp. 1423–1432.

PREHAUD, C., LOPEZ, N., BLOK, M.J., OBRY, V. and BOULOY, M., 1997. Analysis of the 3' terminal sequence recognized by the Rift Valley fever virus transcription complex in its ambisense S segment. *Virology,* **227**(1), pp. 189-197.

PRINS, K.C., DELPEUT, S., LEUNG, D.W., REYNARD, O., VOLCHKOVA, V.A., REID, S.P., RAMANAN, P., CARDENAS, W.B., AMARASINGHE, G.K., VOLCHKOV, V.E. and BASLER, C.F., 2010. Mutations abrogating VP35 interaction with double-stranded RNA render Ebola virus avirulent in guinea pigs. *Journal of Virology,* **84**(6), pp. 3004-3015.

PROKUNINA-OLSSON, L., MUCHMORE, B., TANG, W., PFEIFFER, R. M., PARK, H., DICKENSHEETS, H., et al. 2013. A variant upstream of *IFNL3* (*IL28B*) creating a new interferon gene *IFNL4* is associated with impaired clearance of hepatitis C virus. *Nature Genetics,* **45**, pp. 164–171.

RAYMOND J., BRADFUTE S., BRAY M. 2011. Filovirus infection of stat-1 knockout mice. *Journal of Infectious Diseases*, **204**, pp. 986-990.

RAYMOND, D.D., PIPER, M.E., GERRARD, S.R., SMITH, J.L. 2010. Structure of the Rift Valley fever virus nucleocapsid protein reveals another arquitecture for RNA encapsidation. *Proceedings of the National Academy of Sciences*, **107**, pp. 11769-11774.

REGUERA, J., WEBER, F. and CUSACK, S., 2010. Bunyaviridae RNA polymerases (L-protein) have an N-terminal, influenza-like endonuclease domain, essential for viral cap-dependent transcription. *PLoS Pathogens,* **6**(9), pp. e1001101.

RITTER, M., BOULOY , M., VIALAT, P., JANZEN, C., HALLER, O. and FRESE, M., 2000. Resistance to Rift Valley fever virus in Rattus norvegicus: genetic variability within certain 'inbred' strains. *The Journal of General Virology,* **81**(11), pp. 2683-2688.

ROSS, T.M., BHARDWAJ, N., BISSEL, S.J., HARTMAN, A.L. and SMITH, D.R., 2012. Animal models of Rift Valley fever virus infection. *Virus Research,* **163**(2), pp. 417-423.

ROSTAL, M.K., LIANG, J.E., ZIMMERMANN, D., BENGIS, R., PAWESKA, J. and KARESH, W.B., 2017. Rift Valley Fever: Does Wildlife Play a Role? *Institute of Laboratory Animal Research Journal,* **58**(3), pp. 359-370.

RUSU, M., BONNEAU, R., HOLBROOK, M.R. WATOWICH, S.J., BIRMANNS, S., WRIGGERS, W, FREIBERG, A.N., 2012. An assembly model of Rift Valley fever virus. *Frontiers in Microbiology*, **19,** pp. 3-244.

SALL, A.A., DE A ZANOTTO, P.M., ZELLER, H.G., DIGOUTTE, J.P., THIONGANE, Y. and BOULOY, M., 1997. Variability of the NS(S) protein among Rift Valley fever virus isolates. *The Journal of General Virology,* **78**(11), pp. 2853-2858.

SCHLEE, M., 2013. Master sensors of pathogenic RNA - RIG-I like receptors. *Immunobiology,* **218**(11), pp. 1322-1335.

SCHNEIDER, W.M., CHEVILLOTTE, M.D. and RICE, C.M., 2014. Interferon-stimulated genes: a complex web of host defenses. *Annual Review of Immunology,* **32**, pp. 513-545.

SCHOGGINS, J.W., MACDUFF, D.A., IMANAKA, N., GAINEY, M.D. et al. 2014. Pan-viral specificity of IFN-induced genes reveals new roles for cGAS in innate immunity. *Nature,* **505**(7485), pp. 691-695.

SCHOGGINS, J.W., WILSON, S.J., PANIS, M., MURPHY, M.Y., JONES, C.T., BIENIASZ, P. and RICE, C.M., 2011. A diverse range of gene products are effectors of the type I interferon antiviral response. *Nature,* **472**(7344), pp. 481-485.

SCHUDEL, B.R., HARMON, B., ABHYANKAR, V.V., PRUIT, B.W., NEGRETE, O.A. and SINGH, A.K., 2013. Microfluid platforms for RNA interference screening of virus-host interactions. *Lab on a chip*, **13**, pp. 811-817.

SHERMAN, M.B., FREIBERG, A.N., HOLBROOK, M.R. and WATOWICH, S.J., 2009. Single-particle cryo-electron microscopy of Rift Valley fever virus. *Virology,* **387**(1), pp. 11-15.

SHIEH, W.J., PADDOCK, C.D., LEDERMAN, E., RAO, C.Y., GOULD, L.H., MOHAMED, M., MOSHA, F., MGHAMBA, J., BLOLAND, P., NJENGA, M.K., MUTONGA, D., SAMUEL, A.A., GUARNER, J., BREIMAN, R.F. and ZAKI, S.R., 2010. Pathologic studies on suspect animal and human cases of Rift Valley fever from an outbreak in Eastern Africa, 2006-2007. *The American Journal of Tropical Medicine and Hygiene,* **83**(2), pp. 38-42.

SHIMSHONY A. & BRAZILAI R. 1983. Rift Valley fever. *Advances in Veterinary Science and Comparative Medicine,* **27**, pp 347-425.

SHRESTA, S., SHARAR, K.L., PRIGOZHIN, D.M., SNIDER, H.M., BEATTY, P.R. and HARRIS, E., 2005. Critical roles for both STAT1-dependent and STAT1-independent pathways in the control of primary dengue virus infection in mice. *Journal of immunology,* **175**(6), pp. 3946-3954.

SIDWELL, R.W., HUFFMAN, J.H., BARNARD, D.L., SMEE, D.F., WARREN, R.P., CHIRIGOS, M.A., KENDE, M. and HUGGINS, J., 1994. Antiviral and immunomodulating inhibitors of experimentally-induced Punta Toro virus infections. *Antiviral Research,* **25**(2), pp. 105-122.

SIDWELL, R.W., HUFFMAN, J.H., SMEE, D.F., GILBERT, J., GESSAMAN, A., PEASE, A., WARREN, R.P., HUGGINS, J. and KENDE, M., 1992. Potential role of immunomodulators for treatment of phlebovirus infections of animals. *Annals of the New York Academy of Sciences,* **653**, pp. 344-355.

SIDWELL, R.W., SMEE, D.F., 2003. Viruses of the Bunya-and Togaviridae familyes: Potential as bioterrorism agents and means of control. *Antiviral Research,* **57**, pp. 101-111.

SILVERMAN, R.H. 1994. Fascination with 2-5A-Dependent Rnase: A unique enzyme that functions in Interferon action. *Journal of Interferon Research*, **14,** pp. 101-104.

SIMONS, J.F. and PETTERSSON, R.F., 1991. Host-derived 5' ends and overlapping complementary 3' ends of the two mRNAs transcribed from the ambisense S segment of Uukuniemi virus. *Journal of Virology,* **65**(9), pp. 4741-4748.

SISSOKO, D., MALVY, D., EZZEDINE, K., RENAULT, P., MOSCETTI, F., et al., 2009. Post-Epidemic Chikungunya Disease on Reunion Island: Course of Rheumatic Manifestations and Associated Factors over a 15-Month Period. *PLoS Neglected Tropical Diseases,* **3**(3), pp. e389.

SMIRNOVA, S.E., 1979. A comparative study of the Crimean hemorrhagic fever-Congo group of viruses. *Archives of Virology*, **62**(2), pp. 137-143.

SMITH, D.R., STEELE, K.E., SHAMBLIN, J., HONKO, A., JOHNSON, J., REED, C., KENNEDY, M., CHAPMAN, J.L. and HENSLEY, L.E., 2010. The pathogenesis of Rift Valley fever virus in the mouse model. *Virology,* **407**(2), pp. 256-267.

SPARRER, K.M. and GACK, M.U., 2015. Intracellular detection of viral nucleic acids. *Current Opinion in Microbiology,* **26**, pp. 1-9.

STRUTHERS, J.K., SWANEPOEL, R. and SHEPHERD, S.P., 1984. Protein synthesis in Rift Valley fever virus-infected cells. *Virology,* **134**(1), pp. 118-124.

SWANEPOEL R, PAWESKA J T, 2011. Rift Valley fever. Oxford Textbook of Zoonoses: Biology, Clinical Practice, and Public Health Control, (2nd edition), pp. 421-431.

SWANEPOEL R, STRUTHERS JK, ERASMUS MJ, SHEPHERD SP, MCGILLIVRAY GM, SHEPHERD AJ, HUMMITZ DE, ERASMUS BJ, BARNARD BJ. 1996. *Onderstepoort Journal of Veterinary research*, 63, pp. 341-7.

SWANEPOEL, R. and COETZER, J., 2004. Rift Valley fever. In: J. COETZER and R. TUSTIN, eds, *Infectious diseases of livestock with special reference to South Africa.* 2nd edition, Vol.2 edn. Cape Town: Oxford University Press Southern Africa, pp. 1037-1059.

SWANEPOEL, R. and BLACKBURN, N.K., 1977. Demonstration of nuclear immunofluorescence in Rift Valley fever infected cells. *The Journal of General Virology,* **34**(3), pp. 557-561.

SWANEPOEL, R., GILL, D.E., SHEPHERD, A.J., LEMAN, P.A., MYNHARDT, J.H. and HARVEY, S., 1989. The clinical pathology of Crimean-Congo hemorrhagic fever. *Reviews of Infectious Diseases,* **11**(4), pp. S794-800.

SWANEPOEL, R., STRUTHERS, J.K., ERASMUS, M.J., SHEPHERD, S.P., MCGILLIVRAY, G.M., ERASMUS, B.J. and BARNARD, B.J., 1986. Comparison of techniques for demonstrating antibodies to Rift Valley fever virus. *The Journal of Hygiene,* **97**(2), pp. 317-329.

TERASAKI, K., WON, S. and MAKINO, S., 2013. The C-terminal region of Rift Valley fever virus NSm protein targets the protein to the mitochondrial outer membrane and exerts antiapoptotic function. *Journal of Virology,* **87**(1), pp. 676-682.

TUREL, M.J., DOHM, D.J., MORES, C.N., TERRACINA, L., WALLETE, D.L.J., HRIBAR, L.J., PECOR, J.E., BLOW, J.A. 2008. Potential for North Americn mosquitoes to transmit Rift Valley fever virus. *Journal of the American Mosquito Control Association*, **24**, pp. 502-507.

VALMAS, C. and BASLER, C.F., 2011. Marburg virus VP40 antagonizes interferon signaling in a species-specific manner. *Journal of Virology,* **85**(9), pp. 4309-4317.

VIALAT, P., BILLECOCQ, A., KOHL, A. and BOULOY, M., 2000. The S segment of Rift Valley fever phlebovirus (Bunyaviridae) carries determinants for attenuation and virulence in mice. *Journal of Virology,* **74**(3), pp. 1538-1543.

VON BONSDORFF, C.H. and PETTERSSON, R., 1975. Surface structure of Uukuniemi virus. *Journal of Virology,* **16**(5), pp. 1296-1307.

VON TEICHMAN, B., ENGELBRECHT, A., ZULU, G., DUNGU, B., PARDINI, A. and BOULOY, M., 2011. Safety and efficacy of Rift Valley fever Smithburn and Clone 13 vaccines in calves. *Vaccine,* **29**(34), pp. 5771-5777.

WALKER, K.W. 2016. Site Directed Mutagenesis. Encyclopedia of Cell Biology, Vol.1. Amgen Inc., Thousand Oaks, CA, USA, pp 122-127.

WALPITA, P., FLICK, R. 2005. Reverse genetics of negative-stranded RNA viruses: A global perspective. *FEMS Microbiology letters**,*** **244**, pp 9-18.

WAN, H., LI, Y., FAN, YU et al. 2012. site-directed mutagenesis method particularly useful for creating otherwise difficult-to-make mutants and alanine scanning. *Analytical Biochemistry*, Vol 420 (2), pp 163-170.

WARFIELD, K.L., BRADFUTE, S.B., WELLS, J., LOFTS, L., COOPER, M.T., ALVES, D.A., REED, D.K., VANTONGEREN, S.A., MECH, C.A. and BAVARI, S., 2009. Development and characterization of a mouse model for Marburg hemorrhagic fever. *Journal of Virology,* **83**(13), pp. 6404-6415.

WEBER, F., WAGNER, V., RASMUSSEN, S.B., HARTMANN, R. and PALUDAN, S.R., 2006. Double-stranded RNA is produced by positive-strand RNA viruses and DNA viruses but not in detectable amounts by negative-strand RNA viruses. *Journal of Virology,* **80**(10), pp. 5059-5064.

WEINGARTL, H.M., ZHANG, S., MARSZAL, P., MCGREEVY, A., BURTON, L. and WILSON, W.C., 2014. Rift Valley fever virus incorporates the 78 kDa glycoprotein into virions matured in mosquito C6/36 cells. *PloS One,* **9**(1), pp. e87385.

WICHGERS SCHREUR, P.J. and KORTEKAAS, J., 2016. Single-Molecule FISH Reveals Non-selective Packaging of Rift Valley Fever Virus Genome Segments. *PLoS Pathogens,* **12**(8), pp. e1005800.

WILLIAMS, B.R., 1999. PKR; a sentinel kinase for cellular stress. *Oncogene*, **18**, pp. 6112-6120.

WON S, IKEGAMI T, PETERS CJ, MAKINO S. 2006. NSm and 78 kilodaltons protein of RVFV are non essential for viral replication in culture cells. *Journal of Virology*, **80**(16): 8274-8278.

WON, S., IKEGAMI, T., PETERS, C.J., MAKINO, S., 2007. NSs protein of Rift Valley fever virus suppresses virus-induced apoptosis. *Journal of Virology*, **81**, pp. 13335-133345.

WOODS, C.W., KARPATI, A.M., GREIN, T. et al. 2002. An outbreak of Rift Valley fever in Northeastern Kenya, 1997-98. *Emerging Infectious Diseases,* **8**(2), pp. 138-144.

WUERTH, J.D. and WEBER, F., 2016. Phleboviruses and the Type I Interferon Response. *Viruses,* **8**(6), pp. e174.

YADANI, F.Z., KOHL, A., PREHAUD, C., BILLECOCQ, A. and BOULOY, M., 1999. The carboxy-terminal acidic domain of Rift Valley Fever virus NSs protein is essential for the formation of filamentous structures but not for the nuclear localization of the protein. *Journal of Virology,* **73**(6), pp. 5018-5025.

YONEYAMA, M., ONOMOTO, K., JOGI, M., AKABOSHI, T. and FUJITA, T., 2015. Viral RNA detection by RIG-I-like receptors. *Current Opinion in Immunology,* **32**, pp. 48-53.

YUN, N.E., POUSSARD, A.L. SEREGIN, A.V., WALKER, A.G., SMITH, J.K., ARONSON, J.F., SMITH, J.N., SOONG, L., PAESSLER, S., 2012. Functional interferon system is required for clearance of Lassa virus. *Journal of Virology*, **86**, pp. 3389-3392.

ZIELECKI, F., WEBER, M., EICKMANN, M., SPIEGELBERG, L., ZAKI, A.M., MATROSOVICH, M., BECKER, S. and WEBER, F., 2013. Human cell tropism and innate immune system interactions of human respiratory coronavirus EMC compared to those of severe acute respiratory syndrome coronavirus. *Journal of Virology,* **87**(9), pp. 5300-5304.

ZURITA, M. and MERINO, C., 2003. The transcriptional complexity of the TFIIH complex. *Trends in genetics: TIG,* **19**(10), pp. 578-584.

8 APPENDICES

APPENDIX 1.

Table 1. Conversion of $TCID_{50}$/mL into PFU/mL

$TCID_{50}$/mL RVFV inoculum	**$Log_{10}TCID_{50}$**	**Conversion Factor (*0.7)**	**PFU/mL**
1.00E+07	7.00E+00	0.7	4.90
1.00E+04	4.00E+00	0.7	2.80
1.00E+02	2.00E+00	0.7	1.40
1.00E+03	3.00E+00	0.7	2.10

Table 2. IFN-ß gene expression relative quantification data analysis. Fold induction calculated based on the double delta Ct method (Livak method).

Well	Sample Name	Target Gene	Cт	-0,717*C	e^D	E*1388,9	IFN-b1 corrected for GAPDH	Fold induction
A1	Control 4h R1	IFNb1	31.93365288	-22.8964291	1.14E-10	1.58E-07	0.000428541	
A2	Control 4h R2	IFNb1	31.71027374	-22.7362663	1.34E-10	1.86E-07	0.000345194	
A3	Control 4h R3	IFNb1	31.71562767	-22.740105	1.33E-10	1.85E-07	0.000496193	0.000423309
A4	Control 8h R1	IFNb1	30.78997421	-22.0764115	2.58E-10	3.59E-07	0.000603029	
A5	Control 8h R2	IFNb1	30.93320084	-22.179105	2.33E-10	3.24E-07	0.000817376	
A6	Control 8h R3	IFNb1	31.15592957	-22.3388015	1.99E-10	2.76E-07	0.000455851	0.000625419
A7	Control 12h R1	IFNb1	31.20089722	-22.3710433	1.92E-10	2.67E-07	0.00037069	
A8	Control 12h R2	IFNb1	31.99601555	-22.9411431	1.09E-10	1.51E-07	0.000321889	
A9	Control 12h R3	IFNb1	32.15501404	-23.0551451	9.71E-11	1.35E-07	0.000251243	0.000314607
A10	WtTVFV 4h1	IFNb1	30.21843529	-21.6666181	3.89E-10	5.41E-07	0.000425322	1.004755855
A11	WtRVFV 4h2	IFNb1	31.64691734	-22.6908397	1.40E-10	1.94E-07	6.54074E-05	0.154514566
A12	WtRVFV 4h3	IFNb1	30.23448181	-21.6781235	3.85E-10	5.35E-07	0.000509114	1.202699917
B1	WtRVFV 8h1	IFNb1	30.42395782	-21.8139778	3.36E-10	4.67E-07	0.000785963	1.256699299
B2	WtRVFV 8h2	IFNb1	29.80470085	-21.3699705	5.24E-10	7.27E-07	0.001571705	2.513043786
B3	WtRVFV 8h3	IFNb1	30.50739861	-21.8738048	3.16E-10	4.40E-07	0.001085723	1.735993
B4	WtRVFV 12h1	IFNb1	27.94683266	-20.037879	1.98E-09	2.76E-06	0.006640066	21.10589262
B5	WtRVFV 12h2	IFNb1	27.64494896	-19.8214284	2.46E-09	3.42E-06	0.005514156	17.527111

B6	WtRVFV 12h3	IFNb1	27.40440178	-19.6489561	2.93E-09	4.07E-06	0.008012542	25.46840007
B7	M39/40 4h1	IFNb1	30.46296883	-21.8419486	3.27E-10	4.54E-07	0.004277303	10.10444427
B8	M39/40 4h2	IFNb1	29.63431358	-21.2478028	5.92E-10	8.22E-07	0.001016376	2.40102466
B9	C39S/C40S 4h3	IFNb1	29.77049637	-21.3454459	5.37E-10	7.46E-07	0.00105287	2.48723594
B10	C39S/C40S 8h1	IFNb1	28.58961487	-20.4987539	1.25E-09	1.74E-06	0.004242825	6.783974198
B11	C39S/C40S 8h2	IFNb1	28.13067245	-20.1696922	1.74E-09	2.42E-06	0.002936117	4.694641415
B12	C39S/C40S 8h3	IFNb1	29.6031456	-21.2254554	6.05E-10	8.41E-07	0.004754651	11.23210235
C1	C39S/C40S 12h1	IFNb1	26.88155746	-19.2740767	4.26E-09	5.92E-06	0.029940374	95.16747181
C2	C39S/C40S 12h2	IFNb1	27.43817329	-19.6731703	2.86E-09	3.97E-06	0.017929133	56.98894348
C3	C39S/C40S 12h3	IFNb1	27.98971558	-20.0686261	1.92E-09	2.67E-06	0.014075287	44.73923703
C4	H2O	IFNb1	Undetermined					
C5	H2O	IFNb1	Undetermined					

APPENDIX 2

This appendice shows the alignment of the NSs protein of the rescued mutants (C39S, C149S, C178S, C194S /C40S) with the S segment reference sequence accession number JF784388 (Kortekaas et al., 2011).

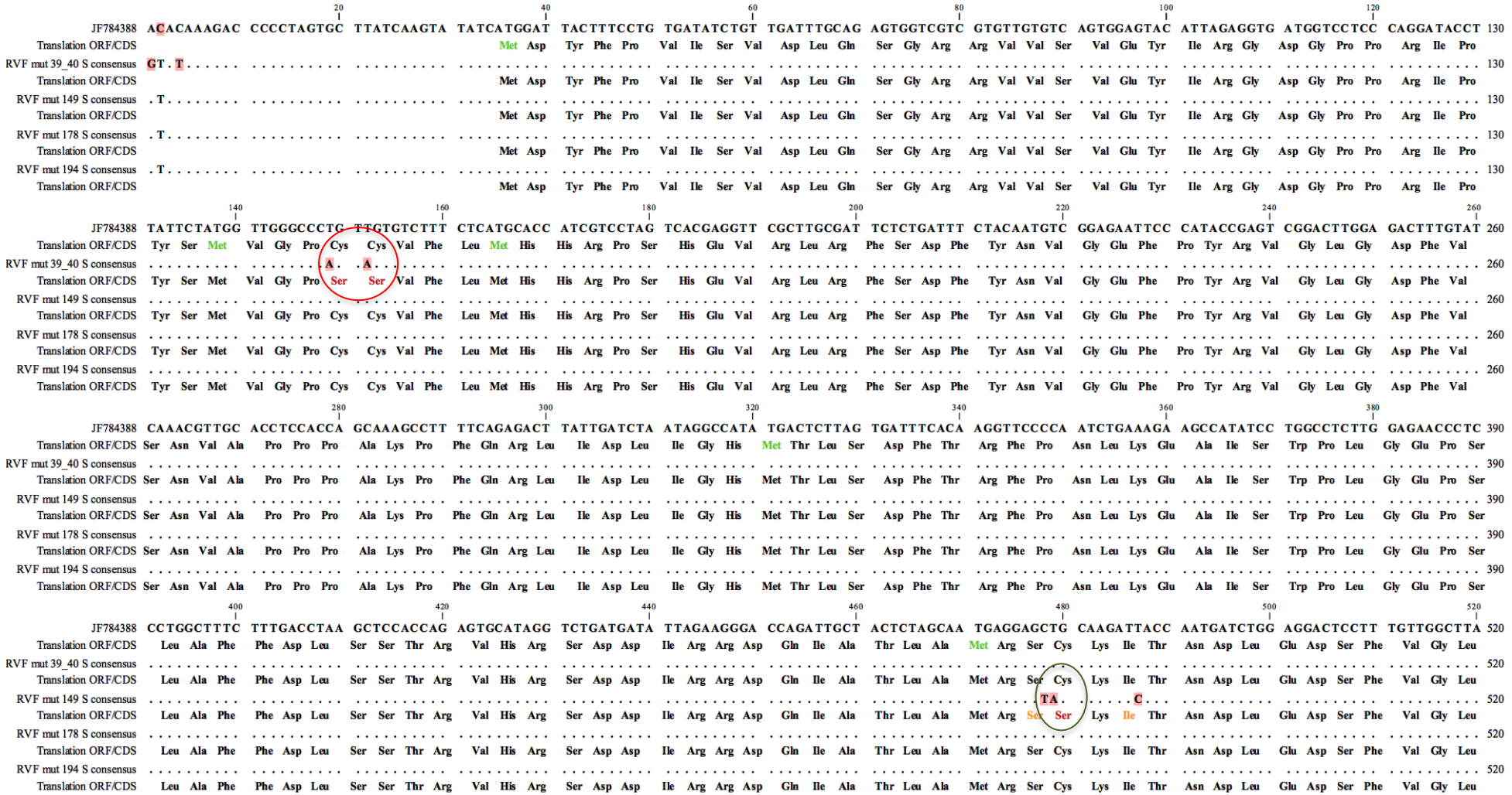
JF784388 ACACAAAGAC CCCCTAGTGC TTATCAAGTA TATCATGGAT TACTTTCCTG TGATATCTGT TGATTTGCAG AGTGGTCGTC GTGTTGTGTC AGTGGAGTAC ATTAGAGGTG ATGGTCCTCC CAGGATACCT 130
Translation ORF/CDS Met Asp Tyr Phe Pro Val Ile Ser Val Asp Leu Gln Ser Gly Arg Arg Val Val Ser Val Glu Tyr Ile Arg Gly Asp Gly Pro Pro Arg Ile Pro
RVF mut 39_40 S consensus GT.T 130
RVF mut 149 S consensus .T 130
RVF mut 178 S consensus .T 130
RVF mut 194 S consensus .T 130
JF784388 TATTCTATGG TTGGGCCCTG TTGTGTCTTT CTCATGCACC ATCGTCCTAG TCACGAGGTT CGCTTGCGAT TCTCTGATTT CTACAATGTC GGAGAATTCC CATACCGAGT CGGACTTGGA GACTTTGTAT 260
Translation ORF/CDS Tyr Ser Met Val Gly Pro Cys Cys Val Phe Leu Met His His Arg Pro Ser His Glu Val Arg Leu Arg Phe Ser Asp Phe Tyr Asn Val Gly Glu Phe Pro Tyr Arg Val Gly Leu Gly Asp Phe Val
RVF mut 39_40 S consensus A A 260
Translation ORF/CDS Tyr Ser Met Val Gly Pro Ser Ser Val Phe Leu Met His His Arg Pro Ser His Glu Val Arg Leu Arg Phe Ser Asp Phe Tyr Asn Val Gly Glu Phe Pro Tyr Arg Val Gly Leu Gly Asp Phe Val
RVF mut 149 S consensus 260
Translation ORF/CDS Tyr Ser Met Val Gly Pro Cys Cys Val Phe Leu Met His His Arg Pro Ser His Glu Val Arg Leu Arg Phe Ser Asp Phe Tyr Asn Val Gly Glu Phe Pro Tyr Arg Val Gly Leu Gly Asp Phe Val
RVF mut 178 S consensus 260
Translation ORF/CDS Tyr Ser Met Val Gly Pro Cys Cys Val Phe Leu Met His His Arg Pro Ser His Glu Val Arg Leu Arg Phe Ser Asp Phe Tyr Asn Val Gly Glu Phe Pro Tyr Arg Val Gly Leu Gly Asp Phe Val
RVF mut 194 S consensus 260
Translation ORF/CDS Tyr Ser Met Val Gly Pro Cys Cys Val Phe Leu Met His His Arg Pro Ser His Glu Val Arg Leu Arg Phe Ser Asp Phe Tyr Asn Val Gly Glu Phe Pro Tyr Arg Val Gly Leu Gly Asp Phe Val
JF784388 CAAACGTTGC ACCTCCACCA GCAAAGCCTT TTCAGAGACT TATTGATCTA ATAGGCCATA TGACTCTTAG TGATTTCACA AGGTTCCCCA ATCTGAAAGA AGCCATATCC TGGCCTCTTG GAGAACCCTC 390
Translation ORF/CDS Ser Asn Val Ala Pro Pro Pro Ala Lys Pro Phe Gln Arg Leu Ile Asp Leu Ile Gly His Met Thr Leu Ser Asp Phe Thr Arg Phe Pro Asn Leu Lys Glu Ala Ile Ser Trp Pro Leu Gly Glu Pro Ser
RVF mut 39_40 S consensus 390
Translation ORF/CDS Ser Asn Val Ala Pro Pro Pro Ala Lys Pro Phe Gln Arg Leu Ile Asp Leu Ile Gly His Met Thr Leu Ser Asp Phe Thr Arg Phe Pro Asn Leu Lys Glu Ala Ile Ser Trp Pro Leu Gly Glu Pro Ser
RVF mut 149 S consensus 390
Translation ORF/CDS Ser Asn Val Ala Pro Pro Pro Ala Lys Pro Phe Gln Arg Leu Ile Asp Leu Ile Gly His Met Thr Leu Ser Asp Phe Thr Arg Phe Pro Asn Leu Lys Glu Ala Ile Ser Trp Pro Leu Gly Glu Pro Ser
RVF mut 178 S consensus 390
Translation ORF/CDS Ser Asn Val Ala Pro Pro Pro Ala Lys Pro Phe Gln Arg Leu Ile Asp Leu Ile Gly His Met Thr Leu Ser Asp Phe Thr Arg Phe Pro Asn Leu Lys Glu Ala Ile Ser Trp Pro Leu Gly Glu Pro Ser
RVF mut 194 S consensus 390
Translation ORF/CDS Ser Asn Val Ala Pro Pro Pro Ala Lys Pro Phe Gln Arg Leu Ile Asp Leu Ile Gly His Met Thr Leu Ser Asp Phe Thr Arg Phe Pro Asn Leu Lys Glu Ala Ile Ser Trp Pro Leu Gly Glu Pro Ser
JF784388 CCTGGCTTTC TTTGACCTAA GCTCCACCAG AGTGCATAGG TCTGATGATA TTAGAAGGGA CCAGATTGCT ACTCTAGCAA TGAGGAGCTG CAAGATTACC AATGATCTGG AGGACTCCTT TGTTGGCTTA 520
Translation ORF/CDS Leu Ala Phe Phe Asp Leu Ser Ser Thr Arg Val His Arg Ser Asp Asp Ile Arg Arg Asp Gln Ile Ala Thr Leu Ala Met Arg Ser Cys Lys Ile Thr Asn Asp Leu Glu Asp Ser Phe Val Gly Leu
RVF mut 39_40 S consensus 520
Translation ORF/CDS Leu Ala Phe Phe Asp Leu Ser Ser Thr Arg Val His Arg Ser Asp Asp Ile Arg Arg Asp Gln Ile Ala Thr Leu Ala Met Arg Ser Cys Lys Ile Thr Asn Asp Leu Glu Asp Ser Phe Val Gly Leu
RVF mut 149 S consensus TA C 520
Translation ORF/CDS Leu Ala Phe Phe Asp Leu Ser Ser Thr Arg Val His Arg Ser Asp Asp Ile Arg Arg Asp Gln Ile Ala Thr Leu Ala Met Arg Ser Ser Lys Ile Thr Asn Asp Leu Glu Asp Ser Phe Val Gly Leu
RVF mut 178 S consensus 520
Translation ORF/CDS Leu Ala Phe Phe Asp Leu Ser Ser Thr Arg Val His Arg Ser Asp Asp Ile Arg Arg Asp Gln Ile Ala Thr Leu Ala Met Arg Ser Cys Lys Ile Thr Asn Asp Leu Glu Asp Ser Phe Val Gly Leu
RVF mut 194 S consensus 520
Translation ORF/CDS Leu Ala Phe Phe Asp Leu Ser Ser Thr Arg Val His Arg Ser Asp Asp Ile Arg Arg Asp Gln Ile Ala Thr Leu Ala Met Arg Ser Cys Lys Ile Thr Asn Asp Leu Glu Asp Ser Phe Val Gly Leu

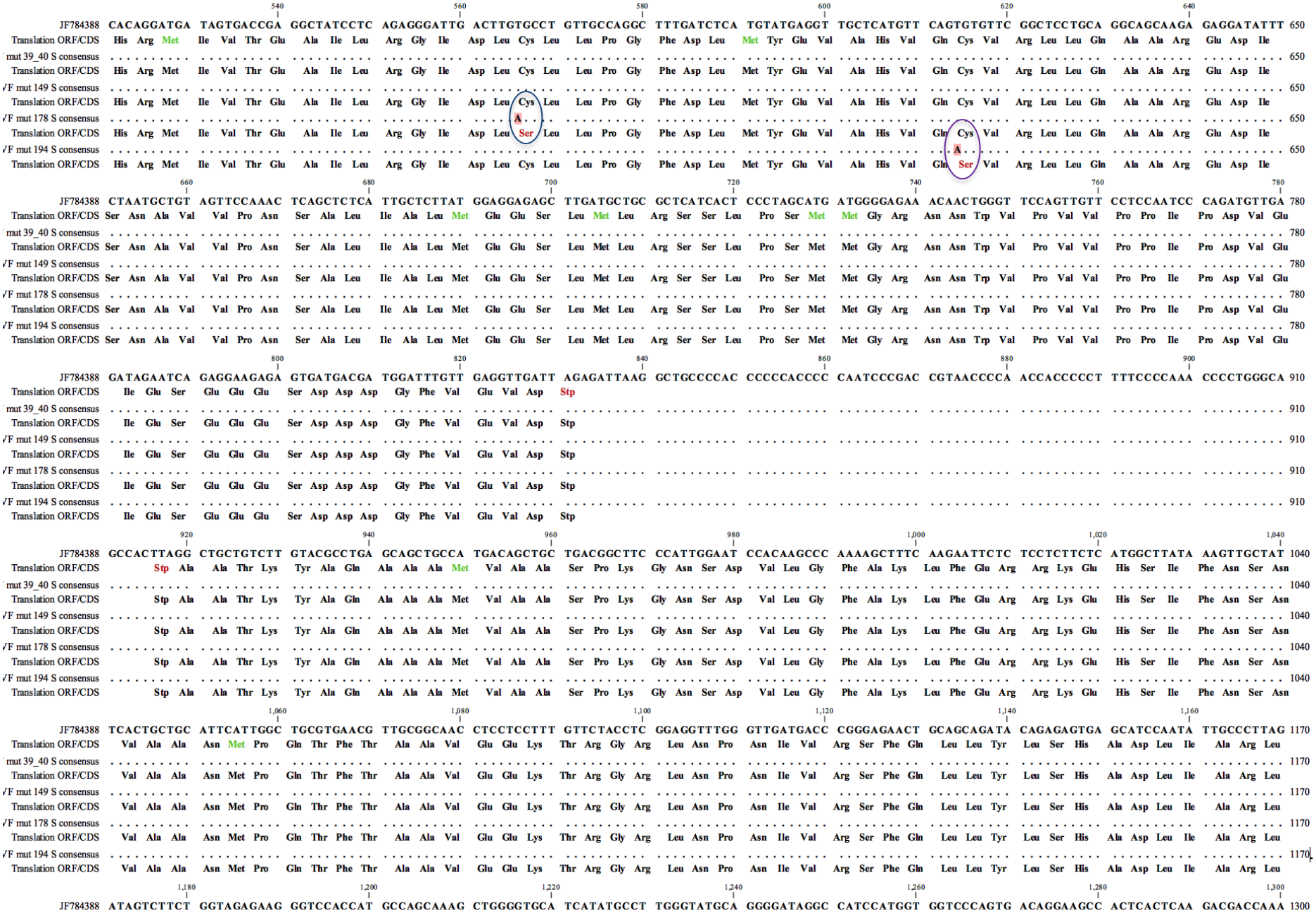
JF784388
Translation ORF/CDS
mut 39_40 S consensus
√F mut 149 S consensus
√F mut 178 S consensus
√F mut 194 S consensus

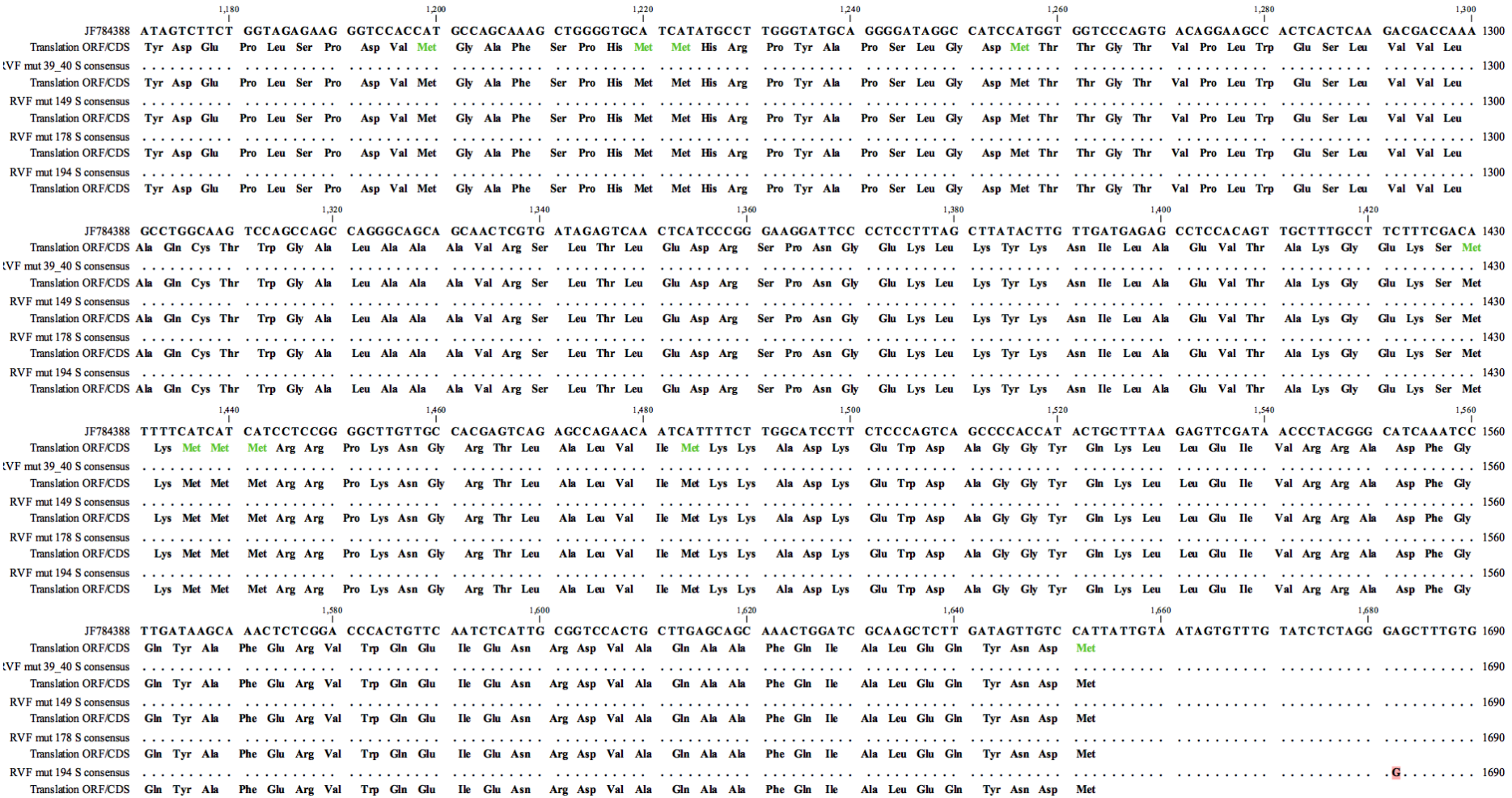
1,180 1,200 1,220 1,240 1,260 1,280 1,300
JF784388 ATAGTCTTCT GGTAGAGAAG GGTCCACCAT GCCAGCAAAG CTGGGGTGCA TCATATGCCT TGGGTATGCA GGGGATAGGC CATCCATGGT GGTCCCAGTG ACAGGAAGCC ACTCACTCAA GACGACCAAA 1300
Translation ORF/CDS Tyr Asp Glu Pro Leu Ser Pro Asp Val Met Gly Ala Phe Ser Pro His Met Met His Arg Pro Tyr Ala Pro Ser Leu Gly Asp Met Thr Thr Gly Thr Val Pro Leu Trp Glu Ser Leu Val Val Leu
RVF mut 39_40 S consensus 1300
Translation ORF/CDS Tyr Asp Glu Pro Leu Ser Pro Asp Val Met Gly Ala Phe Ser Pro His Met Met His Arg Pro Tyr Ala Pro Ser Leu Gly Asp Met Thr Thr Gly Thr Val Pro Leu Trp Glu Ser Leu Val Val Leu
RVF mut 149 S consensus 1300
Translation ORF/CDS Tyr Asp Glu Pro Leu Ser Pro Asp Val Met Gly Ala Phe Ser Pro His Met Met His Arg Pro Tyr Ala Pro Ser Leu Gly Asp Met Thr Thr Gly Thr Val Pro Leu Trp Glu Ser Leu Val Val Leu
RVF mut 178 S consensus 1300
Translation ORF/CDS Tyr Asp Glu Pro Leu Ser Pro Asp Val Met Gly Ala Phe Ser Pro His Met Met His Arg Pro Tyr Ala Pro Ser Leu Gly Asp Met Thr Thr Gly Thr Val Pro Leu Trp Glu Ser Leu Val Val Leu
RVF mut 194 S consensus 1300
Translation ORF/CDS Tyr Asp Glu Pro Leu Ser Pro Asp Val Met Gly Ala Phe Ser Pro His Met Met His Arg Pro Tyr Ala Pro Ser Leu Gly Asp Met Thr Thr Gly Thr Val Pro Leu Trp Glu Ser Leu Val Val Leu
1,320 1,340 1,360 1,380 1,400 1,420
JF784388 GCCTGGCAAG TCCAGCCAGC CAGGGCAGCA GCAACTCGTG ATAGAGTCAA CTCATCCCGG GAAGGATTCC CCTCCTTTAG CTTATACTTG TTGATGAGAG CCTCCACAGT TGCTTTGCCT TCTTTCGACA 1430
Translation ORF/CDS Ala Gln Cys Thr Trp Gly Ala Leu Ala Ala Ala Val Arg Ser Leu Thr Leu Glu Asp Arg Ser Pro Asn Gly Glu Lys Leu Lys Tyr Lys Asn Ile Leu Ala Glu Val Thr Ala Lys Gly Glu Lys Ser Met
RVF mut 39_40 S consensus 1430
Translation ORF/CDS Ala Gln Cys Thr Trp Gly Ala Leu Ala Ala Ala Val Arg Ser Leu Thr Leu Glu Asp Arg Ser Pro Asn Gly Glu Lys Leu Lys Tyr Lys Asn Ile Leu Ala Glu Val Thr Ala Lys Gly Glu Lys Ser Met
RVF mut 149 S consensus 1430
Translation ORF/CDS Ala Gln Cys Thr Trp Gly Ala Leu Ala Ala Ala Val Arg Ser Leu Thr Leu Glu Asp Arg Ser Pro Asn Gly Glu Lys Leu Lys Tyr Lys Asn Ile Leu Ala Glu Val Thr Ala Lys Gly Glu Lys Ser Met
RVF mut 178 S consensus 1430
Translation ORF/CDS Ala Gln Cys Thr Trp Gly Ala Leu Ala Ala Ala Val Arg Ser Leu Thr Leu Glu Asp Arg Ser Pro Asn Gly Glu Lys Leu Lys Tyr Lys Asn Ile Leu Ala Glu Val Thr Ala Lys Gly Glu Lys Ser Met
RVF mut 194 S consensus 1430
Translation ORF/CDS Ala Gln Cys Thr Trp Gly Ala Leu Ala Ala Ala Val Arg Ser Leu Thr Leu Glu Asp Arg Ser Pro Asn Gly Glu Lys Leu Lys Tyr Lys Asn Ile Leu Ala Glu Val Thr Ala Lys Gly Glu Lys Ser Met
1,440 1,460 1,480 1,500 1,520 1,540 1,560
JF784388 TTTTCATCAT CATCCTCCGG GGCTTGTTGC CACGAGTCAG AGCCAGAACA ATCATTTTCT TGGCATCCTT CTCCCAGTCA GCCCCACCAT ACTGCTTTAA GAGTTCGATA ACCCTACGGG CATCAAATCC 1560
Translation ORF/CDS Lys Met Met Met Arg Arg Pro Lys Asn Gly Arg Thr Leu Ala Leu Val Ile Met Lys Lys Ala Asp Lys Glu Trp Asp Ala Gly Gly Tyr Gln Lys Leu Leu Glu Ile Val Arg Arg Ala Asp Phe Gly
RVF mut 39_40 S consensus 1560
Translation ORF/CDS Lys Met Met Met Arg Arg Pro Lys Asn Gly Arg Thr Leu Ala Leu Val Ile Met Lys Lys Ala Asp Lys Glu Trp Asp Ala Gly Gly Tyr Gln Lys Leu Leu Glu Ile Val Arg Arg Ala Asp Phe Gly
RVF mut 149 S consensus 1560
Translation ORF/CDS Lys Met Met Met Arg Arg Pro Lys Asn Gly Arg Thr Leu Ala Leu Val Ile Met Lys Lys Ala Asp Lys Glu Trp Asp Ala Gly Gly Tyr Gln Lys Leu Leu Glu Ile Val Arg Arg Ala Asp Phe Gly
RVF mut 178 S consensus 1560
Translation ORF/CDS Lys Met Met Met Arg Arg Pro Lys Asn Gly Arg Thr Leu Ala Leu Val Ile Met Lys Lys Ala Asp Lys Glu Trp Asp Ala Gly Gly Tyr Gln Lys Leu Leu Glu Ile Val Arg Arg Ala Asp Phe Gly
RVF mut 194 S consensus 1560
Translation ORF/CDS Lys Met Met Met Arg Arg Pro Lys Asn Gly Arg Thr Leu Ala Leu Val Ile Met Lys Lys Ala Asp Lys Glu Trp Asp Ala Gly Gly Tyr Gln Lys Leu Leu Glu Ile Val Arg Arg Ala Asp Phe Gly
1,580 1,600 1,620 1,640 1,660 1,680
JF784388 TTGATAAGCA AACTCTCGGA CCCACTGTTC AATCTCATTG CGGTCCACTG CTTGAGCAGC AAACTGGATC GCAAGCTCTT GATAGTTGTC CATTATTGTA ATAGTGTTTG TATCTCTAGG GAGCTTTGTG 1690
Translation ORF/CDS Gln Tyr Ala Phe Glu Arg Val Trp Gln Glu Ile Glu Asn Arg Asp Val Ala Gln Ala Ala Phe Gln Ile Ala Leu Glu Gln Tyr Asn Asp Met
RVF mut 39_40 S consensus 1690
Translation ORF/CDS Gln Tyr Ala Phe Glu Arg Val Trp Gln Glu Ile Glu Asn Arg Asp Val Ala Gln Ala Ala Phe Gln Ile Ala Leu Glu Gln Tyr Asn Asp Met
RVF mut 149 S consensus 1690
Translation ORF/CDS Gln Tyr Ala Phe Glu Arg Val Trp Gln Glu Ile Glu Asn Arg Asp Val Ala Gln Ala Ala Phe Gln Ile Ala Leu Glu Gln Tyr Asn Asp Met
RVF mut 178 S consensus 1690
Translation ORF/CDS Gln Tyr Ala Phe Glu Arg Val Trp Gln Glu Ile Glu Asn Arg Asp Val Ala Gln Ala Ala Phe Gln Ile Ala Leu Glu Gln Tyr Asn Asp Met
RVF mut 194 S consensus . . . . . G 1690
Translation ORF/CDS Gln Tyr Ala Phe Glu Arg Val Trp Gln Glu Ile Glu Asn Arg Asp Val Ala Gln Ala Ala Phe Gln Ile Ala Leu Glu Gln Tyr Asn Asp Met

APPENDIX 3

Gene expression data

Table A1. Statistical analysis of the Type-I IFN gene expression array. The “p values” are calculated based on a Student’s t-test of the replicate 2^(- Delta Ct) values for each gene in the control group and treatment groups, and p values less than 0.05 are indicated in red. SABiosciences PCR Array Data Analysis Template Excel Utility, version 4.0 (http://sabiosciences.com/pcrarraydataanalysis.php).

Symbol	Well	AVG ΔC_t (Ct(GOI) - Ave Ct (HKG))		$2^{-\Delta C_t}$		Fold Change	T-TEST	Fold Up- or Down-Regulation
		RVFVM39/40 Day 3	Control Sample	RVFVC39S/C 40S Day 3	Control Sample	RVFVM39/40 Day 3 /Control Sample	p value	RVFVM39/40 Day 3 /Control Sample
Adar	A01	7.67	7.42	4.9E-03	5.8E-03	0.84	0.980369	-1.19
Bag3	A02	5.36	5.03	2.4E-02	3.1E-02	0.79	0.519517	-1.26
Bst2	A03	4.07	3.44	5.9E-02	9.2E-02	0.65	0.349819	-1.55
Casp1	A04	6.02	7.00	1.5E-02	7.8E-03	1.97	0.289209	1.97
Cav1	A05	7.64	8.43	5.0E-03	2.9E-03	1.73	0.297971	1.73
Ccl2	A06	7.85	8.86	4.3E-03	2.2E-03	2.01	0.339417	2.01
Ccl4	A07	10.35	10.98	7.7E-04	4.9E-04	1.55	0.372940	1.55
Ccl5	A08	7.47	6.59	5.6E-03	1.0E-02	0.54	0.064127	-1.84
Cd69	A09	12.10	11.56	2.3E-04	3.3E-04	0.68	0.560085	-1.46
Cd70	A10	13.51	13.42	8.6E-05	9.2E-05	0.93	0.542922	-1.07
Cd80	A11	11.09	11.03	4.6E-04	4.8E-04	0.96	0.821744	-1.04
Cd86	A12	7.57	7.68	5.3E-03	4.9E-03	1.08	0.662058	1.08
Cdkn1b	B01	3.55	4.02	8.6E-02	6.2E-02	1.39	0.076557	1.39

Ciita	B02	11.17	10.93	4.3E-04	5.1E-04	0.85	0.825687	-1.18
Crp	B03	-0.38	0.40	1.3E+00	7.6E-01	1.72	0.227373	1.72
Cxcl10	B04	6.23	6.26	1.3E-02	1.3E-02	1.02	0.572953	1.02
Ddx58	B05	4.08	4.88	5.9E-02	3.4E-02	1.74	0.273194	1.74
Eif2ak2	B06	4.07	4.97	5.9E-02	3.2E-02	1.86	0.252313	1.86
Gbp2b	B07	6.33	6.44	1.2E-02	1.2E-02	1.08	0.628023	1.08
H2-Bl	B08	8.39	7.61	3.0E-03	5.1E-03	0.58	0.559295	-1.72
H2-D1	B09	13.51	13.79	8.6E-05	7.1E-05	1.21	0.437670	1.21
H2-K1	B10	3.45	2.20	9.1E-02	2.2E-01	0.42	0.195960	-2.39
H2-M10.1	B11	13.09	12.93	1.1E-04	1.3E-04	0.90	0.471585	-1.12
H2-M3	B12	6.07	6.66	1.5E-02	9.9E-03	1.51	0.344998	1.51
H2-T10	C01	13.51	13.79	8.6E-05	7.1E-05	1.21	0.437670	1.21
Ifi204	C02	6.60	6.95	1.0E-02	8.1E-03	1.27	0.384301	1.27
Ifi30	C03	6.16	5.93	1.4E-02	1.6E-02	0.86	0.317680	-1.17
Ifih1	C04	7.78	9.01	4.6E-03	1.9E-03	2.35	0.148236	2.35
Ifit1	C05	4.68	5.32	3.9E-02	2.5E-02	1.55	0.436023	1.55
Ifit2	C06	6.63	6.69	1.0E-02	9.7E-03	1.04	0.600800	1.04
Ifit3	C07	5.60	5.88	2.1E-02	1.7E-02	1.21	0.481030	1.21
Ifitm1	C08	3.16	3.93	1.1E-01	6.6E-02	1.70	0.309877	1.70
Ifitm2	C09	1.55	1.52	3.4E-01	3.5E-01	0.98	0.980324	-1.02
Ifitm3	C10	-2.81	-1.69	7.0E+00	3.2E+00	2.18	0.183578	2.18
Ifna2	C11	13.51	13.35	8.6E-05	9.6E-05	0.89	0.604799	-1.12
Ifna4	C12	10.79	11.15	5.7E-04	4.4E-04	1.28	0.437099	1.28
Ifnar1	D01	7.01	5.56	7.7E-03	2.1E-02	0.37	0.392574	-2.74

Ifnar2	D02	1.64	1.94	3.2E-01	2.6E-01	1.24	0.436138	1.24
Ifnb1	D03	13.51	13.64	8.6E-05	7.8E-05	1.09	0.471120	1.09
Ifne	D04	13.51	13.79	8.6E-05	7.1E-05	1.21	0.437670	1.21
Ifnz	D05	13.51	13.79	8.6E-05	7.1E-05	1.21	0.437670	1.21
Il10	D06	12.81	13.17	1.4E-04	1.1E-04	1.28	0.663471	1.28
Il15	D07	6.88	6.77	8.5E-03	9.1E-03	0.93	0.709551	-1.08
Il6	D08	13.34	13.34	9.7E-05	9.7E-05	1.00	0.516794	-1.00
Irf1	D09	5.01	4.70	3.1E-02	3.8E-02	0.80	0.524557	-1.24
Irf2	D10	2.89	3.19	1.3E-01	1.1E-01	1.23	0.168182	1.23
Irf3	D11	1.95	2.54	2.6E-01	1.7E-01	1.50	0.354591	1.50
Irf5	D12	8.70	7.42	2.4E-03	5.9E-03	0.41	0.516137	-2.44
Irf7	E01	4.65	4.23	4.0E-02	5.3E-02	0.75	0.741358	-1.34
Irf9	E02	4.06	4.41	6.0E-02	4.7E-02	1.27	0.437831	1.27
Isg15	E03	1.67	2.48	3.1E-01	1.8E-01	1.75	0.372824	1.75
Isg20	E04	7.35	7.41	6.1E-03	5.9E-03	1.04	0.780850	1.04
Jak1	E05	1.60	2.38	3.3E-01	1.9E-01	1.72	0.262642	1.72
Jak2	E06	5.17	5.83	2.8E-02	1.8E-02	1.58	0.115200	1.58
Mal	E07	7.30	8.09	6.4E-03	3.7E-03	1.74	0.399539	1.74
Met	E08	3.56	3.43	8.5E-02	9.3E-02	0.91	0.838031	-1.09
Mx1	E09	8.07	9.14	3.7E-03	1.8E-03	2.10	0.252215	2.10
Mx2	E10	6.58	6.88	1.0E-02	8.5E-03	1.23	0.567298	1.23
Myd88	E11	10.98	10.37	5.0E-04	7.5E-04	0.66	0.914739	-1.52
Nmi	E12	1.78	3.03	2.9E-01	1.2E-01	2.38	0.242912	2.38
Nos2	F01	11.53	10.93	3.4E-04	5.1E-04	0.66	0.718529	-1.52

Oas1a	F02	6.75	6.45	9.3E-03	1.1E-02	0.81	0.697300	-1.23
Oas1b	F03	5.91	7.12	1.7E-02	7.2E-03	2.30	0.176641	2.30
Oas2	F04	11.83	11.70	2.8E-04	3.0E-04	0.92	0.929236	-1.09
Pml	F05	8.68	7.80	2.4E-03	4.5E-03	0.54	0.876664	-1.84
Prkcz	F06	5.27	5.41	2.6E-02	2.3E-02	1.11	0.402580	1.11
Psme2	F07	1.19	1.48	4.4E-01	3.6E-01	1.22	0.463635	1.22
Sh2d1a	F08	11.11	9.99	4.5E-04	9.9E-04	0.46	0.198548	-2.18
Shb	F09	6.58	6.05	1.0E-02	1.5E-02	0.70	0.466870	-1.43
Socs1	F10	11.11	9.98	4.5E-04	9.9E-04	0.46	0.096420	-2.20
Stat1	F11	2.89	3.49	1.4E-01	8.9E-02	1.52	0.353252	1.52
Stat2	F12	5.17	4.74	2.8E-02	3.7E-02	0.74	0.517363	-1.35
Stat3	G01	3.64	3.48	8.0E-02	9.0E-02	0.89	0.742296	-1.12
Tap1	G02	7.10	5.82	7.3E-03	1.8E-02	0.41	0.497171	-2.42
Ticam1	G03	9.66	8.06	1.2E-03	3.8E-03	0.33	0.918752	-3.05
Timp1	G04	12.77	12.42	1.4E-04	1.8E-04	0.79	0.649407	-1.27
Tlr3	G05	7.04	7.34	7.6E-03	6.2E-03	1.23	0.395134	1.23
Tlr7	G06	9.45	9.37	1.4E-03	1.5E-03	0.94	0.817114	-1.06
Tlr8	G07	8.59	8.43	2.6E-03	2.9E-03	0.89	0.746933	-1.12
Tlr9	G08	11.25	12.45	4.1E-04	1.8E-04	2.29	0.313000	2.29
Tnfsf10	G09	6.55	6.71	1.1E-02	9.6E-03	1.12	0.549492	1.12
Traf3	G10	7.31	7.53	6.3E-03	5.4E-03	1.17	0.692315	1.17
Tyk2	G11	6.96	6.50	8.0E-03	1.1E-02	0.73	0.899398	-1.38
Vegfa	G12	2.78	2.69	1.5E-01	1.6E-01	0.94	0.598095	-1.06
Actb	H01	0.16	0.06	8.9E-01	9.6E-01	0.93	0.828872	-1.07

B2m	H02	-4.70	-3.61	2.6E+01	1.2E+01	2.14	0.260826	2.14
Gapdh	H03	0.28	-0.25	8.3E-01	1.2E+00	0.69	0.603049	-1.44
Gusb	H04	4.85	4.45	3.5E-02	4.6E-02	0.76	0.218259	-1.32
Hsp90ab1	H05	-0.59	-0.65	1.5E+00	1.6E+00	0.95	0.768339	-1.05

Table A.2. Fold changes in expression of 84 genes involved in activation of inflammatory cytokines and receptors in the liver and spleen. Fold changes are shown for mice infected with wildtype RVFV SA35/74 or mutant NSsC39S/C40S relative to expression in mock inoculated mice as average of replicates (n=3 mice per group) on day 3 and 5 pi. Statistically significant fold-changes ($p<0.05$) are indicated by an asterisk (*) next to the fold change value.

		Liver								Spleen							
		Day 3				Day 5				Day 3				Day 5			
Gene Symbol	**Description**	**SA 35/74**	***p*-values**	**M39 /40**	***p*-values**	**SA 35/74**	***p*-values**	**M39 /40**	***p*-values**	**SA 35/74**	***p*-values**	**M39 /40**	***p*-values**	**SA 35/74**	***p*-values**	**M39 /40**	***p*-values**
Aimp1	Aminoacyl tRNA synthetase complex-interacting multifunctional protein 1	-3.56	0.333779	-1.85	0.404455	-3.23	0.339418	-3.14	0.340398	-1.10	0.813350	-1.18	0.113117	1.26	0.174458	1.31	0.226824
Bmp2	Bone morphogenetic protein 2	-3.40	0.296128	-1.45	0.384752	-4.08	0.281042	-2.93	0.323705	-3.93*	0.000818	1.16	0.286349	-4.81*	0.001213	-1.87	0.169177
Ccl1	Chemokine (C-C motif) ligand 1	-2.31	0.234944	-5.70	0.063828	-1.66	0.451440	-5.60	0.073386	-2.10	0.220391	-1.64	0.226900	-2.41	0.135146	1.89	0.412450
Ccl11	Chemokine (C-C motif) ligand 11	28.79	0.167800	-1.83	0.419610	95.72*	0.016292	-1.58	0.418611	8.88	0.088375	-1.60	0.017938	6.63*	0.025762	1.47	0.362390
Ccl12	Chemokine (C-C motif) ligand 12	9.74	0.307203	-8.28	0.162751	26.09*	0.000612	-9.50	0.395223	65.84*	0.013853	1.18	0.781129	64.40*	0.000007	4.11	0.259305
Ccl17	Chemokine (C-C motif) ligand 17	1.39	0.671862	-3.44	0.373527	3.77	0.791935	-4.96	0.354509	1.38	0.328225	-1.06	0.611781	2.16	0.077334	1.40	0.455020
Ccl19	Chemokine (C-C motif) ligand 19	3.35	0.291922	-6.56	0.256654	3.55	0.241452	-10.74	0.242956	1.19	0.611491	-1.77	0.124288	1.78	0.171104	2.01	0.169283
Ccl2	Chemokine (C-C motif) ligand 2	142.86*	0.024600	-5.07	0.200604	167.07*	0.000657	-4.16	0.285086	183.83*	0.020027	1.30	0.223378	111.90*	0.001334	5.24	0.129476
Ccl20	Chemokine (C-C motif) ligand 20	4.36	0.404913	-9.51	0.299215	13.44	0.087438	-9.75	0.301338	5.93	0.244128	1.32	0.475316	20.60*	0.027309	2.08	0.157721

Ccl22	Chemokine (C-C motif) ligand 22	6.81	0.550676	-2.56	0.393934	6.60	0.605353	-3.95	0.389184	-1.77	0.161534	1.02	0.814738	-2.59*	0.003655	-2.01	0.098338
Ccl24	Chemokine (C-C motif) ligand 24	-26.77	0.181106	-3.90	0.243670	-15.61	0.188173	-5.49	0.219651	-9.28*	0.003665	2.06	0.133453	-9.31*	0.002534	2.19	0.127526
Ccl3	Chemokine (C-C motif) ligand 3	15.64*	0.015792	-7.02	0.232986	21.46*	0.000118	-5.30	0.309661	12.06*	0.008619	-1.13	0.394957	8.99*	0.016786	2.32	0.132929
Ccl4	Chemokine (C-C motif) ligand 4	45.65*	0.010702	-2.40	0.270704	42.33	0.016631	-1.03	0.998912	12.11	0.098039	-1.14	0.518836	6.76	0.066066	1.16	0.581103
Ccl5	Chemokine (C-C motif) ligand 5	3.75	0.113582	-4.46	0.254107	6.44*	0.016982	-2.80	0.324083	-1.01	0.979936	-1.25	0.133291	-1.11	0.449904	1.16	0.461549
Ccl6	Chemokine (C-C motif) ligand 6	-1.81	0.492521	-3.75	0.239524	1.66	0.858882	-3.40	0.258448	-1.10	0.847283	1.01	0.989782	1.73	0.125952	2.14	0.079521
Ccl7	Chemokine (C-C motif) ligand 7	167.18*	0.033123	-6.18	0.292781	220.45*	0.000458	-4.04	0.723116	675.39*	0.001129	1.43	0.528634	659.66*	0.007357	12.11	0.267306
Ccl8	Chemokine (C-C motif) ligand 8	1.36	0.551698	-10.94	0.336303	2.60	0.798853	-4.87	0.357783	3.47	0.064515	1.08	0.691634	3.90	0.072556	5.66	0.168634
Ccl9	Chemokine (C-C motif) ligand 9	-7.29	0.265888	-3.89	0.297793	-5.33	0.284218	-3.99	0.297404	1.53	0.432511	-1.13	0.355103	4.18	0.207621	1.16	0.559191
Ccr1	Chemokine (C-C motif) receptor 1	63.87	0.083394	-3.54	0.373955	101.79*	0.009666	-3.01	0.385811	1.90	0.033891	-1.22	0.072470	2.06	0.102117	-1.27	0.346674
Ccr10	Chemokine (C-C motif) receptor 10	-11.93	0.242037	-1.04	0.477316	-9.10	0.253469	-2.33	0.336118	-7.89*	0.000821	1.26	0.203067	-13.10*	0.000336	-3.20*	0.004434
Ccr2	Chemokine (C-C motif) receptor 2	1.20	0.758173	-3.38	0.344845	1.73	0.850136	-3.45	0.337787	-2.33*	0.013596	1.17	0.241229	-2.16*	0.017761	-1.14	0.950540
Ccr3	Chemokine (C-C motif) receptor 3	-3.64	0.317398	-2.17	0.365086	-2.22	0.356772	-3.21	0.322052	-4.24*	0.000230	1.91	0.002713	-4.38*	0.000012	-1.00	0.848167
Ccr4	Chemokine (C-C motif) receptor 4	-1.41	0.235322	-2.82	0.111841	-2.04	0.389890	-2.56	0.041592	-2.03*	0.009456	1.22	0.204409	-2.92*	0.006047	-1.38	0.219044
Ccr5	Chemokine (C-C motif) receptor 5	-2.33	0.386949	-2.89	0.336027	-1.05	0.560343	-3.80	0.319489	1.34	0.358977	-1.26	0.066448	1.62	0.014565	-1.57	0.435472
Ccr6	Chemokine (C-C motif) receptor 6	-10.92	0.230785	-9.12	0.236220	-9.22	0.251984	-9.91	0.229385	-2.85*	0.009962	-1.26	0.243085	-1.30	0.092462	1.18	0.143392
Ccr8	Chemokine (C-C motif) receptor 8	-3.43	0.407627	6.59	0.373943	-1.37	0.425547	-16.43	0.231423	1.50	0.274269	-1.09	0.581911	2.27	0.145962	-2.55*	0.021287
Cd40lg	CD40 ligand	-3.99	0.248737	-6.43	0.176129	-4.83	0.191595	-5.78	0.177833	-2.93*	0.002039	-1.17	0.301881	-2.99*	0.000660	1.10	0.624023
Csf1	Colony stimulating factor 1 (macrophage)	9.59*	0.023822	-1.54	0.410705	8.18*	0.018083	-1.43	0.428174	1.44	0.100151	1.71	0.079908	1.22	0.302822	-1.04	0.994680
Csf2	Colony stimulating factor 2 (granulocyte-macrophage)	-4.01	0.263382	-3.74	0.275548	-3.80	0.273241	-6.90	0.224812	2.37	0.068833	1.47	0.384711	1.47	0.455112	1.40	0.433330

Csf3	Colony stimulating factor 3 (granulocyte)	578.73	0.211738	-6.00	0.052064	924.42*	0.014326	-6.92*	0.049885	103.65	0.087831	1.10	0.797133	210.53	0.131099	-1.99	0.675908
Cx3cl1	Chemokine (C-X3-C motif) ligand 1	-1.04	0.567331	1.18	0.586161	1.32	0.621741	-1.40	0.479330	-1.09	0.855517	1.34	0.090395	-2.44*	0.003605	-2.20*	0.025398
Cxcl1	Chemokine (C-X-C motif) ligand 1	11.99	0.079234	-3.18	0.244969	15.42*	0.011961	-8.12	0.176077	82.75*	0.038325	-1.33	0.413691	115.56	0.279481	2.81	0.191467
Cxcl10	Chemokine (C-X-C motif) ligand 10	16.96	0.067706	-3.27	0.305434	7.84	0.151679	-4.28	0.381095	7.10	0.217070	1.05	0.723201	2.42	0.129665	1.64	0.358091
Cxcl11	Chemokine (C-X-C motif) ligand 11	40.13*	0.045421	-2.45	0.281750	35.80*	0.025549	-3.69	0.250860	58.96*	0.032206	-1.31	0.945263	40.95*	0.006034	3.02	0.352452
Cxcl12	Chemokine (C-X-C motif) ligand 12	-4.53	0.274553	-2.94	0.308534	-4.76	0.264703	-4.57	0.272941	-1.54	0.113760	1.07	0.381430	-1.40	0.088159	-1.40	0.484370
Cxcl13	Chemokine (C-X-C motif) ligand 13	-1.86	0.423955	-4.95	0.222108	1.28	0.896724	-8.83	0.192018	1.94	0.134490	-1.24	0.186951	5.00	0.131715	1.89	0.148086
Cxcl15	Chemokine (C-X-C motif) ligand 15	-1.40	0.576461	-7.04	0.198997	-2.17	0.371923	-5.68	0.210720	2.73	0.072508	1.14	0.675135	2.92	0.114245	1.35	0.422804
Cxcl5	Chemokine (C-X-C motif) ligand 5	83.48	0.072314	-3.40	0.379004	125.57*	0.011643	-9.65	0.352104	20.79	0.114109	1.24	0.356279	27.42	0.125809	5.05	0.043823
Cxcl9	Chemokine (C-X-C motif) ligand 9	17.23*	0.003396	-6.07	0.058041	13.82*	0.006018	-4.63	0.129440	17.49*	0.000287	-1.31	0.078074	16.29*	0.001825	2.64	0.177404
Cxcr2	Chemokine (C-X-C motif) receptor 2	72.82	0.098470	-2.05	0.398677	98.26*	0.000467	-1.51	0.425869	-1.08	0.780502	-1.08	0.354409	-1.47	0.854364	-1.75*	0.043945
Cxcr3	Chemokine (C-X-C motif) receptor 3	-2.29	0.380827	-3.52	0.297884	-3.62	0.336008	-3.40	0.291545	-3.03*	0.019039	-1.21	0.297046	-2.48*	0.017647	-1.13	0.457447
Cxcr5	Chemokine (C-X-C motif) receptor 5	-2.38	0.302163	-6.92	0.181912	-4.88	0.210569	-6.57	0.187337	-1.69	0.211378	1.12	0.092900	-1.98	0.000108	-1.53	0.120815
Fasl	Fas ligand (TNF superfamily, member 6)	4.75	0.143864	-4.19	0.183335	3.50	0.200036	-3.24	0.202626	2.93*	0.018042	-1.13	0.639120	2.69*	0.001322	2.07	0.120178
Ifng	Interferon gamma	3.46	0.361967	-6.11	0.302778	1.04	0.571770	-3.55	0.321316	5.35	0.170894	1.31	0.334733	2.35	0.107167	1.24	0.551685
Il10ra	Interleukin 10 receptor, alpha	1.60	0.776841	-1.80	0.402136	2.68	0.873610	-1.89	0.394790	-1.18	0.109624	1.29	0.005645	-1.02	0.905888	-1.55	0.120055
Il10rb	Interleukin 10 receptor, beta	-1.07	0.593107	-2.23	0.357668	1.05	0.610461	-3.51	0.308715	-2.15*	0.001495	1.17	0.044692	-2.10*	0.001545	-1.11	0.539469
Il11	Interleukin 11	15.31	0.104252	-5.70	0.063828	24.66*	0.014094	-6.36	0.060176	4.80	0.096461	1.15	0.581001	3.65*	0.025372	1.70	0.155955
Il13	Interleukin 13	1.20	0.743871	-3.01	0.133738	1.30	0.551463	-5.43	0.065761	1.38	0.389258	-1.11	0.556792	1.01	0.710606	1.79	0.283629
Il15	Interleukin 15	-1.07	0.611508	-3.15	0.302213	-1.64	0.437450	-4.01	0.279468	1.27	0.433025	1.27	0.092829	-1.40	0.254987	1.51	0.068758
Il16	Interleukin 16	1.07	0.631055	-2.01	0.369323	1.27	0.736319	-3.07	0.322049	-1.99	0.010316	1.06	0.584109	-1.91	0.006779	-2.25	0.050123

Il17a	Interleukin 17A	-2.31	0.234944	-5.70	0.063828	-1.66	0.451440	-7.23	0.057822	1.77	0.209614	-1.15	0.560083	1.72	0.346968	-1.17	0.919233
Il17b	Interleukin 17B	4.32	0.166772	-5.70	0.063828	8.38*	0.018214	-5.20	0.068253	14.04	0.103332	1.08	0.732641	20.40*	0.005359	3.05*	0.026704
Il17f	Interleukin 17F	1.06	0.687573	-2.05	0.350984	-1.27	0.497686	-2.96	0.284659	1.85	0.109488	1.05	0.953058	1.75	0.105320	-1.34	0.295285
Il1a	Interleukin 1 alpha	4.43	0.102407	-3.70	0.122963	4.13*	0.027920	-3.21	0.138122	1.94	0.064027	1.25	0.192953	1.51	0.065400	1.99	0.075696
Il1b	Interleukin 1 beta	4.04	0.192482	-4.13	0.256470	4.35	0.052063	-2.77	0.295541	-1.14	0.816236	-1.06	0.545672	-1.64	0.183510	1.18	0.413513
Il1r1	Interleukin 1 receptor, type-I	1.08	0.864504	-1.33	0.495564	1.41	0.919805	-2.70	0.336284	1.05	0.667569	1.37	0.067806	1.41	0.376082	-1.71	0.175954
Il1rn	Interleukin 1 receptor antagonist	3.88	0.116361	-2.82	0.242004	7.66*	0.007221	-8.55	0.163491	19.63*	0.008701	-1.02	0.941808	15.08*	0.013127	1.62	0.404897
Il21	Interleukin 21	-2.31	0.234944	-5.70	0.063828	-1.66	0.451440	-7.23	0.057822	-1.68	0.121161	-2.11*	0.004402	-1.24	0.697757	-1.19	0.437006
Il27	Interleukin 27	8.28*	0.047169	-4.89	0.274637	4.85	0.203795	-7.55	0.289083	4.71	0.155217	1.49	0.254533	2.05	0.091276	-1.05	0.856558
Il2rb	Interleukin 2 receptor, beta chain	4.12	0.588489	-1.04	0.447982	4.76	0.460163	-1.30	0.409593	1.22	0.412561	1.17	0.399793	1.36	0.075233	-2.29	0.032065
Il2rg	Interleukin 2 receptor, gamma chain	7.36	0.104593	-1.87	0.388993	7.06*	0.020993	-1.79	0.417913	-1.16	0.543830	-1.07	0.390860	-1.52	0.021404	-1.57	0.061912
Il3	Interleukin 3	2.02	0.210826	-5.70	0.063828	-1.05	0.786975	-7.23	0.057822	3.23	0.208318	1.44	0.253664	2.90	0.073231	1.28	0.478552
Il33	Interleukin 33	2.44	0.320050	-2.37	0.329012	3.07	0.278912	-2.91	0.306956	5.13*	0.011814	1.36	0.090740	3.90*	0.028563	1.56	0.054343
Il4	Interleukin 4	-1.23	0.461742	-6.69*	0.032188	-1.95	0.138267	-3.63*	0.044040	-3.46*	0.000667	-1.38	0.004452	-3.95*	0.000019	1.49	0.273345
Il5	Interleukin 5	-1.25	0.789113	-2.45	0.206391	1.16	0.702970	-7.23	0.057822	1.17	0.490778	-1.87	0.266096	1.28	0.497034	1.11	0.543811
Il5ra	Interleukin 5 receptor, alpha	-1.67	0.436394	-8.28	0.153964	-2.05	0.491996	-9.92	0.148607	-1.98	0.098888	-1.45	0.206412	-2.07	0.087150	-1.90	0.112996
Il6ra	Interleukin 6 receptor, alpha	-3.52	0.331600	-1.12	0.517286	-3.32	0.336963	-2.78	0.355319	-2.58	0.011707	1.39	0.108788	-2.22*	0.011155	-1.85	0.088930
Il6st	Interleukin 6 signal transducer	-1.45	0.455668	-2.79	0.334845	-1.79	0.408196	-4.26	0.302931	-1.17	0.470802	-1.05	0.558034	-1.05	0.967348	-1.43	0.181130
Il7	Interleukin 7	1.97	0.421843	-3.52	0.171126	-1.41	0.396170	-1.88	0.285964	-6.50	0.006234	1.28	0.133112	-4.04*	0.049444	1.03	0.656570
Lta	Lymphotoxin A	2.43	0.306040	-4.18*	0.021137	-1.10	0.944670	-5.82*	0.014396	-5.90	0.005494	-1.19	0.301405	-8.70*	0.002347	-3.38*	0.015651
Ltb	Lymphotoxin B	8.33	0.447949	1.16	0.426009	9.37	0.349060	-1.29	0.381968	-5.10	0.001971	1.00	0.966591	-9.86*	0.000466	-3.56*	0.001535

Mif	Macrophage migration inhibitory factor	-5.49	0.215299	-3.63	0.241946	-6.60	0.204946	-5.19	0.216232	1.58	0.078812	-1.50	0.046873	1.85	0.004401	1.64	0.223885
Nampt	Nicotinamide phosphoribosyltransferase	-2.31	0.317047	-4.41	0.234375	-3.43	0.260990	-4.79	0.229604	3.25*	0.011383	1.15	0.322798	2.28*	0.004480	1.40	0.292229
Osm	Oncostatin M	58.94	0.203629	-5.22*	0.029672	79.40*	0.001486	-3.97	0.077196	3.27*	0.025512	1.27	0.279395	2.80*	0.006166	-1.34	0.335368
Pf4	Platelet factor 4	5.49	0.324537	-1.04	0.558306	9.12	0.054680	-2.65	0.360873	-1.08	0.666114	1.44	0.280412	-1.14	0.724945	-1.34	0.708487
Spp1	Secreted phosphoprotein 1	-2.01	0.419814	-5.28	0.242400	1.77	0.682950	-6.68	0.232148	3.52	0.162737	-2.13	0.221649	8.46*	0.000200	1.91	0.283854
Tnf	Tumor necrosis factor	205.90	0.078965	1.45	0.363248	165.68*	0.005952	1.11	0.606866	2.34	0.126134	1.16	0.702358	1.49	0.289700	-2.24	0.260328
Tnfrsf11b	Tumor necrosis factor receptor superfamily, member 11b (osteoprotegerin)	5.10	0.139508	-1.72	0.415656	4.37	0.157992	-2.42	0.401171	2.08	0.182391	1.25	0.324025	1.59	0.110084	1.01	0.796779
Tnfsf10	Tumor necrosis factor (ligand) superfamily, member 10	1.24	0.824753	-4.25	0.292907	-2.08	0.386275	-4.46	0.290480	2.03	0.269941	-1.01	0.935608	1.36	0.287609	1.08	0.697077
Tnfsf11	Tumor necrosis factor (ligand) superfamily, member 11	2.71	0.298639	-5.49	0.064877	4.73*	0.003828	-4.45	0.084541	-2.48*	0.002002	-1.02	0.744610	-1.50	0.065242	1.02	0.771609
Tnfsf13	Tumor necrosis factor (ligand) superfamily, member 13	-2.51	0.355442	-1.88	0.390381	-2.28	0.362198	-2.98	0.341069	-5.71*	0.003194	1.48	0.022656	-5.32*	0.002439	-1.17	0.473984
Tnfsf13b	Tumor necrosis factor (ligand) superfamily, member 13b	7.25	0.121431	-2.17	0.384149	5.34	0.163977	-2.04	0.396251	-1.09	0.603132	1.04	0.474928	-1.08	0.657523	-1.26	0.256617
Tnfsf4	Tumor necrosis factor (ligand) superfamily, member 4	-2.15	0.239233	-5.70	0.063828	-1.66	0.451440	-7.23	0.057822	-1.76	0.132384	-1.54	0.193182	-1.26	0.262291	-1.47	0.332520
Vegfa	Vascular endothelial growth factor A	-1.51	0.507360	-2.56	0.190510	-1.64	0.354910	-3.56	0.149710	-2.05	0.020848	-1.10	0.378146	-1.71	0.171314	-1.34	0.221748
Actb	Actin, beta	68.14	0.035268	32.17	0.031306	73.77	0.004839	38.24	0.017268	-1.62	0.049249	1.28	0.086689	-1.98	0.021528	-1.36	0.353288
B2m	Beta-2 microglobulin	-2.31	0.297913	-2.91	0.262563	-2.45	0.287374	-3.09	0.255572	1.86	0.008543	-1.13	0.289533	1.74	0.022095	1.78	0.069025
Gapdh	Glyceraldehyde-3-phosphate dehydrogenase	-2.25	0.359805	-1.32	0.469522	-2.59	0.341089	-1.45	0.441736	1.17	0.240495	1.16	0.330799	1.31	0.024143	-1.43	0.095148
Gusb	Glucuronidase, beta	-5.35	0.301618	-3.31	0.329886	-3.74	0.320299	-3.78	0.319981	-1.86	0.003665	-1.15	0.100382	-1.43	0.037736	1.02	0.811099
Hsp90ab1	Heat shock protein 90 alpha (cytosolic), class B member 1	-2.45	0.359540	-2.53	0.348737	-3.11	0.329738	-2.25	0.363508	1.39	0.107995	-1.15	0.361873	1.25	0.217316	1.07	0.717336

Table A.3. Fold changes in expression of 84 genes involved in activation of type-I interferon response in the liver and spleen. Fold changes are shown for mice infected with wild type RVFV SA35/74 or mutant NSsC39S/C40S relative to expression in mock inoculated mice as average of replicates (n=3 mice per group) on day 3 and 5 pi. Statistically significant fold-changes (p<0.05) are indicated by an asterisk (*) next to the fold change value.

		Liver								Spleen							
		Day 3				Day 5				Day 3				Day 5			
Gene Symbol	**Description**	**SA 35/74**	***p*-values**	**M39 /40**	***p*-values**	**SA 35/74**	***p*-values**	**M39 /40**	***p*-values**	**SA 35/74**	***p*-values**	**M39 /40**	***p*-values**	**SA 35/74**	***p*-Values**	**M39 /40**	***p*-values**
Adar	Adenosine deaminase, RNA-specific	2.83*	0.031131	-1.19	0.980369	2.02	0.214202	1.26	0.298827	-7.25	0.374479	-10.10	0.374087	-9.96	0.374072	-14.59	0.373845
Bag3	Bcl2-associated athanogene 3	2.07	0.486404	-1.26	0.519517	2.31	0.367689	1.24	0.853311	-9.93	0.374091	-15.95	0.373930	-8.25	0.374139	-16.80	0.373924
Bst2	Bone marrow stromal cell antigen 2	4.01*	0.002797	-1.55	0.349819	2.82*	0.019803	1.12	0.575209	-1.20	0.376999	-6.62	0.374323	-1.84	0.375908	-5.60	0.374779
Casp1	Caspase 1	2.44*	0.003818	1.97	0.289209	4.06	0.160428	-1.42	0.802159	-11.08	0.372653	-9.83	0.372907	-12.53	0.372335	-8.25	0.373573
Cav1	Caveolin 1, caveolae protein	-1.35	0.865139	1.73	0.297971	1.17	0.563086	1.05	0.761132	-43.87	0.373128	-10.36	0.373923	-35.24	0.373203	-14.52	0.373644
Ccl2	Chemokine (C-C motif) ligand 2	570.86*	0.012548	2.01	0.339417	850.21*	0.009670	1.35	0.438873	6.31	0.386377	-18.23	0.373934	2.80	0.379297	-10.06	0.374062
Ccl4	Chemokine (C-C motif) ligand 4	74.51*	0.019088	1.55	0.372940	56.29	0.051459	1.72	0.430139	20.10	0.086991	1.54	0.377060	11.48	0.057605	1.89	0.392178
Ccl5	Chemokine (C-C motif) ligand 5	7.41*	0.029267	-1.84	0.064127	10.82	0.052802	-1.59	0.855753	-7.10	0.373531	-8.12	0.372871	-7.83	0.373014	-7.98	0.373071
Cd69	CD69 antigen	18.24	0.097871	-1.46	0.560085	12.20*	0.009336	1.00	0.900588	-1.11	0.408989	-6.29	0.372480	-1.51	0.397046	-4.76	0.375042
Cd70	CD70 antigen	2.26	0.060089	-1.07	0.542922	1.28	0.511121	-2.08	0.892719	-49.36	0.373888	-72.23	0.373879	-46.40	0.373887	-56.92	0.373883
Cd80	CD80 antigen	9.11	0.069935	-1.04	0.821744	25.29*	0.016473	1.12	0.783372	-23.52	0.373915	-31.79	0.373907	-21.09	0.373920	-45.45	0.373899

Cd86	CD86 antigen	2.83	0.209363	1.08	0.662058	7.46*	0.006555	-1.05	0.663870	-8.58	0.374118	-13.99	0.373970	-9.53	0.374085	-14.61	0.373964
Cdkn1b	Cyclin-dependent kinase inhibitor 1B	-2.22*	0.038823	1.39	0.076557	-1.78	0.123604	-1.36	0.181126	-3.84	0.317305	-2.48	0.356292	-3.06	0.337052	-3.36	0.327107
Ciita	Class II transactivator	1.23	0.455041	-1.18	0.825687	-1.39	0.721132	-1.42	0.453512	-6.99	0.344574	-2.85	0.374939	-7.30	0.341901	-4.41	0.355872
Crp	C-reactive protein, pentraxin-related	-3.96*	0.027121	1.72	0.227373	-6.11*	0.014146	1.03	0.979615	-59.00	0.373410	-89.58	0.373323	-48.15	0.373381	-17.71	0.373685
Cxcl10	Chemokine (C-X-C motif) ligand 10	34.48	0.075161	1.02	0.572953	19.57	0.091747	-1.69	0.796148	3.38	0.407386	-2.08	0.412373	1.04	0.588850	-1.52	0.496177
Ddx58	DEAD (Asp-Glu-Ala-Asp) box polypeptide 58	5.18*	0.047313	1.74	0.273194	3.16	0.058180	1.56	0.399489	-1.50	0.432891	-3.17	0.377065	-1.79	0.407201	-2.96	0.385477
Eif2ak2	Eukaryotic translation initiation factor 2-alpha kinase 2	3.67*	0.040111	1.86	0.252313	2.45	0.104292	1.37	0.460355	-1.29	0.538147	-2.66	0.377367	-2.30	0.383757	-3.22	0.362576
Gbp2b	Guanylate binding protein 1	51.67*	0.024074	1.08	0.628023	25.58*	0.020334	1.10	0.573077	2.23	0.766711	-3.32	0.375346	1.13	0.491996	-2.28	0.401474
H2-Bl	Histocompatibility 2, blastocyst	1.71	0.241676	-1.72	0.559295	1.24	0.450991	-1.13	0.885849	-4.85	0.375513	-5.66	0.374696	-4.59	0.376293	-4.56	0.376156
H2-D1	Histocompatibility 2, D region locus 1	1.54	0.451349	1.21	0.437670	1.67	0.373926	-1.87	0.978359	-22.46	0.373433	-76.91	0.373221	-18.43	0.373547	-29.21	0.373381
H2-K1	Histocompatibility 2, K1, K region	2.86*	0.001850	-2.39	0.195960	2.12*	0.037394	-1.10	0.779194	1.66	0.015658	-1.08	0.762077	1.39	0.078019	1.06	0.712335
H2-M10.1	Histocompatibility 2, M region locus 10.1	-1.18	0.452141	-1.12	0.471585	1.44	0.439551	-1.90	0.820036	-90.55	0.373880	-243.93	0.373875	-67.50	0.373886	-136.29	0.373878
H2-M3	Histocompatibility 2, M region locus 3	4.63*	0.014245	1.51	0.344998	5.40	0.076079	1.09	0.632465	-3.51	0.378070	-4.33	0.373190	-3.45	0.378606	-5.07	0.371428
H2-T10	Histocompatibility 2, T region locus 10	1.54	0.451349	1.21	0.437670	1.67	0.373926	-2.06	0.995271	-64.99	0.373848	-161.30	0.373836	-48.85	0.373855	-116.32	0.373839
Ifi204	Interferon activated gene 204	33.47*	0.025026	1.27	0.384301	35.98*	0.007510	-1.03	0.630792	1.18	0.385731	-6.31	0.374801	-1.33	0.381114	-5.93	0.375538
Ifi30	Interferon gamma inducible protein 30	1.40	0.443799	-1.17	0.317680	2.80*	0.019916	1.28	0.405391	-1.56	0.021840	1.27	0.063827	-2.05*	0.003433	1.09	0.626176
Ifih1	Interferon induced with helicase C domain 1	10.43*	0.018407	2.35	0.148236	5.88	0.105709	2.12	0.353135	1.51	0.510401	-2.21	0.393727	-1.16	0.428526	-2.56	0.397250

Ifit1	Interferon-induced protein with tetratricopeptide repeats 1	35.02*	0.014498	1.55	0.436023	23.25	0.077063	1.72	0.416634	2.07	0.540739	-5.80	0.378022	1.47	0.456907	-4.22	0.393237
Ifit2	Interferon-induced protein with tetratricopeptide repeats 2	66.38*	0.008243	1.04	0.600800	33.74*	0.042813	1.28	0.469608	1.59	0.396718	-6.95	0.374765	-1.16	0.382902	-5.12	0.377282
Ifit3	Interferon-induced protein with tetratricopeptide repeats 3	87.30*	0.011486	1.21	0.481030	30.18	0.071556	2.80	0.380319	8.22	0.101546	-1.20	0.814533	5.39	0.082058	1.07	0.629665
Ifitm1	Interferon induced transmembrane protein 1	5.41*	0.031336	1.70	0.309877	6.05*	0.020954	-1.59	0.056970	-1.30	0.473795	-3.04	0.343951	-1.54	0.434338	-2.61	0.356778
Ifitm2	Interferon induced transmembrane protein 2	1.03	0.999325	-1.02	0.980324	-1.08	0.806338	-1.38	0.238814	2.10	0.074638	1.28	0.004813	2.34*	0.012379	1.19	0.050076
Ifitm3	Interferon induced transmembrane protein 3	2.02*	0.005637	2.18	0.183578	1.86	0.000797	1.33	0.474132	2.42	0.196007	-1.61	0.410116	2.10	0.280448	-1.41	0.587040
Ifna2	Interferon alpha 2	104.12*	0.001423	-1.12	0.604799	61.88	0.075555	1.79	0.153246	1.61	0.376345	-88.64	0.373824	1.37	0.376238	-18.94	0.373922
Ifna4	Interferon alpha 4	202.15*	0.001015	1.28	0.437099	125.75	0.058554	-1.78	0.468706	3.02	0.456961	-20.36	0.370375	2.59	0.445485	-11.56	0.371747
Ifnar1	Interferon (alpha and beta) receptor 1	-1.08	0.877160	-2.74	0.392574	-1.50	0.296146	-1.59	0.299268	-6.55	0.371523	-4.46	0.375153	-6.62	0.371595	-7.37	0.370613
Ifnar2	Interferon (alpha and beta) receptor 2	-1.08	0.619564	1.24	0.436138	-1.18	0.317287	-1.50	0.091342	-1.50	0.136778	-1.08	0.588438	-1.49	0.115288	-1.33	0.136707
Ifnb1	Interferon beta 1, fibroblast	2597.38*	0.001830	1.09	0.471120	2237.59*	0.035011	1.95	0.399117	6.97	0.420185	-70.16	0.373318	7.28	0.420437	-21.17	0.373690
Ifne	Interferon epsilon	2.58	0.136907	1.21	0.437670	2.54	0.255466	-1.15	0.737864	-20.52	0.373754	-83.56	0.373433	-16.41	0.373666	-75.10	0.373440
Ifnz	Interferon zeta	11.47	0.053824	1.21	0.437670	7.74*	0.000973	-2.06	0.995271	-44.59	0.373619	-80.96	0.373566	-28.17	0.373659	-107.02	0.373553
Il10	Interleukin 10	11.78	0.111843	1.28	0.663471	20.10*	0.042798	-2.75	0.609783	1.29	0.389840	-14.18	0.373558	2.08	0.393379	-16.57	0.373624
Il15	Interleukin 15	1.87	0.071052	-1.08	0.709551	1.31	0.313050	-1.75	0.027716	-6.35	0.375115	-7.14	0.374196	-12.45	0.373176	-6.24	0.374581

Il6	Interleukin 6	290.11	0.195771	-1.00	0.516794	494.73*	0.010153	-1.07	0.536197	1.89	0.374787	-52.44	0.373901	1.27	0.374640	-25.80	0.373912
Irf1	Interferon regulatory factor 1	6.97	0.089388	-1.24	0.524557	4.44	0.089876	-1.67	0.073215	-2.73	0.384350	-4.65	0.374724	-4.29	0.375720	-4.49	0.375256
Irf2	Interferon regulatory factor 2	1.24	0.475472	1.23	0.168182	-1.14	0.942925	-1.40	0.045759	-8.76	0.371414	-5.71	0.373343	-9.58	0.370145	-7.01	0.371863
Irf3	Interferon regulatory factor 3	-1.98	0.027738	1.50	0.354591	-1.51	0.261228	-1.44	0.353407	-6.95	0.352867	-4.61	0.361589	-6.73	0.353329	-4.92	0.359870
Irf5	Interferon regulatory factor 5	2.21	0.067022	-2.44	0.516137	1.82	0.115745	-1.79	0.702725	-4.68	0.370869	-2.83	0.382510	-4.46	0.371856	-3.89	0.374549
Irf7	Interferon regulatory factor 7	44.15*	0.001831	-1.34	0.741358	29.11*	0.035613	1.44	0.456963	3.60	0.799896	-3.41	0.379369	2.60	0.897329	-2.37	0.524820
Irf9	Interferon regulatory factor 9	2.20*	0.021158	1.27	0.437831	2.16*	0.000403	1.02	0.751503	-3.47	0.378052	-4.02	0.376157	-3.46	0.377995	-5.22	0.371687
Isg15	ISG15 ubiquitin-like modifier	18.76*	0.041843	1.75	0.372824	14.14*	0.000088	1.73	0.415015	1.51	0.855680	-4.16	0.353941	-1.08	0.581284	-2.86	0.414683
Isg20	Interferon-stimulated protein	61.04*	0.006060	1.04	0.780850	47.58*	0.007095	1.28	0.424549	-3.54	0.349151	-5.09	0.317391	-6.42	0.310954	-5.78	0.309394
Jak1	Janus kinase 1	2.48*	0.009009	1.72	0.262642	2.74*	0.037141	-1.12	0.960131	3.71	0.594246	3.46	0.719686	4.24	0.419710	3.19	0.855576
Jak2	Janus kinase 2	4.07*	0.014992	1.58	0.115200	3.83*	0.005300	-1.15	0.443057	-1.41	0.482369	-1.85	0.361778	-1.31	0.555662	-2.17	0.321151
Mal	Myelin and lymphocyte protein, T-cell differentiation protein	-1.50	0.445148	1.74	0.399539	2.99	0.363075	-1.65	0.210075	-6.76	0.000906	-1.35	0.166346	-8.29*	0.000567	-1.31	0.213228
Met	Met proto-oncogene	-2.30	0.058226	-1.09	0.838031	-2.97	0.022586	-1.27	0.362781	1.59	0.679537	1.94	0.382957	1.97	0.378885	1.65	0.610312
Mx1	Myxovirus (influenza virus) resistance 1	91.47*	0.047484	2.10	0.252215	71.73*	0.000357	1.63	0.426149	24.64	0.072372	1.56	0.683917	11.83*	0.017392	1.79	0.450732
Mx2	Myxovirus (influenza virus) resistance 2	17.73*	0.000041	1.23	0.567298	14.13*	0.049356	1.22	0.592922	13.98	0.087455	1.66	0.477954	8.61*	0.008162	1.21	0.540662
Myd88	Myeloid differentiation primary response gene 88	13.56	0.072366	-1.52	0.914739	6.56	0.079936	-1.03	0.609612	-4.87	0.374576	-7.54	0.374233	-6.11	0.374399	-8.17	0.374228
Nmi	N-myc (and STAT) interactor	1.68	0.181140	2.38	0.242912	1.64	0.124887	1.15	0.559486	-1.52	0.434537	-3.53	0.356342	-2.13	0.401741	-2.46	0.388705
Nos2	Nitric oxide synthase 2, inducible	5.64	0.244199	-1.52	0.718529	4.50	0.082627	1.34	0.396588	-1.74	0.433612	-1.51	0.436034	-1.57	0.418104	-2.19	0.343774
Oas1a	2'-5' oligoadenylate synthetase 1A	32.41*	0.010660	-1.23	0.697300	24.30*	0.028527	1.30	0.478855	13.20	0.064868	2.54	0.352029	7.82	0.055780	2.49	0.418122

Oas1b	2'-5' oligoadenylate synthetase 1B	16.81*	0.032475	2.30	0.176641	17.77*	0.008639	-1.19	0.518856	-11.62	0.373741	-15.64	0.373099	-14.47	0.373267	-11.76	0.373769
Oas2	2'-5' oligoadenylate synthetase 2	15.91	0.162575	-1.09	0.929236	10.01	0.132110	-1.11	0.679684	1.13	0.381779	-8.28	0.374503	-2.04	0.376510	-10.83	0.375981
Pml	Promyelocytic leukemia	5.42*	0.023632	-1.84	0.876664	2.40	0.239598	1.13	0.592582	-3.59	0.379305	-4.76	0.375948	-5.39	0.374905	-6.42	0.374530
Prkcz	Protein kinase C, zeta	-8.42*	0.001291	1.11	0.402580	-18.24*	0.000558	-2.01*	0.015809	-14.84	0.371850	-7.63	0.373516	-24.53	0.371125	-10.22	0.372608
Psme2	Proteasome (prosome, macropain) 28 subunit, beta	1.64	0.080186	1.22	0.463635	1.65*	0.006388	-1.43	0.657049	-1.06	0.705920	-1.70	0.233508	-1.61	0.273102	-1.50	0.343917
Sh2d1a	SH2 domain protein 1A	1.98	0.288561	-2.18	0.198548	4.14	0.293205	-2.68	0.390743	-4.24	0.364946	-4.39	0.360942	-4.50	0.359235	-2.93	0.376707
Shb	Src homology 2 domain-containing transforming protein B	1.05	0.664879	-1.43	0.466870	-1.32	0.326928	-1.07	0.783676	-2.98	0.386127	-2.08	0.396140	-3.05	0.384236	-3.60	0.374304
Socs1	Suppressor of cytokine signaling 1	21.03	0.080650	-2.20	0.096420	10.93	0.173825	-1.28	0.383123	-3.01	0.376147	-11.19	0.374057	-5.81	0.374558	-11.26	0.374132
Stat1	Signal transducer and activator of transcription 1	7.71	0.095575	1.52	0.353252	4.10*	0.027347	1.22	0.503492	1.33	0.580768	-1.44	0.388537	-1.21	0.593404	-1.46	0.575120
Stat2	Signal transducer and activator of transcription 2	3.48	0.073245	-1.35	0.517363	1.95	0.232110	-1.01	0.971477	10.45	0.077743	3.88	0.279660	6.55*	0.024131	3.58	0.413430
Stat3	Signal transducer and activator of transcription 3	2.50*	0.026066	-1.12	0.742296	1.87*	0.034747	1.17	0.536036	-1.21	0.431266	-2.96	0.380579	-1.20	0.434457	-3.77	0.373760
Tap1	Transporter 1, ATP-binding cassette, sub-family B (MDR/TAP)	10.65*	0.010692	-2.42	0.497171	5.30	0.091328	-1.06	0.714687	7.80*	0.012547	3.54	0.287772	6.40	0.061665	3.18	0.443886
Ticam1	Toll-like receptor adaptor molecule 1	-1.05	0.749788	-3.05	0.918752	-2.89	0.342131	-1.50	0.860885	-13.35	0.373922	-5.51	0.374685	-11.91	0.373990	-10.60	0.374055
Timp1	Tissue inhibitor of metalloproteinase 1	64.98	0.091361	-1.27	0.649407	201.99	0.185533	-1.09	0.693039	25.59	0.123417	1.10	0.506015	29.79*	0.002445	1.77	0.202045
Tlr3	Toll-like receptor 3	16.07*	0.008706	1.23	0.395134	7.74	0.067210	1.11	0.638615	-1.20	0.528118	-1.56	0.428091	-1.75	0.415783	-1.48	0.468917
Tlr7	Toll-like receptor 7	4.59	0.170070	-1.06	0.817114	9.24	0.053937	-1.07	0.861583	-1.33	0.397982	-2.43	0.383468	-1.53	0.393777	-2.58	0.384763
Tlr8	Toll-like receptor 8	1.71	0.384040	-1.12	0.746933	2.11*	0.046362	-1.17	0.672286	-8.02	0.372830	-2.09	0.384732	-10.42	0.371676	-3.45	0.378487

Tlr9	Toll-like receptor 9	21.89	0.116063	2.29	0.313000	27.41*	0.004590	3.39	0.197733	-3.42	0.380903	-3.80	0.376068	-7.09	0.367679	-3.91	0.377511
Tnfsf10	Tumor necrosis factor (ligand) superfamily, member 10	3.72	0.093226	1.12	0.549492	1.57	0.207564	-1.17	0.957911	-2.84	0.382368	-6.88	0.373914	-4.88	0.375745	-6.46	0.374769
Traf3	Tnf receptor-associated factor 3	4.28*	0.002653	1.17	0.692315	5.98	0.063827	1.45	0.309696	1.40	0.479834	1.65	0.190761	1.23	0.698003	1.21	0.761830
Tyk2	Tyrosine kinase 2	-1.30	0.598074	-1.38	0.899398	-1.87	0.048891	-1.32	0.565756	-6.65	0.365511	-3.07	0.380261	-8.08	0.363222	-4.54	0.371303
Vegfa	Vascular endothelial growth factor A	1.55	0.330050	-1.06	0.598095	1.24	0.413445	-1.37	0.124249	-12.87	0.372223	-7.19	0.373773	-10.91	0.372758	-9.42	0.372966
Actb	Actin, beta	3.56	0.020962	-1.07	0.828872	3.04	0.000779	1.73	0.058493	-1.33	0.416903	1.56	0.059316	-1.40	0.198619	1.31	0.309668
B2m	Beta-2 microglobulin	1.25	0.124593	2.14	0.260826	1.29	0.250475	-1.00	0.750551	3.65	0.055582	1.97	0.673329	3.04	0.129524	2.32	0.435142
Gapdh	Glyceraldehyde-3-phosphate dehydrogenase	-1.34	0.203950	-1.44	0.603049	-1.74	0.077977	1.05	0.794259	3.62	0.186001	3.15	0.322424	3.95	0.124183	2.80	0.459195
Gusb	Glucuronidase, beta	-2.71	0.009729	-1.32	0.218259	-1.56	0.117862	-1.80	0.016505	-5.57	0.354956	-3.23	0.371843	-4.64	0.358845	-3.60	0.367681
Hsp90ab	Heat shock protein 90 alpha (cytosolic), class B member 1	-1.23	0.401035	-1.05	0.768339	-1.44	0.104711	-1.01	0.843437	-1.78	0.412121	-3.00	0.368486	-1.85	0.406969	-2.36	0.387013

APPENDIX 4

Animal Ethics Approval

Letters of approval for the PhD “Mutation of adjacent cysteine residues in the NSs protein of Rift Valley fever virus results in loss of virulence in a murine model infection”. Note that the letters present the old title “Molecular basis of Rift Valley fever virus virulence”. The certificates were issued by Animal Ethics Committees of the University of Pretoria and the National Health Laboratory Service (clearance certificate no V013-14 and 142/14, respectively) and also by the Department of Agriculture, Forestry and Fisheries of the Republic of South Africa (permission no. 12/11/1/1/13). PHD THESIS GABY FINAL VERSION 22.01.19 PHD THESIS GABY FINAL VERSION 22.01.19

UNIVERSITEIT VAN PRETORIA
UNIVERSITY OF PRETORIA
YUNIBESITHI YA PRETORIA

Animal Ethics Committee

PROJECT TITLE	**Molecular basis of rift Valley fever virus virulence**
PROJECT NUMBER	**V013-14 (Revised version number 3)**
RESEARCHER/PRINCIPAL INVESTIGATOR	**Dr. G Monteiro**

STUDENT NUMBER (where applicable)	**121 204 31**
DISSERTATION/THESIS SUBMITTED FOR	**PhD**

ANIMAL SPECIES	**Rodents**	
NUMBER OF ANIMALS	**387**	
Approval period to use animals for research/testing purposes		**August 2014 – August 2015**
SUPERVISOR	**Prof. JT Paweska**	

KINDLY NOTE:

Should there be a change in the species or number of animal/s required, or the experimental procedure/s - please submit an amendment form to the UP Animal Ethics Committee for approval before commencing with the experiment

APPROVED	Date	**4 August 2014**
CHAIRMAN: UP Animal Ethics Committee	Signature	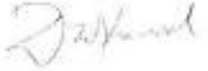

Version: CC 2/10 Date: Dec 2012

NATIONAL HEALTH LABORATORY SERVICE
ANIMAL ETHICS COMMITTEE

Chairperson: A/Prof John Frean	Technical Advisor:
NICD/NHLS Parasitology Reference Unit	SAVP/NHLS Animal Unit
P/Bag X4	P.O. Box 28999
Sandringham	Sandringham
2131	2131
Phone: +27(011) 555 0308	Phone: + 27 (011) 386 6039
Email: johnf@nicd.ac.za	E-mail: ingridl@savp.co.za

ANIMAL ETHICS CLEARANCE CERTIFICATE

CLEARANCE CERTIFICATE NO. 142/14

APPLICANT: DR G MONTEIRO

DEPARTMENT/COMPANY: CEZD, NICD

PROJECT TITLE: Molecular basis of Rift Valley fever virus virulence

SPECIES	NUMBER	TYPE OF APPLICATION
Rattus norvegicus Wistar-Furth	102	EXPERIMENTAL
Rattus norvegicus Sprague-Dawley	102	
Mus musculus BALB/c	102	

Approval is hereby given for the procedure/s described in the above application.

The use of this material is subject to the National Standard SANS 10386: 2008 guidelines as used by the NHLS AEC. If an application is for a routine procedure then the recommended guidelines or SOP must be followed. It is limited to the procedure/s specified in the application form.

SIGNED---------- DATE: 17 March 2014
(Chairperson: Animal Ethics Committee)

i) I am satisfied that the persons listed in this application are competent to perform the procedures therein, in terms of Section 23(1) (C) of the Veterinary and Para-Veterinary Professions Act (19 of 1982)

SIGNED---------- DATE: 18 March 2014
(Registered Veterinarian)

agriculture,
forestry & fisheries

Department:
Agriculture, Forestry and Fisheries
REPUBLIC OF SOUTH AFRICA

Directorate Animal Health, Department of Agriculture, Forestry and Fisheries
Private Bag X138, Pretoria 0001

Enquiries: Mr Herry Gololo • Tel: +27 12 319 7532 • Fax: +27 12 319 7470 • E-mail: HerryG@daff.gov.za
Reference: 12/11/1/1/13

Prof Janusz Tadeusz Paweska
Center for emerging and Zoonotic Diseases
2131 Sandringham
1 Modderfontein RD
Gauteng

Dear Prof Pawaseka,

RE: Permission to do research in terms of Section 20 of the ANIMAL DISEASES ACT, 1984 (ACT NO. 35 of 1984)

Your fax / memo / letter/ Email dated 23 June 2014, requesting permission under Section 20 of the Animal Disease Act, 1984 (Act No. 35 of 1984) to perform a research project or study, refers.

I am pleased to inform you that permission is hereby granted to perform the following research/study, with the following conditions :

Conditions:

1. This permission does not relieve the researcher of any responsibility which may be placed on him by any other act of the Republic of South Africa;
2. All potentially infectious material utilised or collected during the study is to be destroyed at the completion of the study. Records must be kept for five years for audit purposes. A dispensation application may be made to the Director Animal Health in the event that any of the above is to be stored or distributed;
3. A Veterinary Import Permit must be obtained prior to the importation of the plasmids containing RVFV ZH50.

Title of research/study: Molecular basis of Rift Valley fever virus virulence.
Researcher (s): Prof Janusz Tadeusz Paweska.
Institution: Center for emerging and Zoonotic Diseases, NICD.
Your Ref./ Project Number:
Our ref Number: 12/11/1/1/13.

Kind regards,

DR. MPHO MAJA
DIRECTOR OF ANIMAL HEALTH
Date: 2014 -07- 15

agriculture,
forestry & fisheries

Department:
Agriculture, Forestry and Fisheries
REPUBLIC OF SOUTH AFRICA

Directorate Animal Health, Department of Agriculture, Forestry and Fisheries
Private Bag X138, Pretoria 0001

Enquiries: Mr Henry Gololo • Tel: +27 12 319 7532 • Fax: +27 12 319 7470 • E-mail: HenryG@daff.gov.za
Reference: 12/11/1/1/13

Prof Janusz Tadeusz Paweska
Center for Emerging and Zoonotic Diseases
Special Viral Pathogens Laboratory
NICD

Dear Prof Paweska,

RE: Dispensation on Section 20 Approval in Terms of the Animal Diseases Act, 1984 (Act No 35 of 1984) for: Molecular basis of Rift valley fever virus virulence

Your email dated 23 June 2014 refers.

A dispensation is hereby granted on point 2 of the Section 20 approval that was issued for the above mentioned study (attached):

The samples collected from rodents including serum and various tissues may be stored:

(i) Within the -70°C freezer in the access controlled freezer room OR
(ii) Samples collected in buffered formalin may be stored at room temperature

Kind regards,

Maja

DR. MPHO MAJA
DIRECTOR: ANIMAL HEALTH

Date: 2014 -07- 25

APPENDIX 5

Communications related to this thesis

The following scientific presentations and publications were generated during the course of this research study and emanated directly from this study:

Publication:

Monteiro GER, Jansen van Vuren P, Wichgers Schreur PJ, Odendaal L, Clift SJ, Kortekaas J and Paweska JT. 2018. **Mutation of adjacent cysteine residues in the NSs protein of Rift Valley fever virus results in loss of virulence in mice**. Virus Research, 249, 31-44. https://doi.org/10.1016/j.virusres.2018.03.005.

Scientific meetings and forums:

Monteiro GER, Jansen van Vuren P, Wichgers PJ, Odendaal L, Clift SJ, Kortekaas J and Paweska JT. **Evaluation of phenotypic attenuation of Rift Valley fever virus NSs cysteine mutants in mice**. ASM Biothreats Congress: Baltimore, USA, February 2018 (poster presentation).

Monteiro GER, Jansen van Vuren P, Odendaal L, Clift SJ, Kortekaas J and Paweska JT. **Point mutation of conserved NSs cysteine residues prevents the outcome of Rift Valley fever virus infection in mice.** 3rd One Health Ecohealth congress. Melbourne, Australia, December 2016 (poster presentation).

Monteiro GER, Jansen van Vuren P, Kortekaas J, Moormann R, Coetzer JAW and Paweska JT. **Study of the virulence among reassortants of Egyptian and sub-Saharan lineage of Rift Valley fever virus**. 2nd One health Conference in Africa, Arusha-Tanzania, April 2013 (oral presentation).

Monteiro GER, Jansen van Vuren P, Kortekaas J, Moormann R, Coetzer JAW and Paweska JT. **Molecular basis of the Rift Valley fever virus virulence.** 2nd Southern African Student Symposium, University of Pretoria, September 2012 (oral presentation).